Process Modelling of Thermoset Composites

Ahmad Kamal Zulkifle

Submitted for
Degree of Doctor of Philosophy,
Department of Mathematics,
University of Strathclyde.

1999

Acknowledgements

Firstly, I would like to express my sincere and warmest thanks to my supervisor, Professor Sean McKee (and Joyce), for giving me the opportunity to work on this project and for his enduring and persevering guidance, patience and encouragement without which this thesis would not have been possible. I wish also to thank Dr. Brian Duffy and Dr. David Blest for their very helpful discussions on the fluid flow section of the thesis. I wish to express my gratitude to the Institute Technology of MARA, Malaysia for the financial support throughout my long and extended stay here.

Over the last six years, I have received much help from lecturers, friends and colleagues in the Mathematics Department of Strathclyde University and would like to thank them all. A special 'thank you' also goes to Dr. Ishak Hashim, Dr. Reezal Latif, Dr. Nizam Hassan, Dr. Rosli Saleh and Mr. Saiful whose friendship nourished the completion of this thesis. A thank you note also goes to all my friends whom I've known here and family back home for their encouragement throughout my studies. I would like to dedicate the thesis to my mother, my late father and especially to my daughter Nurul whom I was unable to be there for her and will never be. And last but not least, I am grateful to God Almighty for giving me the strength to persevere and for whatever He has bestowed upon.

Abstract

The process modelling of autoclave composites has received much attention over the years. This thesis concentrates on two types of processes namely the prepreg processing method and the resin infusion processing method. The work focuses on the modelling and simulation of the resin flow, heat transfer and cure processes of the composites during processing.

The Hercules 3501-6/AS4 composite was chosen for the simulation and the data for its thermal properties was obtained from Loos and Springer [12]. The composite is considered as a multilayered system consisting of prepregs or dry fibre layers with alternate layers of resin. A similarity analysis for the prepreg process was carried out allowing the velocity field, in both the prepreg and the resin, to be analytically determined. This then permitted the temperature and the degree of cure to be computed numerically. A similar, but different analysis was then carried out for the resin film infusion process, allowing the temperature and rate of cure to be computed directly.

The simulation results of the prepreg case of Hercules 3501-6/AS4 were compared to known experimental results and good agreement has been found. Experimental work was performed on the flow dynamics of the resin infusion case and good agreement has also been observed.

Contents

1 Introduction **5**

1.1 Manufacturing Processes 9

1.2 Process Modelling 15

1.2.1 Resin Flow and Consolidation Model 16

1.2.2 Thermo-chemical Model 27

1.3 Scope and framework of this thesis 30

2 Prepreg Processing **32**

2.1 Introduction 32

2.2 Modelling the Heat Flow 32

2.3 Fluid Flow 35

2.3.1 Fluid Flow Equations 36

2.3.2 A Similarity Solution 38

2.3.3 Variable Viscosity 44

2.4 Numerical Solution Techniques 44

2.4.1 Discretization 46

2.4.2 ADI Method 48

2.5 Numerical Results and Discussion 50
2.6 Concluding Remarks 53

3 Resin Infusion Process **68**
3.1 Introduction 68
3.2 Modelling the Resin Flow 68
3.3 Heat Transfer Model 75
3.4 Solution Techniques 78
3.4.1 Scaling 78
3.5 Numerical Result 81
3.6 Experimental Investigation 92
3.7 Concluding Remarks 97

4 Conclusion and Recommendation **98**

A Derivation of Prepreg Flow Equations. **101**

B Derivation of RFI Flow Equations. **116**

C ADI Method **131**

Bibliography **141**

List of Figures

1.1 Schematic diagram of crossply dry fibre weave 6

1.2 Dry fibre weave 7

1.3 Schematic diagram of materials selection and processing methods. 11

1.4 Schematic diagram of the RTM. 12

1.5 Schematic diagram of an autoclave [8]. 13

1.6 A typical autoclave stepped cure cycle. 17

1.7 The expert system approach for selecting the autoclave cure cycle. 18

1.8 The processing model approach for selecting the autoclave cure cycle. 18

2.1 Set up for n prepregs 55

2.2 Comparison of average resin thickness vs time of 32 ply for different heating rates. 56

2.3 Comparison of the computed (variable) viscosity (see equation (2.62)) versus time for different heating rates for 64 ply laminate at the centre of the composite. 57

2.4 Comparison of temperature at $y/h_{2n+1}(t)$=0.25 with experimental data of Loos and Springer[12] for 64 plies. 58

2.5 Comparison of temperature at the centre of the composite with experimental data of Loos and Springer[12] for 64 plies. 59

2.6 Comparison of temperature at $y/h_{2n+1}(t) = 0.75$ with experimental data of Loos and Springer[12] for 64 plies. 60

2.7 Comparison of the temperature versus time at the centre of composite for Hercules 3501-6 resin for the heating rate 2.8 K/min. 61

2.8 Comparison of temperature versus time at the centre of composite for Hercules 3501-6 resin for the heating rate 11.1 K/min. 62

2.9 Comparison of the degree of cure versus temperature at centre of composite for Hercules 3501-6 resin for different heating rates. 63

2.10 Comparison of the degree of cure versus time at the centre of composite for different heating rates for varying thickness. . . 64

2.11 Comparison of the temperature versus time at the centre of a 64 ply laminate for varying prepreg thickness for the heating rate 2.8 K/min. 65

2.12 Through-the-thickness degree of cure of 16 ply laminate for the heating rate 2.8 K/min. 66

2.13 Through-the-thickness degree of cure of 64 ply laminate for the heating rate 11.1 K/min. 67

3.1 Set-up for n dry fibre plies 69

3.2 Resin thickness vs Time. 83

3.3 Temperature vs Time at the centre of the composites at heating rate 2.8 K/min. 84

3.4 Temperature vs Time at the centre of the composites at heating rate 11.1 K/min. 85

3.5 Cure vs Time at the centre of the composites at heating rate 2.8 K/min. 86

3.6 Cure vs Time at the centre of the composites at heating rate 11.1 K/min. 87

3.7 Comparison of Temperature vs Time at the centre of the composites at different heating rates. 88

3.8 Comparison of Degree of cure vs Time at the centre of the composite at different heating rates. 89

3.9 Temperature vs Normalized height at different times during the process for n=16 plies. 90

3.10 Temperature vs Normalized height at different times during the process for n=32 plies. 91

3.11 Micrograph 1. 94

3.12 Micrograph 2. 95

3.13 Micrograph 3. 96

C.1 Grid for n prepregs. 140

List of Tables

1.1 **Functions of vacuum bag components [8].** 14

2.1 Material properties of Hercules 3501-6 resin and fibre. 51

2.2 Flow parameters from Blest [61]. 51

2.3 Curing constants of Hercules 3501-6 resin. 52

Chapter 1

Introduction

Composite materials are now well established in many industries. Their high specific stiffness and strength-to-weight ratio in addition to their tendency to offer cost savings are their principal advantages. Composite materials are made up of reinforcements in the form of unidirectional fibres, stitched-fibres or woven fibres. These are held by a matrix material which can be either polymeric, ceramic or metallic. The resulting composite will generally be composed of layers (laminae) of the fibre material and the matrix stacked to achieve the desired properties in one or more directions. This will produce material properties that will be influenced by the individual properties of the selected reinforcement material and the matrix material. This in effect allows the designer to obtain either isotropic or anisotropic properties of the material according to the requirements of the design. *Figure 1.1* shows a schematic diagram of fibre weave lay-up and *Figure 1.2* displays the actual dry fibre weave.

Composites of metal-matrix and ceramic-matrix are suitable for high - temperature uses whereas polymer matrix composites offer significant cost savings (see Dominy [1]). Polymer-based structural composites are usually reinforced with continuous fibres. The mechanical properties of the components built from such materials depend not only on the material type but also on

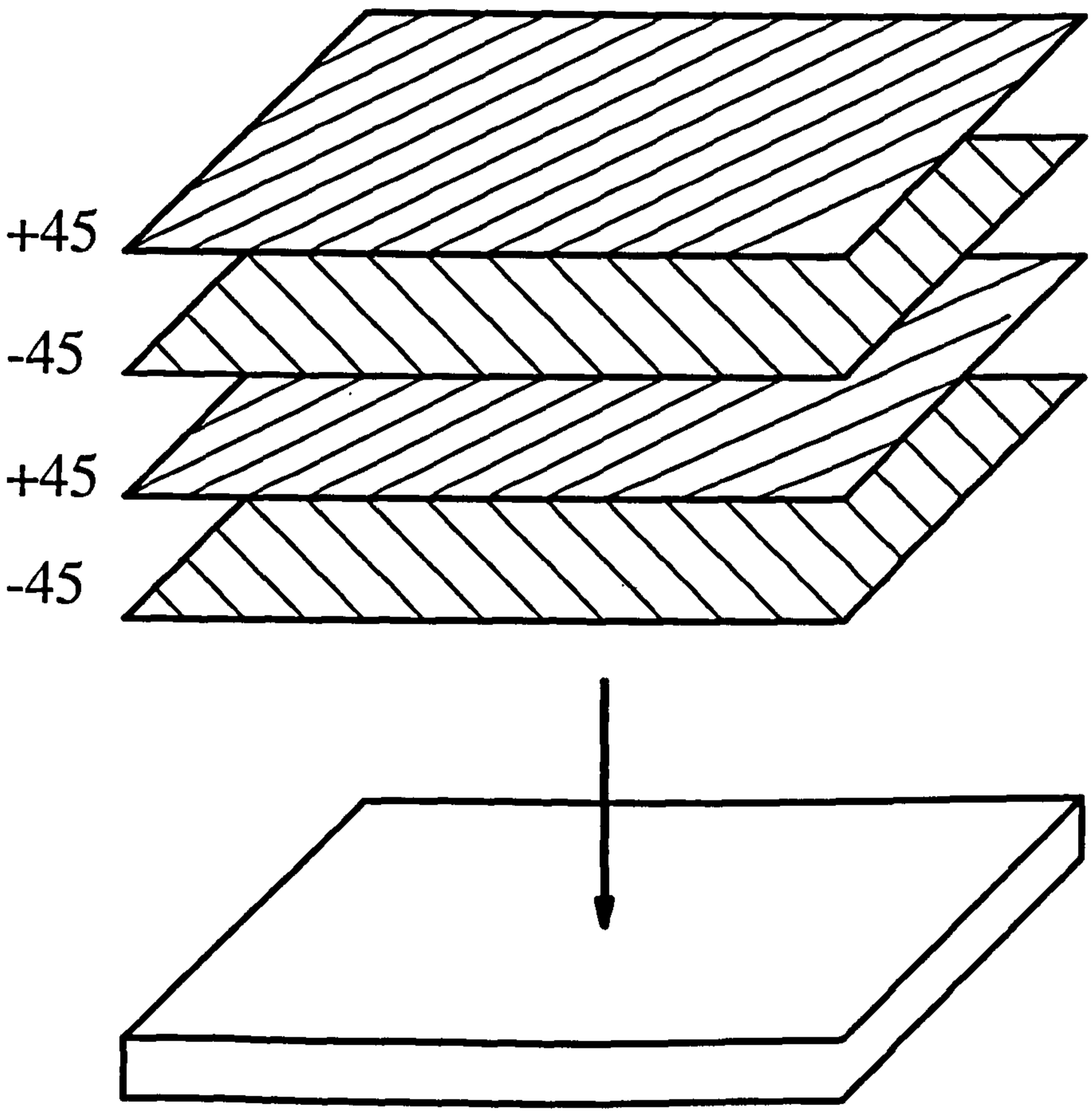

Figure 1.1: Schematic diagram of crossply dry fibre weave

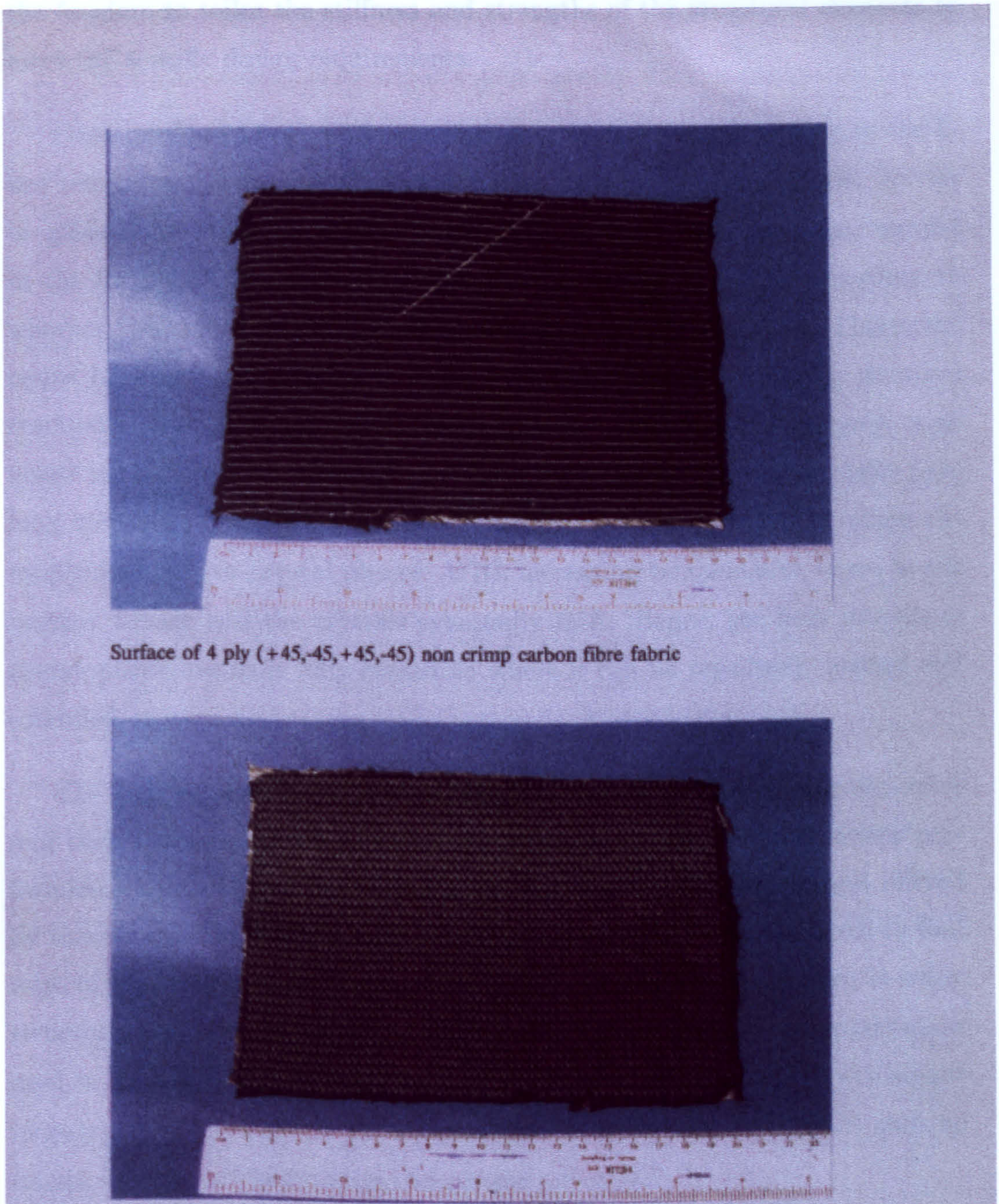

Figure 1.2: Dry fibre weave

the fibre volume fraction, distribution, and orientation. This gives the designer the freedom to tailor the stiffness and strengths of the structural elements to meet the specific design requirements.

Fibre-reinforced polymer composites may be classified according to the fibre reinforcement employed. These fibres, such as graphite, boron, Kevlar or glass fibres, may be discontinuous or they may be continuous, usually in the form of a weave. Composites can be further classified according to whether they are thermoset or thermoplastic matrix composites. Thermoset resins have network structures called crosslinks, which are set by chemical reactions. Crosslinks are irreversible, and hence, once made, thermoset composite parts cannot be reshaped. On the other hand, thermoplastic resins have long molecular chains that are held together by secondary bonds, chain entanglement and/or crystal phases. With increasing temperature, these bonds become weaker and the crystals eventually melt. Hence, the heat process in thermoplastic resins is fully reversible where it can be repeatedly melted and solidified.

The high strength or stiffness-to-weight ratios of the advanced composites and their non-corrosive behaviour are well known: they provide better performance and a longer life time for the structures. The advantages offered by these composite materials have stimulated much work and research to find ways of replacing conventional materials such as metals by composites in many structural parts; for example, in the transportation industry, composites are used in the airplanes, automobiles and small ships or boats and in the leisure industry they are used in the manufacture of many sporting goods such as tennis, squash and badminton rackets and golf clubs.

1.1 Manufacturing Processes

The goal of processing is to make a good quality fibre reinforced composite where the resin forms a void-free continuous phase, surrounds each filament, is evenly distributed, is present in the desired amount relative to the fibre and is fully cured.

Figure 1.3 displays the wide range of options involved in the selection of material, preform and processing techniques. When constituent materials have been selected, the designer has to select the best composite fabrication process which will provide an acceptable quality component at the lowest possible cost. High-performance laminates usually of fibre-reinforced-epoxy systems are usually produced using the autoclave process. This process is usually chosen for its reproducibility, high quality, low void content and reasonable production rates. Its main drawback is the high cost of material involved in production. For large complex-shaped composite structures, non-autoclave curing methods such as ovens or presses are used. Major issues related to non-autoclave methods are effective compaction of plies and elimination of trapped interlaminar and intralaminar air pockets. Interlaminar air pockets are air bubbles that occurs between the laminates during the lay-up process and intralaminar air pockets are the air voids that are present within each individual layer.

Resin Transfer Moulding (RTM) offers low processing cost and fast cycle times. RTM is a closed mould process in which matched male and female moulds, preplaced with fibre preform are clamped to form composite components. Mixed resins are then injected into the cavity through ports which displace the air escaping through vents thus avoiding dry spots. A schematic diagram of the RTM process is shown in *Figure* 1.4. The cure cycle of the process is dependent on part thickness, type of resin and temperature of the mould and resin. The cured part is normally heated by a controller and is removed from the mould after sufficient green strength has been achieved. The

RTM process has been successfully used for moulding parts such as cabinet walls, water tanks, bathtubs and boat hulls. Other processes similar to RTM includes Structural Reaction Injection Molding (SRIM), and hybrid versions of vacuum assisted RTM. The difference between SRIM and RTM is mainly in the resin reactivity employed by the two processes (see Mallick [2]).

For aerospace and aircraft applications, most components are produced using the autoclave. Flat or curved composite panels are some of the parts produced by autoclave moulding. This technique ensures high quality, but is labour intensive and expensive. Autoclave moulding is mainly used for processing thermosetting composites, because thermoplastic composites can be more quickly and less expensively processed using other methods. The material most often employed in autoclave moulding is composite prepregs (see Hoa [3]). In this process, the pre-impregnated unidirectional or woven fibres or prepregs, are stacked on the mould surface and covered with a flexible bag where the assembly is then placed in the autoclave for consolidation and curing to take place by the application of an external pressure at an elevated temperature. *Figure* 1.5 shows the basic components of the tooling for vacuum bag or autoclave processed components and *Table* 1.1 shows the function of each part of the system.

For several decades, there has been a great deal of activity in modelling the fabrication process of composites using an autoclave. In this study, two autoclave processes of manufacturing flat plate composites will be investigated. The first process involves the use of prepregs and the second involves the infusion of resin through initially dry fibre layers. In both processes, the laminae are stacked on a tool plate, vacuum bagged and placed in an autoclave to be acted upon by simultaneous heat and pressure. For the prepreg lay-up, the applied pressure will force out excess resin and entrapped volatiles from the saturated fibre layers of the laminate and the elevated heat will initiate the curing reactions and the polymerization process of the thermoset resin. In the case of the infusion process, the applied pressure will force the

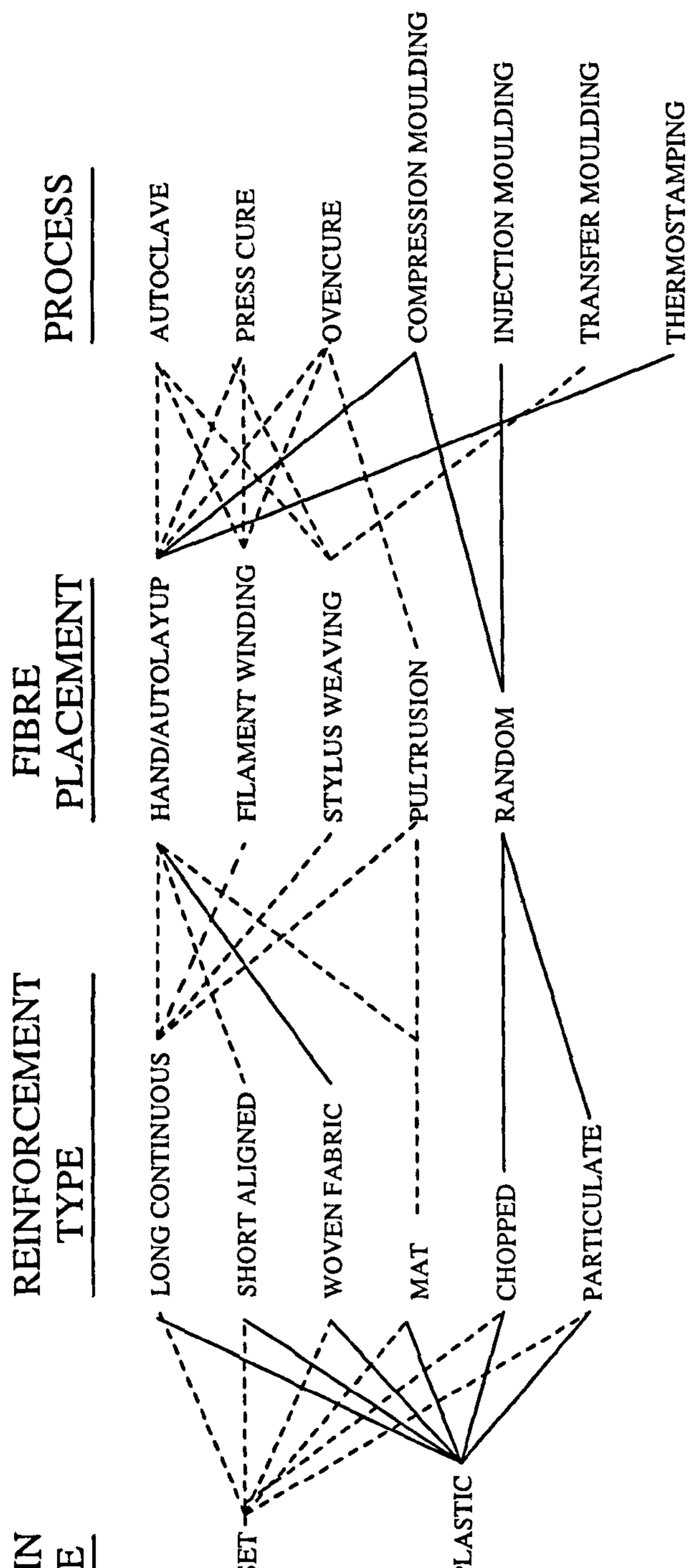

Figure 1.3: Schematic diagram of materials selection and processing methods.

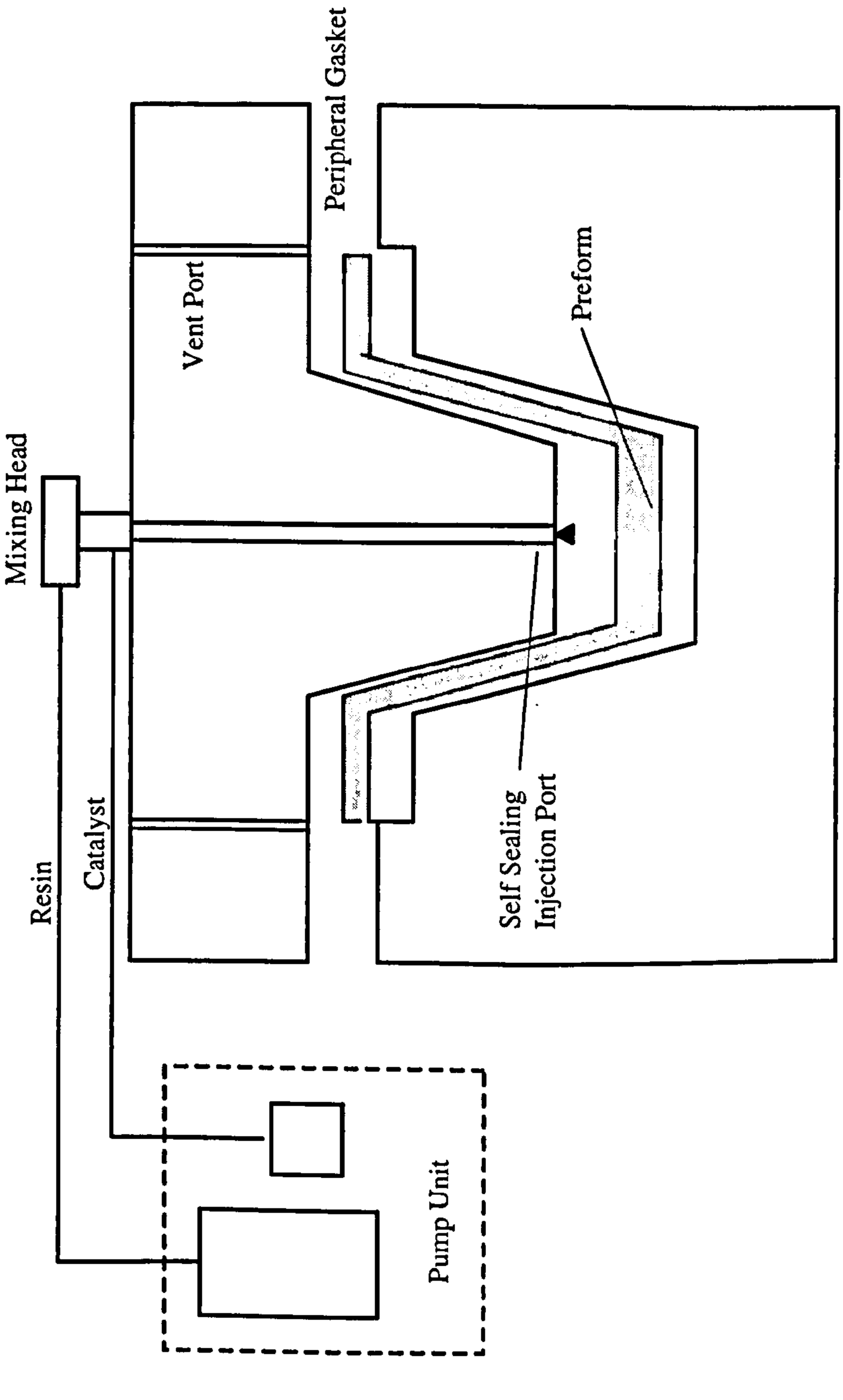

Figure 1.4: Schematic diagram of the RTM.

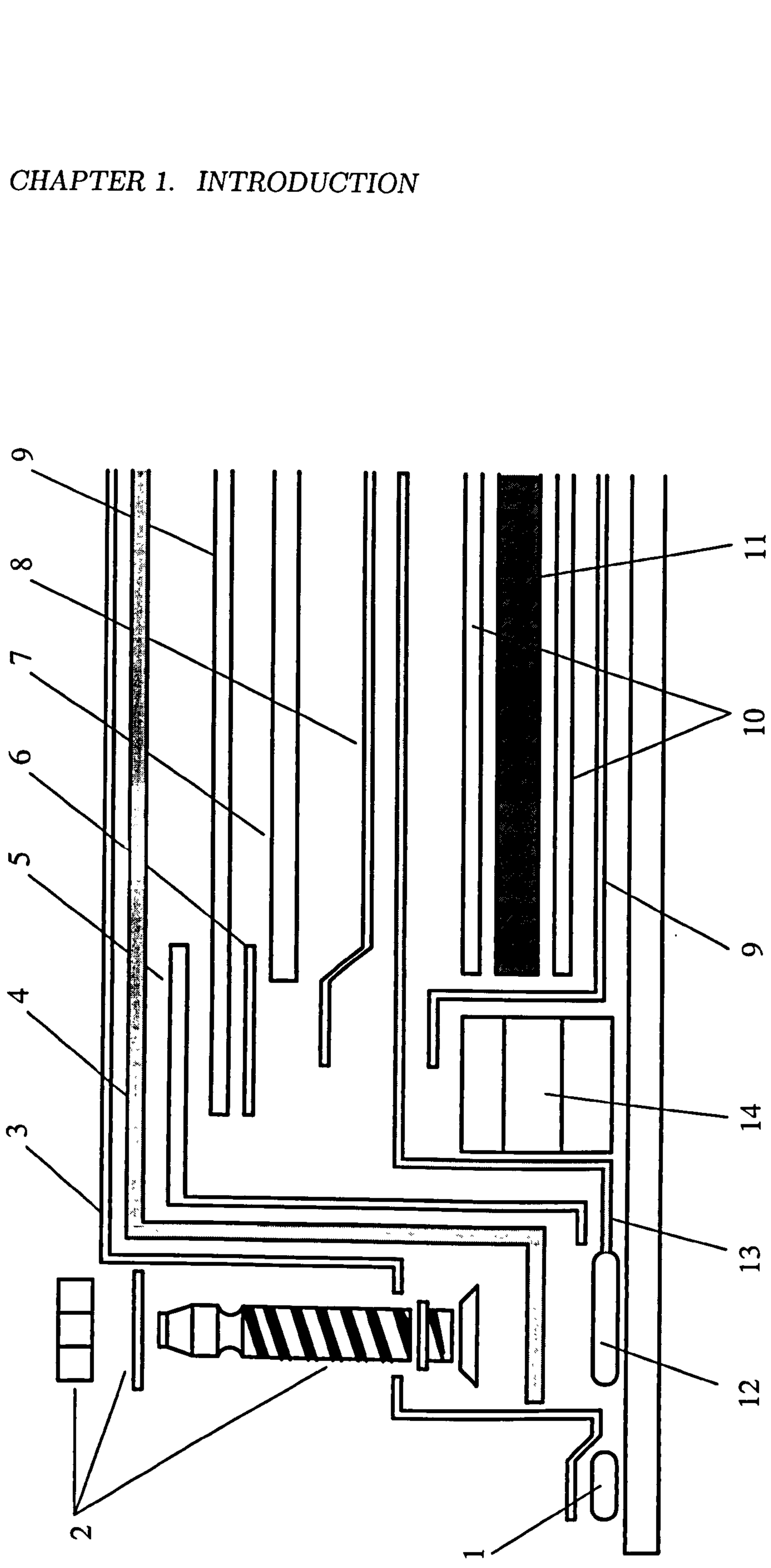

Figure 1.5: Schematic diagram of an autoclave [8].

*Component**	*Functions*
1 Bag sealant	Temporarily bonds vacuum bag tool
2 Vacuum fitting and hardware	Exhausts air, provides convenient connection to vacuum pump
3 Bagging film	Encloses part, allows for vacuum and pressure
4 Open weave breather mat	Allows air or vacuum transfer to all of part
5 Polyester tape(wide)	Holds other components of bag in place
6 Polyester tape(narrow)	Holds components in place
7 Caul sheet	Imparts desired contour and surface finish to composite
8 Perforated release film	Allows flow of resin or air without adhesion
9 Non-perforated release film	Prevents adhesion of laminate resin to tool surface
10 Peel ply	Imparts a bondable surface to cured laminate
11 Laminate	
12 1581-style glass breather manifold	Allows transfer of air or vacuum
13 1581-style glass bleeder ply	Soaks up excess resin
14 Stacked silicon edge dam	Forces excess resin to flow vertically, increasing fluid pressure

*numbers refer to *Figure* 1.5

Table 1.1: Functions of vacuum bag components [8].

resin which are interspersed in between the dry fibre layers to infiltrate and impregnate the fibre layers as well as eliminating the voids. Both fabrication procedure, thus, involves a combination of processes involving resin flow, heat transfer of the laminate and polymerisation: it is vital (certainly in the case of resin film infusion) that the resin infiltrates the fibre completely before the chemical reactions start to take place. Currently, the Seemann Composites Resin Infusion Manufacture Process (SCRIMP) [4, 5] and the Resin Infusion under Flexible Tooling (RIFT) [5] process have been widely and successfully used in industry. In Hasko et al. [6], variations in the processing techniques of RTM, RFI and SCRIMP process are described. Guy et al. [7] successfully demonstrated the use of the RFI process to construct a low-cost, large scale, low observable (LO), high performance aircraft structure.

1.2 Process Modelling

In fabricating composite parts of high quality, the selection of the the autoclave temperature and pressure, i.e. the cure cycle, is important. *Figure* 1.6 displays a typical autoclave stepped cure cycle and its relationship with the resin viscosity for a typical 120 deg C curing epoxy resin system [8]. It can be observed that the resin viscosity changes considerably, typically in the order of $O(10^2)$, as the temperature is varied in the cure cycle. Typically, the viscosity, μ, of a thermosetting resin during the curing process is a function of cure temperature T, shear rate $\dot{\gamma}$, and degree of cure α:

$$\mu = \mu(T, \dot{\gamma}, \alpha).$$

For thermoplastics, since no in-situ chemical reaction occurs during processing, its viscosity function is significantly different from that of thermosets, i.e., only dependent on temperature and shear rate (see Mallick [2]). Using this information (usually available from material suppliers), a cure cycle can be defined to obtain maximum performance in fabricating a specific composite

structure. The cure cycle becomes more important as the structure becomes more complex.

There are various ways that can help the fabricator choose the appropriate cure cycle. One procedure is to follow the manufacturer's recommendation of the cure cycle but this is limited since it is clearly very dependent on the part geometry and thickness. For a part that does not satisfy the manufacturer's recommended specification, then a trial and error experimental procedure can be performed but this is not cost-effective.

A more cost effective and convenient means of determining the cure cycle is by an on-line control through in-situ expert system of sensors, a decision making program and closed loop control. The expert system controls the processing parameters by detecting the physical and chemical changes in the resin through the in-situ sensors [9] (*Figure* 1.7).

Alternatively, the parameters of the cure cycle can be selected using processing models which describe the physical processes based on conservation laws, and computer simulations can be performed using the codes developed for the numerical procedures [9] (*Figure* 1.8).

1.2.1 Resin Flow and Consolidation Model

The resin flow problem in composite processing is usually treated as flow through fibrous porous media. The equation of motion used to describe the average or macroscopic flow properties is in the form of Darcy's law which relates the volumetric flow per unit area, $\mathbf{v}$, to the pressure gradient, ∇p driving the flow through the porous medium. The anisotropic form of this equation is,

$$\mathbf{v} = -\mu^{-1}\mathbf{K}\nabla p \tag{1.1}$$

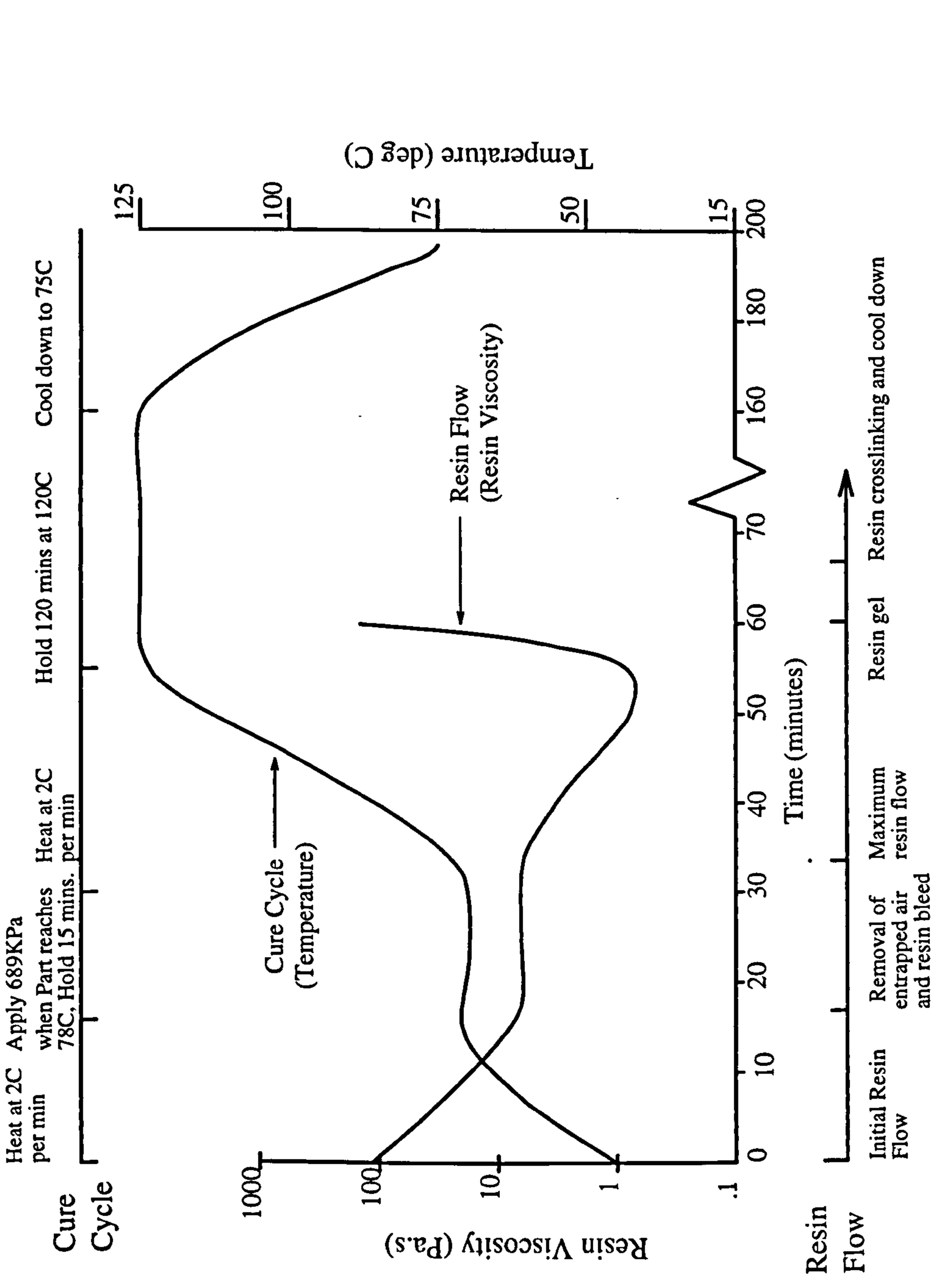

Figure 1.6: A typical autoclave stepped cure cycle.

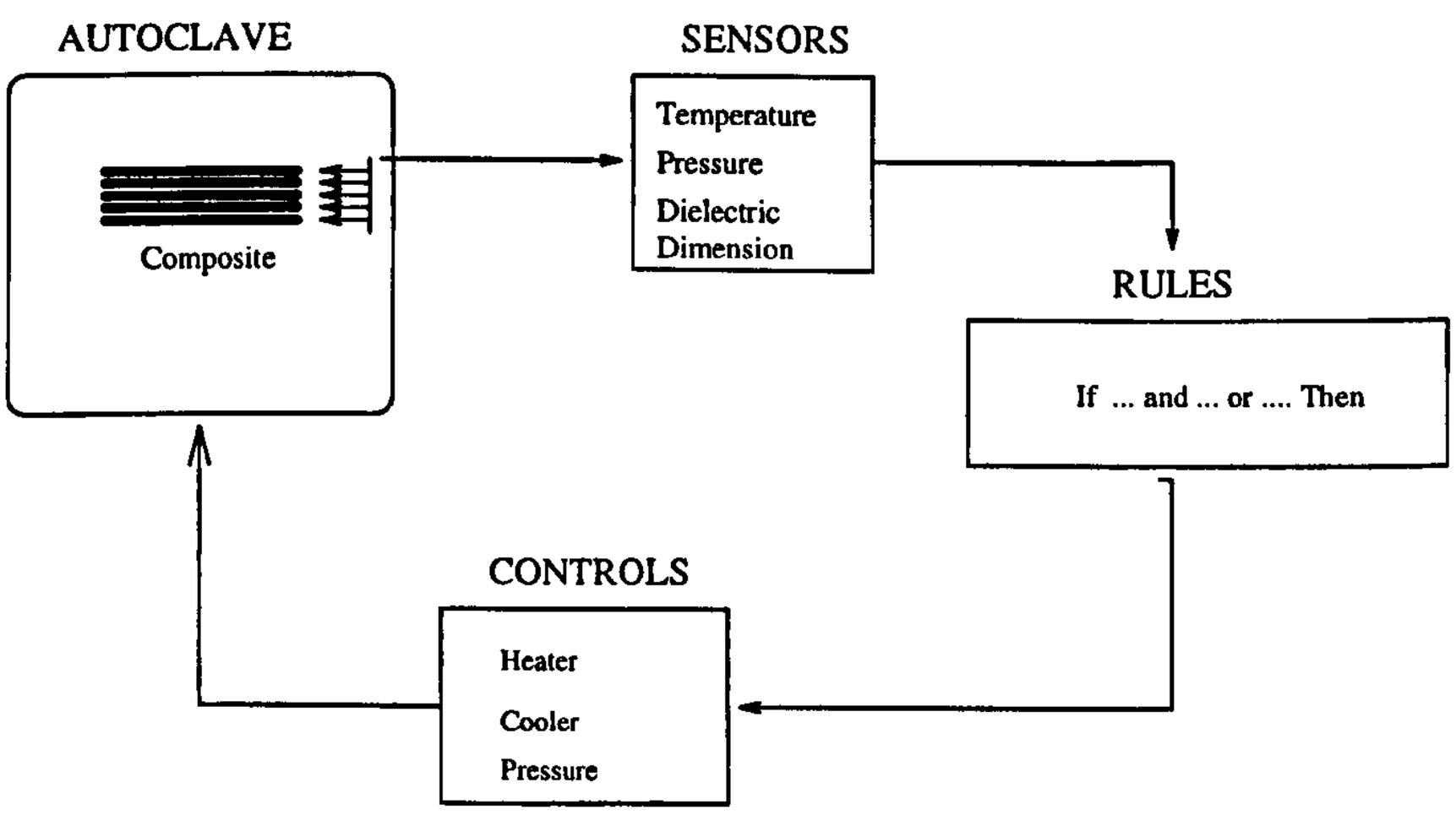

Figure 1.7: The expert system approach for selecting the autoclave cure cycle.

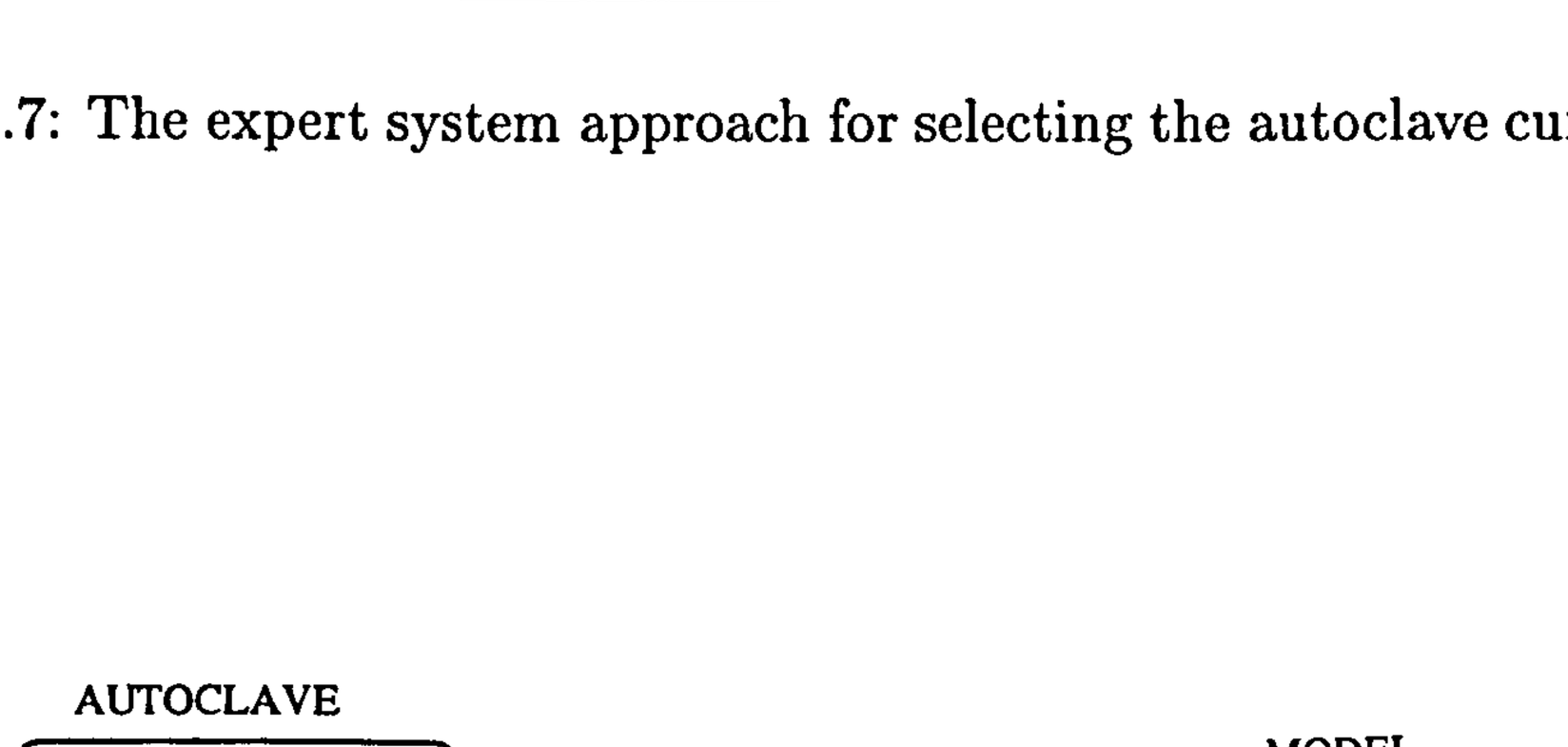

Figure 1.8: The processing model approach for selecting the autoclave cure cycle.

where μ is the viscosity of the resin and $\mathbf{K}$ is the permeability tensor. In general, the permeability tensor is

$$\mathbf{K} = \begin{bmatrix} \kappa_{xx} & \kappa_{xy} & \kappa_{xz} \\ \kappa_{yx} & \kappa_{yy} & \kappa_{yz} \\ \kappa_{zx} & \kappa_{zy} & \kappa_{zz} \end{bmatrix}. \tag{1.2}$$

For isotropic medium, if the principal components of $\mathbf{K}$ are aligned to the flow directions, then (1.2) reduces to

$$\mathbf{K} = \begin{bmatrix} \kappa_{xx} & 0 & 0 \\ 0 & \kappa_{yy} & 0 \\ 0 & 0 & \kappa_{zz} \end{bmatrix}, \text{ where } \kappa_{xx} = \kappa_{yy} = \kappa_{zz} = \kappa. \tag{1.3}$$

Resin Flow in Prepregs

Various consolidation and cure models, based on physical laws, have been proposed to simulate the autoclave curing process of prepreg laminates. Lindt [10] presented a two-dimensional squeeze flow model due to the compaction of the laminates. In his model, the composites are treated as layers of aligned fibres in parallel rows and columns and suspended in a viscous fluid. Subject to the external force applied normal to the tool, the fibres are assumed to move vertically downwards resulting in the relative motion of the resin. The squeezing action between the vertical fibres causes horizontal flow below the fibres and normal flow in the vertical gaps between the fibres. In practice, the fibres may not all be completely aligned in rows and columns.

Gutowski [11] presented a one-dimensional flow model of the composite in the direction of the fibres. Loos and Springer [12] developed a thermo-chemical flow model and provided a one-dimensional solution of the cure and temperature distribution for flat-plate composites. They calculated the flow variables by considering the normal and parallel directions separately, and assumed a non-deformable porous system. In contrast to the Loos and Springer

[12] flow model, Gutowski [13] and Dave et al. [14] independently proposed a squeezed sponge three-dimensional flow model with coupled vertical and horizontal directions and one-dimensional consolidation of the composite. They also considered a deformable unidirectional fibre reinforcement system where the load is shared by the fibre network and the resin. Dave [15] presented a generalized theory of resin flow and applied the unified flow model to different processing techniques such as bleeder ply moulding, autoclave processing, pultrusion and resin transfer moulding. Young [16] extended the general three-dimensional flow model of Gutowski [13] and Dave et al. [14] by considering multi-directional fibre arrangements and predicted the pressure, velocity and laminate thickness. Young [17] proposed a viscoelastic solid model for the consolidation of the laminate and considered variable permeability and thermal properties due to the change in fibre volume content during processing.

The conventional autoclave cure cycle recommended by the manufacturers is usually successful for processing thin laminates. For thick laminates (e.g. 100 plies or approx. 15 mm in thickness), studies have shown that the conventional cure cycle resulted in temperature overshoot at the centre of laminate due to the exothermic reactions of the resin. This can cause matrix degradation and thermal residual stress. Hojjati and Hoa [18] used a control-volume method combined with an alternating-direction explicit method to solve a one-dimensional heat conduction equation coupled with the flow equations. Kinsey et al. [19] solved the three dimensional heat conduction problem using an alternating-direction implicit (ADI) finite difference method. Kim and Lee [20] developed an autoclave cure cycle with cooling and reheating steps to reduce the temperature overshoot using a finite difference scheme. In order to validate the Loos and Springer [12] flow model, experimental measurements have been performed by Ciriscioli et al. [21] on Hercules 3501-6 and Fiberite 976 prepreg system; no indication is supplied as to the accuracy of these results.

In most of the previous studies, thermal material properties have been

taken to be constant. Yi and Hilton [22] have considered the thermal properties to be dependent on temperature and degree of cure. They investigated the effects of thermal conductivities, fibre volume fraction ratios, thicknesses of laminates and bagging materials on the viscosity, temperature and degree of cure. They used a non-linear transient heat transfer finite element scheme for the simulation.

The presence of voids, often caused by entrapped air which is not evacuated before resin gelation, reduces the strength bearing capabilities of the part, creates stress risers and can contribute to surface finishing and cosmetic problems. Ahn et al. [23] developed a technique to measure air permeation through the prepreg laminate during the consolidation and the curing process. Harper [24] et al. found that an optimum cure temperature gave maximum fibre volume fraction and composite density, and minimum void content. They proposed a linear relationship between cure pressure and fibre volume fraction to model the void content of the laminate.

Resin Infusion Process

Resin film infusion is an alternative method of fabricating composite materials to the prepreg technique. The lay-up of the infusion process is similar to the prepreg process where in this case the initially dry fibre plies, each separated by a layer of resin, are enclosed in a vacuum bag and placed in an autoclave for curing to take place. Simultaneously heat and pressure are applied to the set-up; this initiates an exothermic chemical reaction and forces the resin to infuse through the dry fibres. As the resin completely impregnates the dry fibres and consolidation takes place, it gels and solidifies into the desired finished product. In the SCRIMP process, the resin infiltrates through the dry fibres by the action of negative pressure.

Several investigators have studied and proposed models for the RFI/RTM processes used in composites manufacturing. Resin flow through the dry fibres

is conventionally modelled as unsaturated flow through porous media where Darcy's Law is employed. The determination of the exact location of the flow front is an important feature in the analysis of the simulation. When high pressure gradients are applied, it is necessary to treat the fibre layers as deformable and a recent study of this fluids-structure interaction problem has been treated by Ambrosi and Preziosi [25].

As in the prepreg process, proper selection of the cure cycle of the autoclave is important in order to produce a high quality part where full resin wet-out and complete, uniform curing are achieved at the end of the process. For steady flow through a wall-bounded porous medium, Givler and Altobelli [26] have used the Brinkman-Forchheimer equation to model the flow. They noted that when a porous flow domain contains an interface, the Brinkman term ($\mu_e \nabla^2 \mathbf{v}$), a diffusion term, is an important determinant in predicting the development of boundary layers which emanates from the interface. However, inaccurate determination of μ_e, the effective viscosity, has in the past tended to hamper the usage of this term. The Forchheimer term, $(C|\mathbf{v}|\mathbf{v})$, C constant, is a quadratic drag term to account for nonlinear behaviour of high velocity flow in porous media (see Nield and Bejan [27]). However, in composites manufacturing where the flows are small ≈ 1, the use of Darcy's Law is sufficient. A comprehensive study of single fluid flow in porous media with application to cylindrical beds of fibrous mats has been presented by Liu and Masliyah [28]. A comprehensive discussion of flow in porous media with application to composite processing has also been presented by Tucker and Dessenger in Advani [29].

Permeability is strongly dependent on the fibre volume fraction i.e. the porosity of the reinforcement. A common theoretical model used in describing the permeability of the reinforcement is the Carman-Kozeny model,

$$\mathbf{K} = \frac{D_f^2 \phi^3}{16 k_0 (1-\phi)^2} \tag{1.4}$$

where ϕ is the porosity, D_f is the fibre diameter and k_0 is the Kozeny constant,

which is usually determined experimentally. The reinforcement material can take different forms such as woven, stitched or unidirectional and flow along a fibre direction has higher permeability compared to the flow in the transverse direction. The use of orthotropic permeability models would be a further improvement. Parnas et al. [30] proposed a database containing a set of permeability results, developed by the National Institute of Standards and Technology. The database, based on carefully controlled measurements for both saturated and unsaturated flows in glass fabrics, could have been used to characterize the fibre reinforcement. Ni et al. [31] investigated a two-regional flow introducing an equivalent permeability parameter for the flow in the fibre free region.

Another important issue is the elimination of trapped air where minimizing the presence of voids can significantly improve the quality of the composite. Pearce et al. [32] conducted experiments to investigate flow behaviour inside moulds where flow fronts conyerged due to multiport injection in RTM processing. They found that when flow fronts meet at a mould edge , they merge and act as a single front and when the flow fronts meet head-on, voids can be formed. One method of reducing the amount of void content and improving fibre wet-out is by locating vents in the set-up to allow for the entrapped volatiles to escape and by using of vacuum impregnation techniques (see Abraham and McIlhagger [33]). The growth and collapse of gas bubbles in relation to process modelling of composites has been studied theoretically and experimentally by Wood and Bader [34, 35]. They proposed a model based on the diffusion theory where, assuming a spherically symmetrical bubble of radius R, the rate of bubble growth or collapse can be described by

$$\frac{dR}{dt} = -\frac{D(C_s - C_\infty)}{\rho R}\left[1 + \frac{R}{(\pi D t)^{1/2}}\right]. \tag{1.5}$$

In the above equation, C_s is the concentration of the mobile species, C_∞ the concentration in the bulk fluid, ρ the density of the gas within the bubble and D is the diffusion coefficient. In their model, the growth or collapse of the gas

bubbles depends upon whether the solution is oversaturated or undersaturated and they suggested that in composite processing, the long curing process may allow for the transient term, $R/(\pi Dt)^{1/2}$ to be neglected, which yields the asymptotic steady-state solution

$$R^2 = R_0^2 - \frac{2D}{\rho}(C_s - C_\infty)t \tag{1.6}$$

where R_0 is the bubble radius at $t = 0$.

Chui et al. [36] developed a two-phase model to study the formation and migration of macrovoids (< 1 mm diameter). Their model predicts a pressure dependence of the residual air saturation level where increasing the local pressure would mobilize the entrapped bubbles in the preform. In their two-phase model describing the transport of the voids, which is based on the Buckley-Leverett equations, they denoted S_r and S_a respectively to be the saturation of the resin phase and the air phase relative to the available pore space. These satisfy

$$S_r + S_a = 1 \tag{1.7}$$

since both phases occupy the available pore space.
They defined ϕ to be the interfibre preform porosity which is the volume fraction not occupied by the fibre and for the incompressible phases and constant ϕ, the mass conservation equations are

$$\phi\frac{\partial S_r}{\partial t} = \nabla \cdot q_r = 0 \tag{1.8}$$

$$\phi\frac{\partial S_a}{\partial t} = \nabla \cdot q_a = 0 \tag{1.9}$$

where q_r and q_a are the volumetric velocities of the two phases described by Darcy's law; they expressed these as

$$q_r = -\frac{k_{rel,r}}{\mu_r}K\nabla P \tag{1.10}$$

$$q_a = -\frac{k_{rel,a}}{\mu_a} K \nabla P \tag{1.11}$$

where they denoted μ_r and μ_a as the phase viscosities, $k_{rel,a}$ and $k_{rel,a}$ the relative phase permeabilities, P the pressure, and K is the absolute preform permeability.

Both finite element and finite difference approaches have been employed to solve the macroscopic and microscopic models. Coulter and Güceri [37] developed a numerical code, TGIMP, for computing a two-dimensional Darcy isothermal resin flow model based on a finite difference method using boundary-fitted coordinates with numerical grid generation. They determined the resin front by relocating the computational nodes using the resultant surface velocities and a pre-determined time increment. Coulter and Güceri [38] then performed experimentation and found reasonable agreement with results predicted by the TGIMP code.

Ahn et al. [39] proposed a model for the RFI vacuum process which predicts the final resin content of the laminate and the desired autoclave processing cycle required to eliminate voids. They defined a dimensionless parameter, the Infusion Flow Number, which describes the degree of impregnation of a preform based on the total pressure, resin viscosity, resin velocity, preform permeability and thickness of fibre preform. They controlled the resin content in the final composite by changing the initial amounts of resin in the bleeder and they detected no voids using this process. This compared well with the prepreg process which displayed voids due to air pockets trapped in between the prepregs layers during the lay-up. Bruschke and Advani [40] presented a non-isothermal viscous flow model, using a finite element control volume method, to predict the free surface of a shear-thinning resin injected through a fibre preform on the in-plane direction of a thin part.

Wymer and Engel [41] developed a numerical model to study the flow of a thermoset resin through, and parallel to a heated unidirectional fibre array, with temperature dependent viscosity. They considered a micro-model

of the nonisothermal incompressible flow of the resin employing the Crank-Nicholson finite difference scheme to the steady one-dimensional convective energy equation of the RTM process. Kang et al. [42] presented numerical and experimental studies of the simulation of resin transfer moulding (both non-isothermal mould filling and curing) using a finite element control volume technique.

Malkin et al. [43] proposed a model for the impregnation of liquid above a porous layer and applied the model to moulding of low viscous resin. Sadiq et al. [44] investigated experimentally the transverse flow through aligned cylinders and provided data for the progress of the flow front and the formation of voids through a heterogeneous fibre bed. Loos and MacRae [45] developed an analytical model to simulate the non-isothermal infiltration of resin in the resin film infusion process for manufacturing a blade-stiffened panel. Their model predicts the temperature, resin viscosity, and extent of cure during infiltration of an anisotropic fibre preform using a finite element/control volume technique.

Williams et al. [5] presented a comprehensive review of the Resin Infusion under Flexible Tooling process (RIFT) which is a variant of the vacuum-driven RTM in which one of the solid tool faces is replaced by a flexible polymeric film. This process potentially is a safer and more economical method of production where resin is drawn into the dry reinforcement in an evacuated vacuum bagged tool using only a partial vacuum to drive the resin. Mogavero and Advani [46] performed flow experiments through preforms composed of multiple layers of reinforcement material and investigated the effect of varying the order of the lay-up of a fixed number of plies and the impact of varying the thickness of individual layers of a thick preform. They found that the weighted average scheme provided a reasonable estimate for the effectiveness of the preforms. Yu and Young [47] proposed an RTM simulation model integrated with genetic algorithms to search for the process parameters (the mould heating rate, mould temperature, resin filling and curing temperatures) that could reduce cycle

time and enhance the uniformity of the final product.

Ambrosi and Preziosi [25] proposed a model of resin flow under isothermal conditions for an injection moulding process. Their model allows for deformation of the reinforcing network of the dry and the wetted part of the preform generated by the infiltration process. Pillai and Advani [48] performed simulations of unsaturated flow of resin in woven and stitched fibre mats used in RTM using an adaptation of the Finite Element/Control Volume (FEM/CV) technique. A dual scale porous media was modelled and the inlet pressures, inlet fill times, and mat saturation were studied. Lekakou and Bader [49] proposed a macro- and a micro-infiltration model based Darcy's law incorporating mechanical, capillary and vacuum pressures.

1.2.2 Thermo-chemical Model

Parts and structures constructed from fibre-reinforced thermosetting resin composites are manufactured by arranging the uncured fibre-resin mixture into the desired shape and then curing the material by exposure to elevated temperatures and pressures for a predetermined length of time. The temperature distribution, the degree of cure of the resin, and the resin viscosity inside the composite depend on the rate at which heat is transmitted from the environment into the material. The temperature inside the composite can be calculated using the conservation of energy together with the appropriate expression for the cure kinetics. In general, the heat transfer process is described by the energy equation which, neglecting convection, can be expressed as

$$\frac{\partial(\rho C T)}{\partial t} = \frac{\partial}{\partial x}\left(k_x \frac{\partial T}{\partial x}\right) + \frac{\partial}{\partial y}\left(k_y \frac{\partial T}{\partial y}\right) + \frac{\partial}{\partial z}\left(k_z \frac{\partial T}{\partial z}\right) + \rho \frac{dH}{dt} \qquad (1.12)$$

where ρ and C are the density and the specific heat of the composite, k_x, k_y and k_z are the thermal conductivities and T is the temperature.

The rate of heat generation by chemical reaction is defined as

$$\frac{dH}{dt} = H_R \frac{d\alpha}{dt} \tag{1.13}$$

where H_R is the total heat of reaction evolved during the process of cure and is dependent on the type of resin.
The cure rate is a function of degree of cure α and temperature T

$$\frac{d\alpha}{dt} = F(\alpha, T); \tag{1.14}$$

this can be characterized using a modified Arrhenius type equation, with the relevant constants of the model determined experimentally using differential scanning calorimetry [50, 51, 52].

Loos and Springer [12] considered a one-dimensional coupled equation. Bogetti and Gillespie [53] performed a two-dimensional cure simulation of thick composites using a heat conduction equation coupled to the cure kinetics of the thermoset. They employed a finite difference scheme on a boundary fitted coordinate system (BFCS) and found that spatial gradients of temperature and cure induced warpage and residual stress during the curing process. The BFCS technique is a mapping technique in which coordinates in a physical curvilinear coordinate system (x, y), are transformed into a computational rectangular coordinate system(ξ, η). Their motivation for using the technique is its advantage to easily accommodate complex shaped geometries. Once the governing equations and boundary equations are transformed into the computational domain, a straightforward finite difference solution technique is applied.

Telikicherla et al. [54] considered a two-dimensional time-dependent heat conduction equation with a heat generation term and employed an Alternating Direction Explicit (ADE) finite difference procedure. They considered the effects of the different thermal properties of the materials such as the bleeder/vacuum bag and the tool plate in the heat transfer process between the composite and the autoclave environment. Tredoux and Westhuizen [55]

proposed a numerical code based on finite element formulations to simulate the heat transfer, resin flow and compaction during composites processing. They also concluded that the finite element method was suitable for modelling the arbitrarily shaped parts and tooling geometry. Young [56] performed numerical simulations of the consolidation and cure process of thick laminates (400 plies with dimensions 15.24 cm × 15.24 cm) and studied the effects of compacting forces and cure cycles on the degree of consolidation. His findings showed that the compacting pressure is the major factor affecting the final degree of consolidation and the cure cycle only controls the thermal response and resin reaction in the laminate and had limited effect on the final degree of consolidation. They used different compacting pressures for the consolidation simulations of the laminate with the same cure cycle. They found that the final consolidation thickness of the laminate decreased with increasing compacting pressure, and the region without any consolidation was smaller using a higher compacting pressure.

Kim and White [57] proposed a staged curing technique for dealing with thermal spiking and non uniform consolidation. In the first step of this procedure, a relatively thin stack of material is built up (either by hand lay-up or using automated methods). This stack is then partially cured (stage 1 cure cycle) where the material is gelled, consolidated and some of the exothermic energy released. Subsequently, another incremental stack of material is placed on top of the first and the entire structure is again subjected to a partial cure cycle. This procedure is repeated until the desired thickness is reached. After the entire structure has been built up and subjected to the stage 1 curing, the final cure is performed in stage 2 cycle where the remaining exothermic energy is released and complete cure is reached. Their results showed no degradation of quality and they also demonstrated the feasibility of reducing the void content. They proposed that this technique addresses two of the major problems in manufacturing of thick composites: non-uniform consolidation and thermal spiking.

In Kim and Lee [20], an autoclave cure cycle is developed for thick composites which reduced temperature overshoots by determining the cure rate and temperature at the centre of a laminate using a finite difference scheme. Buckmaster and Vedarajan [58] predicted the possibility of temperature spikes of thermoset autoclave cure of large specimens using stability analysis. They presented a two-dimensional stability results, and showed that, for nth-order kinetics, the one-dimensional results will suffice. It is necessary to select a cure cycle that could reduce these thermal spikes as it could lead to matrix degradation and thermal residual stress.

1.3 Scope and framework of this thesis

The scope of this thesis is to study and compare the fabrication process of thermoset laminates by two processing techniques namely the autoclave curing using prepregs and the autoclave resin infusion process. The composite is treated as consisting of layers of reinforcements interspersed with layers of resins where in the case of the infusion process, the reinforcement layers are initially dry.

During the curing process of the composite where it is placed in the autoclave and exposed to heat and pressure, the resin undergoes chemical reactions and changes in viscosity. In the case of the prepreg, excess resin is allowed to escape while in the infusion process, the resin flows through and saturates the initially dry reinforcement layers. Further, polymerization of the resin then causes the resin to solidify into the desired product.

In both the fibre-free resin regions and the wetted fibre regions, constant flow parameters, such as viscosity and porosity, are assumed in order to decouple the flow equation and the heat equation. This is not unreasonable as the thermal conduction time scale is small when compared with the viscous time scale. In the fibre-free resin regions, Stokes's slow flow equations are

used. The resin flow in the saturated fibre regions are treated as flow through porous media and Darcy's law is employed.

In both the regions, a similarity solution is developed for the approximately isothermal flow of the resin. The known velocity components are then employed in the convection-diffusion heat equation, which itself is coupled to the cure kinetics of the thermoset, to calculate the temperature and cure profiles of the laminate using the Alternating Direction Implicit Method (ADI), an implicit finite difference scheme. The cure kinetic models of Hercules 3501-6 prepreg system formulated by Lee et al. [51] were used in the simulation, and the numerical computations in the prepreg case were compared with the experimental results obtained by Loos and Springer [12]. Voidage was not considered in this model as it would involve a two-phase model.

In Chapter 2, the autoclave curing of thermoset prepregs is described. The simulated results are compared with selected experimental results, and good agreement is obtained considering the limitations of the model.

In Chapter 3, the autoclave curing of thermoset resin by the infusion process is described. The model of resin flow, heat transfer and curing of the thermoset laminates is derived. The results and discussion of the simulation results are presented. Experimental work is also given and compared with the simulated result.

Chapter 4 presents an overview of the conclusion to the work and lists a number of problems which will have to be solved in the future and recommendations for the continuation of the work.

Chapter 2

Prepreg Processing

2.1 Introduction

In this study, the convective term is included in the heat equation which itself is coupled to the cure kinetics of the thermoset. By decoupling the velocity from the temperature and making other assumptions, the Navier-Stokes slow flow equations (Stokes's equations) can be solved analytically. A finite difference numerical scheme developed by McKee et al. [59] is then employed to simulate the temperature and cure distribution of the composite laminate, using the now known velocity components. The cure kinetic and viscosity models of Hercules 3501-6 prepreg system formulated by Lee et al. [51] were used in the simulation, and the numerical computations were compared with the experimental results obtained by Loos and Springer [12]. Voidage was not considered in this model.

2.2 Modelling the Heat Flow

The temperature and the degree of cure distribution in the multilayered composite, as shown schematically in *Figure* 2.1, is modelled by a system of coupled

heat and rate of cure equations. The multilayer composite system consists of n layers of prepreg, each layer interspersed with a layer of resin. Thus the k^{th} layer of prepreg is defined to lie between $y = h_{2k-1}(t)$ and $y = h_{2k}(t)$. Note the layers, move and change thickness with time as the resin is squeezed from the system under the action of external force, F_a, acting at the top $y = h_{2n+1}(t)$, where n is the number of prepreg layers.

The two dimensional convection-diffusion heat equation with internal heat generation by the cure reaction is given by

$$\frac{\partial T_f}{\partial t} + u^f \frac{\partial T_f}{\partial x} + v^f \frac{\partial T_f}{\partial y} = K_f \left(\frac{\partial^2 T_f}{\partial x^2} + \frac{\partial^2 T_f}{\partial y^2} \right) + \frac{\phi \rho_r H_R}{\rho_f c_f} \frac{\partial \alpha}{\partial t} , \quad (2.1)$$

$$\frac{\partial T_r}{\partial t} + u^r \frac{\partial T_r}{\partial x} + v^r \frac{\partial T_r}{\partial y} = K_r \left(\frac{\partial^2 T_r}{\partial x^2} + \frac{\partial^2 T_r}{\partial y^2} \right) + \frac{H_R}{c_r} \frac{\partial \alpha}{\partial t} \quad (2.2)$$

where $T_f(x, y, t)$ is the temperature in the wetted or saturated fibre layer, $T_r(x, y, t)$ is the temperature in the resin layer, $\alpha(x, y, t)$ is the degree of cure of the resin and $u^i = u^i(x, y, t)$ and $v^i = v^i(x, y, t)$, $i = r, f$ are the velocity components along the x and y directions respectively in the resin and saturated fibre layers. The porosity of the fibre layer or, equivalently, the voidage is ϕ and H_R is the heat of reaction of the resin. The thermal diffusivities in the resin and fibre layers are given by

$$K_i = \frac{k_i}{\rho_i c_i}, \ i = r, f \quad (2.3)$$

where k_i is the thermal conductivity, ρ_i the density and c_i is the specific heat capacity in the respective resin and saturated fibre layers. The thermal conductivity and heat capacity of the saturated fibre layer are defined by the rule of mixtures [27],

$$\begin{aligned} k_f &= \phi k_r + (1 - \phi) k_{df} , \\ c_f \rho_f &= \phi c_r \rho_r + (1 - \phi) c_{df} \rho_{df} \end{aligned}$$

where again r denotes the thermal properties of the resin and df denotes thermal properties of the dry fibre. A more accurate approach would be to

treat the material as being two-phase, but this would very much complicate the computational solution. The exothermic rate of the degree of cure equation for a thermoset resin is obtained from Lee et al.[51]:

$$\frac{\partial \alpha}{\partial t} = (c_1 + c_2\alpha)(1-\alpha)(0.47-\alpha) \quad \text{for} \quad \alpha \leq 0.3\ , \tag{2.4}$$

$$\frac{\partial \alpha}{\partial t} = c_3\ (1-\alpha) \quad \text{for} \quad \alpha > 0.3. \tag{2.5}$$

The temperature dependent functions, $c_i, i = 1, 2, 3$ are given by

$$c_i = A_i \exp\left(\frac{-\Delta E_i}{RT}\right)\ ,\ i = 1, 2, 3 \tag{2.6}$$

where A_i are specified pre-exponential factors, ΔE_i are the known activation energies, R is the universal gas constant and T represents the temperature in the resin or fibre layer, accordingly. As the degree of cure is temperature dependent, it is consequently spatially dependent.

The initial temperature is known and is taken to be uniform; also the multi-layer composite system is assumed to be insulated at the sides (i.e. $x = \pm L$), although in practice there may be a small amount of temperature flux dissipation. Thus

$$T_f(x, y, 0) = T_r(x, y, 0) = T_{ini} \tag{2.7}$$

and

$$T_r(x, 0, t) = T_r(x, h_{2n+1}(t), t) = T_a(t) \tag{2.8}$$

$$\frac{\partial T_f}{\partial x}(-L, y, t) = \frac{\partial T_f}{\partial x}(L, y, t) = 0,$$

$$\text{for } y \in [h_{2k-1}(t), h_{2k}(t)],\ k = 1, 2, ..., n-1 \tag{2.9}$$

$$\frac{\partial T_r}{\partial x}(-L, y, t) = \frac{\partial T_r}{\partial x}(L, y, t) = 0,$$

$$\text{for } y \in [h_{2k}(t), h_{2k+1}(t)],\ k = 0, 1, ..., n \tag{2.10}$$

where T_{ini} is a prescribed known temperature and $T_a(t)$ is a prescribed known function of temperature which can be expressed as

$$T_a(t) = \begin{cases} T_{ini} + \beta t & , t < t_c \\ T_c & , t \geq t_c \end{cases} \tag{2.11}$$

where β is the heat-up or ramp rate and t_c is the time to reach the cure temperature T_c.

The continuity conditions for temperature and flux imposed at the interfaces are given by

$$T_f(x, h_k(t), t) = T_r(x, h_k(t), t),\ k = 1, 2, \ldots, 2n\ , \tag{2.12}$$

$$k_f \frac{\partial T_f}{\partial y}(x, h_k(t), t) = k_r \frac{\partial T_r}{\partial y}(x, h_k(t), t),\ k = 1, 2, \ldots, 2n. \tag{2.13}$$

The initial degree of cure is

$$\alpha(x, y, 0) = 0 \tag{2.14}$$

and theoretically reaches a value of 1 when the composite is fully cured[12].

2.3 Fluid Flow

The composite is considered to consist of alternating layers of resin and resin-saturated fibre mats. The set-up for this model is schematically indicated in

Figure 2.1. In total there are $2n+1$ layers comprising of n fibre regions and $n+1$ resin regions. The fibre regions are assumed to be of constant thickness (i.e. incompressible and non-deformable) with isotropic permeability and the resin in the resin regions is assumed to be both isothermal and Newtonian with an approximately constant viscosity. These assumptions are, of course, not strictly valid, but they do allow us, as we shall see, to obtain approximate analytic solutions for the flow field, thus reducing the computational effort considerably.

2.3.1 Fluid Flow Equations

High values for viscosity lead to a Reynolds number considerably less than unity, and so the viscous terms tend to dominate the inertial terms in the full Navier-Stokes equations for an incompressible resin. Hence, in the resin layers, it will be assumed that the flows are quasi-steady so that the accelerative terms may be omitted; the conditions for Stokes's (slow) flow are thus satisfied and will henceforth be assumed together with the continuity equation. In the principal regions of interest (see *Figure* 2.3, for viscosity values < 10 Pa.s), it is not unreasonable to assume that μ is constant and this will be assumed here. The fibre plies are treated as incompressible movable porous layers saturated with resins and therefore an amended Darcy's Law and the continuity equation are utilised.

The quasi-steady flow equations in the resin layers are

$$\nabla \cdot \mathbf{u}^r = 0 \,, \tag{2.15}$$

$$-\nabla p^r + \mu \nabla^2 \mathbf{u}^r = \mathbf{0}, \tag{2.16}$$

$$\text{for} \quad (x, y) \in [-L, L] \times [h_{2k}(t), h_{2k+1}(t)], \;\; k = 0, 1, ..., n \tag{2.17}$$

while the flow equations in the saturated fibre layers are

$$\nabla \cdot \mathbf{u}^f = 0 \,, \tag{2.18}$$

$$\mathbf{u}^f = \mathbf{w} - \frac{\kappa}{\mu}\nabla p^f, \tag{2.19}$$

$$\text{for } \ (x,y) \in [-L,L] \times [h_{2k-1}(t), h_{2k}(t)], \ k = 1,2,...,n \tag{2.20}$$

where $\mathbf{w} = (0, \dot{h}_{2k}(t))^T$, κ is the isotropic permeability of the fibre mat, μ is the (assumed) constant viscosity of the resin and $\dot{h}_{2k}(t)$ is the velocity of the moving fibre mats for the respective fibre layers. The pressures in the resin and saturated fibre layers are denoted by p^r and p^f respectively. Note that incompressibility implies that $\dot{h}_{2k-1}(t) = \dot{h}_{2k}(t)$, for $k = 1, 2, \ldots, n$.
Boundary conditions for the flow are that there is no-slip and no-flow at the base and at the top plate within which the composite is held so that

$$u^r(x,0,t) \ = \ 0 \ \text{ and } \ v^r(x,0,t) \ = \ 0, \ x \in [-L,L] \,, \tag{2.21}$$

$$\begin{aligned} & u^r(x, h_{2n+1}(t), t) \ = \ 0 \\ & \text{and } \ v^r(x, h_{2n+1}(t), t) \ = \ \dot{h}_{2n+1}(t), \quad x \in [-L,L] \end{aligned} \tag{2.22}$$

and that there is continuity of velocity at the resin-prepreg interfaces

$$u^r(x, h_k(t), t) = u^f(x, h_k(t), t) \tag{2.23}$$

$$\text{and } \ v^r(x, h_k(t), t) = v^f(x, h_k(t), t), \quad k = 1,2,...,2n. \tag{2.24}$$

We shall also require continuity of the pressure at the resin-prepreg interface

$$p^r(x, h_k(t), t) \ = \ p^f(x, h_k(t), t), \ k = 1,2,\ldots,2n. \tag{2.25}$$

We shall further assume that the pressure is constant, say $p = p_0$ at $x = \pm L$ (for all y). Since the pressure only appears in (2.15)-(2.19) as a derivative, we shall use

$$p^r(\pm L, y, t) \;=\; p^f(\pm L, y, t) \;=\; 0. \tag{2.26}$$

The boundary conditions at the resin-prepreg interface are questionable. An alternative would be to use the Beaver-Joseph boundary condition

$$\frac{\partial u^r}{\partial y}(x, h_k(t), t) \;=\; \frac{\alpha_{BJ}}{\kappa^{1/2}}\Big(u^f(x, h_k(t), t) - u^r(x, h_k(t), t)\Big), \quad k = 1, 2, ..., 2n. \tag{2.27}$$

where α_{BJ} is dimensionless and is independent of the viscosity of the fluid but depends upon the material parameters that characterize the structure of the permeable material within the boundary region (see Beavers and Joseph[60]). The continuity of normal stress could also be used. This results in

$$p^f(x, h_k(t), t) \;=\; p^r(x, h_k(t), t) - \mu\frac{\partial v^r}{\partial y}(x, h_k(t), t), \quad k = 1, 2, ..., 2n. \tag{2.28}$$

However, since the object here is to obtain fluid equations which will admit a similarity solution, we restrict ourselves to the boundary conditions (2.23) and (2.24) which are a reasonable approximation for a loosely woven fibre.

2.3.2 A Similarity Solution

A similarity solution is sought in both the resin and the fibre (prepreg) regions (see Blest[61]). We shall begin by denoting the velocity and the pressure in the resin region $[-L, L] \times [h_{2k}, h_{2k+1}]$ by $\mathbf{u}^r_{2k+1}$ and p^r_{2k+1} and the velocity and pressure in the fibre region $[-L, L] \times [h_{2k-1}, h_{2k}]$ by $\mathbf{u}^f_{2k}$ and

$$\times \left(y - h_{2n}(t) + \frac{2\kappa}{h_{2n+1}(t) - h_{2n}(t)} \right) , \qquad (2.36)$$

$$\begin{aligned} v^r_{2n+1}(x,y,t) &= \dot{h}_{2n+1}(t) + A\Big[y^3 - 3h^2_{2n+1}(t)y + 2h^3_{2n+1}(t) \\ &\quad -\frac{3}{2}\Big(y - h_{2n+1}(t)\Big)^2 \\ &\quad \times \Big(h_{2n}(t) + h_{2n+1}(t) - \frac{2\kappa}{h_{2n+1}(t) - h_{2n}(t)}\Big)\Big] , \end{aligned} \qquad (2.37)$$

$$\begin{aligned} p^r_{2n+1}(x,y,t) &= 3\mu A\Big[y^2 - x^2 + L^2 - h^2_{2n}(t) - \Big(y - h_{2n}(t)\Big) \\ &\quad \times \Big(h_{2n}(t) + h_{2n+1}(t) - \frac{2\kappa}{h_{2n+1}(t) - h_{2n}(t)}\Big)\Big] \end{aligned} \qquad (2.38)$$

where $A(x,y,t)$ can be expressed as

$$A(x,y,t) = \frac{F_a}{4\mu L(3\kappa + L^2)}. \qquad (2.39)$$

For a typical intermediate k^{th} resin layer, the velocities and pressures can be computed to be

$$u^r_{2k+1}(x,y,t) = -3Ax\Big[\Big(y - h_{2k}(t)\Big)\Big(y - h_{2k+1}(t)\Big) - 2\kappa\Big], \qquad (2.40)$$

$$\begin{aligned} v^r_{2k+1}(x,y,t) &= \dot{h}_{2k}(t) - 3\kappa A\Big[2y - (h_{2k-1}(t) + h_{2k}(t))\Big] \\ &\quad +A\Big[y^3 - \frac{3}{2}\Big(h_{2k}(t) + h_{2k+1}(t)\Big)y^2 \\ &\quad +3h_{2k}(t)h_{2k+1}(t)y + \frac{1}{2}h^3_{2k}(t) - \frac{3}{2}h^2_{2k}(t)h_{2k+1}(t)\Big], \end{aligned} \qquad (2.41)$$

$$p^r_{2k+1}(x,y,t) = 3\mu A\Big[\Big(y - h_{2k}(t)\Big)\Big(y - h_{2k+1}(t)\Big) - x^2 + L^2\Big] \qquad (2.42)$$

for $k = 1, 2, \ldots, n-1$.

For a typical intermediate k^{th} fibre layer, the velocities and pressures take the

form

$$u^f_{2k}(x,y,t) = 6\kappa A x \ , \tag{2.43}$$

$$v^f_{2k}(x,y,t) = \dot{h}_{2k}(t) - 3\kappa A\Big[2y - \Big(h_{2k-1}(t) + h_{2k}(t)\Big)\Big] \ , \tag{2.44}$$

$$p^f_{2k}(x,y,t) = 3\mu A\Big[\Big(y - h_{2k-1}(t)\Big)\Big(y - h_{2k}(t)\Big) - x^2 + L^2\Big] \tag{2.45}$$

for $k = 1, 2, \ldots, n-1$.

As for the first and topmost resin layer the constant A is given by

$$A(x,y,t) = \frac{F_a}{4\mu L(3\kappa + L^2)}. \tag{2.46}$$

It is possible to write down a system of differential equations for the rate of change of the thickness of each of the resin layers, that is, the rate at which resin is squeezed from the layers as a result of the applied pressure :

$$\dot{h}_1(t) = -\frac{1}{2}Ah_1(t)\Big(h_1^2(t) + 6\kappa\Big), \tag{2.47}$$

$$\begin{aligned}\dot{h}_{2k+1}(t) - \dot{h}_{2k}(t) = -\frac{1}{2}A\Big[&\Big(h_{2k+1}(t) - h_{2k}(t)\Big)^3 \\ &+6\kappa\Big(2h_{2k+1}(t) - 2h_{2k}(t) + d_k + d_{k+1}\Big)\Big], \\ &k = 1, 2, \ldots, n-1\end{aligned} \tag{2.48}$$

$$\begin{aligned}\dot{h}_{2n+1}(t) - \dot{h}_{2n}(t) = -\frac{1}{2}A[&(h_{2n+1}(t) - h_{2n}(t))^3 \\ &+6\kappa\,(h_{2n+1}(t) - h_{2n}(t) + d_n)]\end{aligned} \tag{2.49}$$

where $d_k = h_{2k}(t) - h_{2k-1}(t)$ represents the thickness of the incompressible fibre layer, that is, d_ks are constants. Recall that this implies that $\dot{h}_{2k}(t) =$

$\dot{h}_{2k-1}(t)$. Note also that this allows the different formulation of (2.47)-(2.49) :

$$\dot{\delta}_0(t) = -\frac{1}{2}A\delta_0(t)\Big(\delta_0^2(t) + 6\kappa\Big) \tag{2.50}$$

$$\dot{\delta}_k(t) = -\frac{1}{2}A\Big[\delta_k^3(t) + 6\kappa\Big(2\delta_k(t) + d_k + d_{k+1}\Big)\Big],\ k = 1, 2, \ldots, n-1 \tag{2.51}$$

$$\dot{\delta}_n(t) = -\frac{1}{2}A\Big[\delta_n^3(t) + 6\kappa\Big(\delta_n(t) + d_n\Big)\Big] \tag{2.52}$$

where $\delta_k(t) = h_{2k+1}(t) - h_{2k}(t)$, the thickness of the k^{th} resin layer.

To solve this system we require the thickness of the prepreg layers and the initial thickness of the resin layers, that is

$$d_k, k = 1, 2, \ldots, n \text{ and } \delta_k(0), k = 0, 1, \ldots, n. \tag{2.53}$$

We can then solve (2.50)-(2.52) by any standard numerical method. This will provide the time taken for any two prepregs to come together, or alternatively the time taken to squeeze out all the excess resin. Note that this time will in general be different for different layers. Here, a 2^{nd}-order Runge-Kutta method was used to compute the solution of the system for the rate of change of resin layer thickness equations (2.50)-(2.52) and the decreasing average thickness of the resin layer against time is displayed in *Figure* 2.2 for the case $n = 32$ ply for the Hercules 3501-6 resin for different heating rates. It can be seen that the time computed for the laminates to be compacted is independent of the heating rate for the model with constant viscosity. However, it is possible to solve this system analytically. For constant known prepreg thickness the equations decouple. Thus the k^{th} equation may be written as

$$\dot{\delta} = a\Big(\delta(t)^3 + b\delta(t) + c\Big) \tag{2.54}$$

where the subscripts have been omitted.

Clearly (2.54) has the solution

$$at = I(\delta) + constant \tag{2.55}$$

where

$$I(\delta) = \int \frac{d\delta}{\delta^3 + b\delta + c}. \tag{2.56}$$

Following factorization of the denominator, the integral has a closed form solution

$$I(\delta) = \frac{1}{(P-Q)^2 + R^2}\left[ln\frac{y-P}{\sqrt{y^2 - 2Qy + Q^2 + R^2}} + \frac{(Q-P)}{R}arctan\left(\frac{y-Q}{R}\right)\right] \tag{2.57}$$

where

$$P = \frac{\theta}{6} - \frac{2b}{\theta} \tag{2.58}$$

$$Q = \frac{-\theta}{12} + \frac{b}{\theta} \tag{2.59}$$

$$R = \sqrt{3}(-\frac{\theta}{12} + \frac{b}{\theta}) \tag{2.60}$$

for θ defined by

$$\theta = (12\sqrt{12b^3 + 81c^2} - 108c)^{1/3}. \tag{2.61}$$

The constant in equation (2.55) is determined by the initial condition $\delta(0) = \delta_0$.

2.3.3 Variable Viscosity

In general, viscosity is a function of temperature and cure[51] and can be expressed as

$$\mu(x,y,t) \;=\; \mu_{\infty} exp(U/RT + \chi\alpha) \tag{2.62}$$

where μ_{∞} is a constant, U is the activation energy for viscosity, χ is a constant which is independent of temperature, and R is the universal gas constant. The graph of the computed viscosity against time is shown in *Figure* 2.3 which agrees with known data (see Lee et al.[51]). As the temperature increases, the resin becomes less and less viscous until polymerisation commences and consequently becomes viscous again. We also observe that, independent of the heat-up rate, the viscosity is very high initially and it then drops substantially to around 0.3 Pa.s. Thus, the mathematical model for the fluid flow may still be employed: where initially, no fluid flow takes place, but heat is nonetheless conducted to the centre of the laminate; when the resin begins to flow, viscosity remains approximately constant about a value of 1.0 Pas. Thus the values of the flow variables can be obtained from the analytic solutions of (2.33)-(2.34), (2.36)-(2.37), (2.40)-(2.41) and (2.43)-(2.44), and substituted, as before, into the convection-diffusion equation (2.1) and (2.2).

2.4 Numerical Solution Techniques

Equations (2.1),(2.2),(2.4) and (2.5) are nondimensionalized using the following scalings

$$\tilde{T}_i = \frac{T_i - T_{ini}}{T_c - T_{ini}}, \quad \tilde{x} = \frac{x}{d}, \quad \tilde{y} = \frac{y}{d}, \quad \tilde{u}^i = \frac{u^i}{V}, \quad \tilde{v}^i = \frac{v^i}{V}, \quad \tilde{t} = \frac{K_r\, t}{d^2}$$

for $i = r, f$ in the respective resin and saturated fibre layer. Recall that T_{ini} is the initial temperature of the composite, T_c is the cure temperature applied

to the top and bottom of the composite, d is the typical thickness of a fibre layer, and V is the known velocity of the upper tool plate, $\dot{h}_{2n+1}(t)$. Applying these transformations and omitting *tildes* for clarity gives

$$\frac{\partial T_f}{\partial t} + Pe\left(u^f \frac{\partial T_f}{\partial x} + v^f \frac{\partial T_f}{\partial y}\right) = D\left(\frac{\partial^2 T_f}{\partial x^2} + \frac{\partial^2 T_f}{\partial y^2}\right) + J_f \frac{\partial \alpha}{\partial t} \quad (2.63)$$

$$\frac{\partial T_r}{\partial t} + Pe\left(u^r \frac{\partial T_r}{\partial x} + v^r \frac{\partial T_r}{\partial y}\right) = \left(\frac{\partial^2 T_r}{\partial x^2} + \frac{\partial^2 T_r}{\partial y^2}\right) + J_r \frac{\partial \alpha}{\partial t} \quad (2.64)$$

and

$$\frac{\partial \alpha}{\partial t} = (C_1 + C_2\alpha)(1-\alpha)(0.47-\alpha) \text{ for } \alpha \leq 0.3 \quad (2.65)$$

$$\frac{\partial \alpha}{\partial t} = C_3\,(1-\alpha) \text{ for } \alpha > 0.3 \quad (2.66)$$

where D, J_f and J_r are the dimensionless constants given by

$$D = \frac{K_f}{K_r}, \quad J_f = \frac{\phi \rho_r H_R}{c_f \rho_f (T_c - T_{ini})}, \quad J_r = \frac{H_R}{c_r (T_c - T_{ini})},$$

Pe is the Peclet number

$$Pe = \frac{Vd}{K_r} \quad (2.67)$$

and the constants C_i is given by

$$C_i = \frac{d^2 c_i}{K_r}\ ,\ i = 1, 2, 3. \quad (2.68)$$

The initial and boundary conditions become

$$T_r(x, y, 0) = T_r(x, y, 0) = 0 \quad (2.69)$$

and

$$0 \leq T_f(x, 0, t) = T_r(x, h_{2n+1}(t)/d, t) \leq 1\ , \quad (2.70)$$

$$\frac{\partial T_f}{\partial x}(-L/d, y, t) \;=\; \frac{\partial T_f}{\partial x}(L/d, y, t) \;=\; 0\;,$$
$$\text{for } y \in [\; h_{2k-1}(t)/d,\; h_{2k}(t)/d\;],\; k = 1, 2, \ldots, n \tag{2.71}$$

$$\frac{\partial T_r}{\partial x}(-L/d, y, t) \;=\; \frac{\partial T_r}{\partial x}(L/d, y, t) \;=\; 0\;,$$
$$\text{for } y \in [\; h_{2k}(t)/d,\; h_{2k+1}(t)/d\;],\; k = 1, 2, \ldots, n. \tag{2.72}$$

The continuity of temperature and flux at the resin-fibre interface layers become

$$T_f(x, h_k(t)/d, t) \;=\; T_r(x, h_k(t)/d, t)\;,\; k = 1, 2, \ldots, 2n \tag{2.73}$$

$$D^* \frac{\partial T_f}{\partial y}(x, h_k(t)/d, t) \;=\; \frac{\partial T_r}{\partial y}(x, h_k(t)/d, t) = 0\;,\; k = 1, 2, \ldots, 2n \tag{2.74}$$

where $D^* = k_f/k_r$.

The initial degree of cure remains

$$\alpha(x, y, 0) \;=\; 0. \tag{2.75}$$

2.4.1 Discretization

The nondimensionalised coupled heat and rate of cure equations, i.e. equations (2.63)-(2.66) for each layer, are discretized by applying the finite-difference Alternating-Direction-Implicit Method (ADI)[59]. Before providing a description of the implementation of the method it is necessary to discuss the construction of the moving mesh.

Moving mesh

Since the fibre regions are assumed incompressible they do not change shape; however, resin is continuously being squeezed from the resin layers and so they are monotonically decreasing in thickness. Fortunately, we have, from the solution of (2.50)-(2.52), a good approximation for each layer of the rate at which this occurs. Thus, we shall use a fixed grid in the saturated fibre layers in the vertical direction (y-direction) and a fixed grid in the horizontal direction (x-direction) in all layers. However, we shall employ a moving grid in the vertical direction in the resin layers. The essential strategy will be to employ $\nu(= 2^{\nu_1}, \nu_1 \in \mathbb{N}^+)$ points in each resin layer (independent of their individual thickness) in the y-direction so that the mesh spacing is

$$\Delta y^{(m)} \;=\; (h_{2k+1}(t_m) - h_{2k}(t_m))/\nu \;=\; \delta_{2k+1}(t_m)/\nu. \tag{2.76}$$

The number of points ν will then be held fixed until $t = t^*$ such that

$$\delta_{2k+1}(t^*) < \frac{1}{2}\delta_{2k+1}(0) \tag{2.77}$$

whereupon ν is replaced by $\nu/2$ equally spaced points and appropriate interpolation is performed where necessary. This is continued ν_1 times(in practice $\nu_1 = 3$) and thereafter the number of points are decreased no longer. The resin is deemed to have been removed from that layer when $\delta_{2k+1}(t)$ is less than some prescribed tolerance. The $\delta_{2k+1}(t)$ are determined from solving equations (2.50)-(2.52) by a second order Runge-Kutta method.

In the x-direction we define the fixed grid

$$\Delta x \;=\; 2L/\lambda\;,\; (\lambda \in \mathbb{N}^+) \tag{2.78}$$

both for the resin and saturated fibre layers. In the saturated fibre layers, we also define the fixed grid in the y-direction

$$\Delta y \;=\; d_k/\gamma\;,\; (\gamma \in \mathbb{N}^+)\;,\; d_k \;=\; h_{2k}(t) - h_{2k-1}(t). \tag{2.79}$$

When $d_k = d$ the saturated fibre layers have the same thickness.

2.4.2 ADI Method

The scheme used for a typical fluid layer is given by

$$\left[1 - \frac{ra}{2}\delta_x^2 + \frac{pu^r Pe}{2}\nabla_x\right](T_r)_{i,j}^{m+1^*}$$
$$= \left[1 + sa\delta_y^2 - qv^r Pe\nabla_y + \frac{ra}{2}\delta_x^2 - \frac{pPeu^r}{2}\nabla_x\right](T_r)_{i,j}^m + \Delta t J_r g\left(\alpha_{i,j}^m, (T_r)_{i,j}^m\right) \tag{2.80}$$

$$\left[1 - \frac{sa}{2}\delta_y^2 + \frac{qPev^r}{2}\nabla_y\right](T_r)_{i,j}^{m+1}$$
$$= (T_r)_{i,j}^{m+1^*} - \left[\frac{sa}{2}\delta_y^2 - \frac{qPev^r}{2}\nabla_y\right](T_r)_{i,j}^m \tag{2.81}$$

and the scheme for a typical fibre layer is given by

$$\left[1 - \frac{ra}{2}\delta_x^2 + \frac{pu^f Pe}{2}\nabla_x\right](T_f)_{i,j}^{m+1^*}$$
$$= \left[1 + sa\delta_y^2 - qv^f Pe\nabla_y + \frac{ra}{2}\delta_x^2 - \frac{pPeu^f}{2}\nabla_x\right](T_f)_{i,j}^m + \Delta t J_f g\left(\alpha_{i,j}^m, (T_f)_{i,j}^m\right) \tag{2.82}$$

$$\left[1 - \frac{sa}{2}\delta_y^2 + \frac{qPev^f}{2}\nabla_y\right](T_f)_{i,j}^{m+1}$$
$$= (T_f)_{i,j}^{m+1^*} - \left[\frac{sa}{2}\delta_y^2 - \frac{qPev^f}{2}\nabla_y\right](T_f)_{i,j}^m \tag{2.83}$$

where

$$\nabla_x T_{i,j}^m = T_{i,j}^m - T_{i-1,j}^m$$
$$\nabla_y T_{i,j}^m = T_{i,j}^m - T_{i,j-1}^m$$

$$\begin{aligned}\delta_x^2 T_{i,j}^m &= T_{i-1,j}^m - 2T_{i,j}^m - T_{i+1,j}^m \\ \delta_y^2 T_{i,j}^m &= T_{i,j-1}^m - 2T_{i,j}^m - T_{i,j+1}^m\end{aligned}$$

with T_{ij}^m denoting an approximation to $T(i\Delta x, j\Delta y, m\Delta t)$ where Δt is the time-step and $\Delta x \neq \Delta y$ are the spatial sizes in the x- and y- directions respectively (see Appendix C). The subscripts r and f denote values in a typical resin fluid layer and a saturated fibre layer respectively. Other parameters are defined as follows:

$$a = \begin{cases} D & \text{for fibre layer} \\ 1 & \text{for resin fluid layer,} \end{cases}$$

$$p = \Delta t/\Delta x \ , \ r = \Delta t/\Delta x^2 \ , \ q = \Delta t/\Delta y \ , \ s = \Delta t/\Delta y^2 \ ,$$

and

$$\begin{aligned}g(\alpha_{i,j}^m, (T_r)_{i,j}^m) &= \left(\frac{\partial \alpha}{\partial t}\right)_{i,j}^m \\ g(\alpha_{i,j}^m, (T_f)_{i,j}^m) &= \left(\frac{\partial \alpha}{\partial t}\right)_{i,j}^m\end{aligned}$$

are the exothermic reaction functions.
Note $(T_r)_{i,j}^{m+1^*}$ and $(T_f)_{i,j}^{m+1^*}$ denote an intermediate (non-physical) stage in the calculation.

The mesh spacing in the y-direction in the resin layers is, of course, not a constant: it is monotonically decreasing according to (2.76). However, Δt is chosen so that the decrease in Δy from $t = t_m$ to $t = t_{m+1}$ is small. This allows us to calculate $(T_r)_{i,j}^{m+1^*}$ from $(T_r)_{i,j}^{m^*}$ on a fixed grid, ie. $\Delta x, \Delta y^{(m)}$ and Δt. The new grid is then constructed and the values of T_r on the new grid are taken to be identically those of the old grid. Only if $\delta(t_m) \leq \frac{1}{2^\nu}\delta(0)$ are half the points omitted and the necessary interpolation then undertaken.

2.5 Numerical Results and Discussion

The system of ordinary differential equations (2.50)-(2.52) (the rate of thickness equations) are first solved by a 2^{nd}-order Runge-Kutta Method. This allows the velocity of the fluid, both in the resin and the prepreg, to be determined through equations (2.33)-(2.34), (2.36)-(2.37), (2.40)-(2.41) and (2.43)-(2.44). The velocities are then substituted into the convection-diffusion-reaction equations (2.63)-(2.64) and the ADI method described previously is solved in tandem with the 2^{nd}-order Runge-Kutta Method for the rate of cure equation. The simulation to obtain the temperature distribution and the degree of cure distribution during the process is performed for different thickness of composite, namely 16, 32, 52 and 64 plies. The cure cycle with heat-up rates of 2.8 deg K/min and 11.1 deg K/min with a constant force of 586 kN were used in the simulation.

The material constants for the fibre and Hercules 3501-6 resin employed which can be found in Loos and Springer [12] are listed in *Table* 2.1. The porosity and half-length of the composite, obtained from Blest[61], are given in *Table* 2.2. The value of constants used in the curing equations are obtained from Lee et al.[51] are given in *Table* 2.3.

Figure 2.3 shows the graph of the computed viscosity against time at different heating rates at the centre of the laminate. It can be seen that, as expected, at the lower heat-up rate, the time at which the minimum viscosity occurs is larger than that for the higher heat-up rate. This is important since it is desirable that all excess resin and trapped air is squeezed out before gelation takes place. The gel point of the resin is assumed to occur at 100 Pa.s [12] and the model predicted the time to gelation with satisfactory precision.

Figures 2.4, 2.5 and 2.6 provide a comparison between the temperature computed from the model at different positions through the composite thickness and those measured (by thermocouples) in Loos and Springer[12] for a 64 ply composite. It can be seen that the model agrees well with the data at the

Resin density, ρ_r	1.26×10^3	kg/m^3
Specific heat of resin, c_r	1.26×10^3	J/(kg.K)
Thermal conductivity of resin, k_r	1.67×10^{-1}	W/(m.K)
Heat of reaction of resin, H_R	474	J/g
Fiber density, ρ_{df}	1.79×10^3	kg/m^3
Specific heat of fibre, c_{df}	7.12×10^2	J/(kg.K)
Thermal conductivity of fibre, k_{df}	2.60×10^1	W/(m.K)
Gas constant,R	8.31435	J/Kmol
Applied Force, F_a	586	kN
Permeability of porous mat, κ	10^{-16}	m^{-2}
Thickness of a prepreg, d	0.0001	m
Initial ambient temperature, T_{ini}	300	K
Applied cure temperature, T_c	450	K

Table 2.1: Material properties of Hercules 3501-6 resin and fibre.

Resin viscosity, μ	1	Pa.s
Porosity, ϕ	0.5	
Half-Length of composite, L	0.5	m

Table 2.2: Flow parameters from Blest [61].

three locations inside the composite.

Figures 2.7 and 2.8 display the temperature profiles at the centre of the composite for heating rates of 2.8 and 11.1 deg K/min respectively for a number of different plies. It can be seen that no matter how many number of plies, no significant thermal spiking occurs for the applied temperature of 450 K for either of the two different heat-up rates although the small temperature spike, as would be expected, increases with increasing number of plies.

the prepreg thickness is increased the lag becomes more pronounced, indicating that heat diffusion is no longer "instantaneous"; the thermal spiking is due to the exothermal reaction of the curing process and the more material there is the greater the amount of heat released. The thermal spiking may be overcome to some degree by introducing recooling and reheating steps into the thermal cure cycle (see Kim and Lee [20]).

Figures 2.12 and 2.13 display the curing profile at the vertical midplane of the laminate for 16 and 64 plies laminate, respectively. It can be seen that the model predicts the cure for both thickness is fairly uniform throughout the composite at the low heat-up rate of 2.8 K/min.

2.6 Concluding Remarks

A mathematical model has been developed for the prepreg curing process of a composite laminate with n layers of prepregs. It was shown, subject to certain assumptions, that the velocity components for the flowing resin (both in the resin layers and the prepregs) could be reduced to a problem of solving a system of first-order ordinary differential equations which, in the case where the layers of prepreg are of equal thickness, admit a closed analytic solution. The convection-diffusion equation with a heat generation term was solved by an alternating-direction implicit method (for the temperatures in the prepregs and the excess resin layers) coupled with a 2^{nd}-order Runge-Kutta method for the cure. Numerical results have been compared with experimental data and found to give good agreement, particularly with regard to the temperature of the composite.

This flow model is clearly useful in providing simple solutions to the flow problem but it has its limitations. The resin itself is in general a non-Newtonian

fluid, its rheology determining the precise form of the constitutive relationship to be employed. Another simplification used in the model was to assume that the permeability is isotropic; in general this will not be the case. The minimisation of voidage or its complete elimination is important to the composite manufacturer; this has not been addressed in this thesis. Finally, the permeability is likely to change as curing take place. Indeed, variable permeability models (in the context of filtration through coffee granules) have already been discussed (see Baldini and Petracco[62]). The case when the fibre weave is deformable has recently been treated by Ambrosi and Preziosi[25].

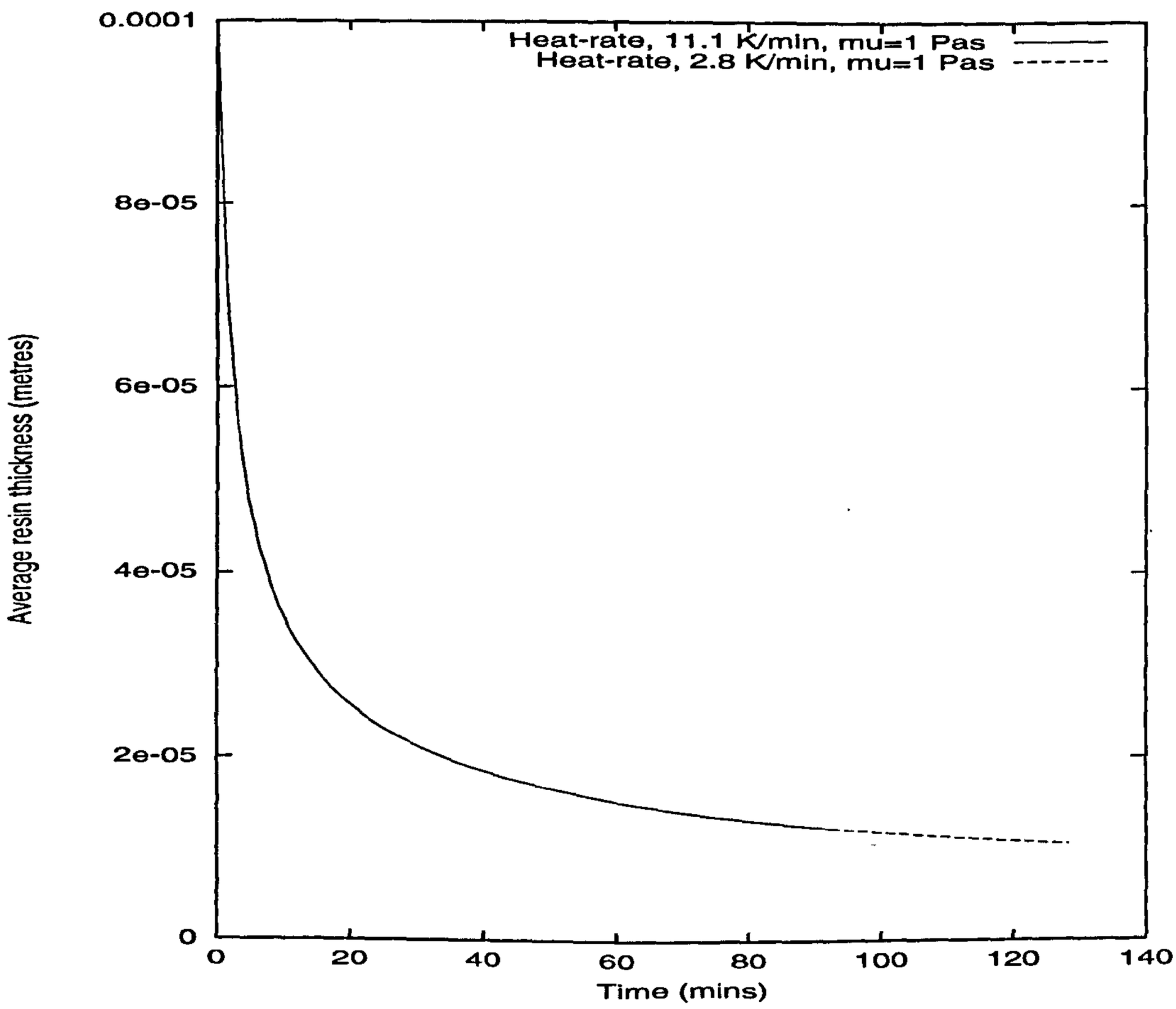

Figure 2.2: Comparison of average resin thickness vs time of 32 ply for different heating rates.

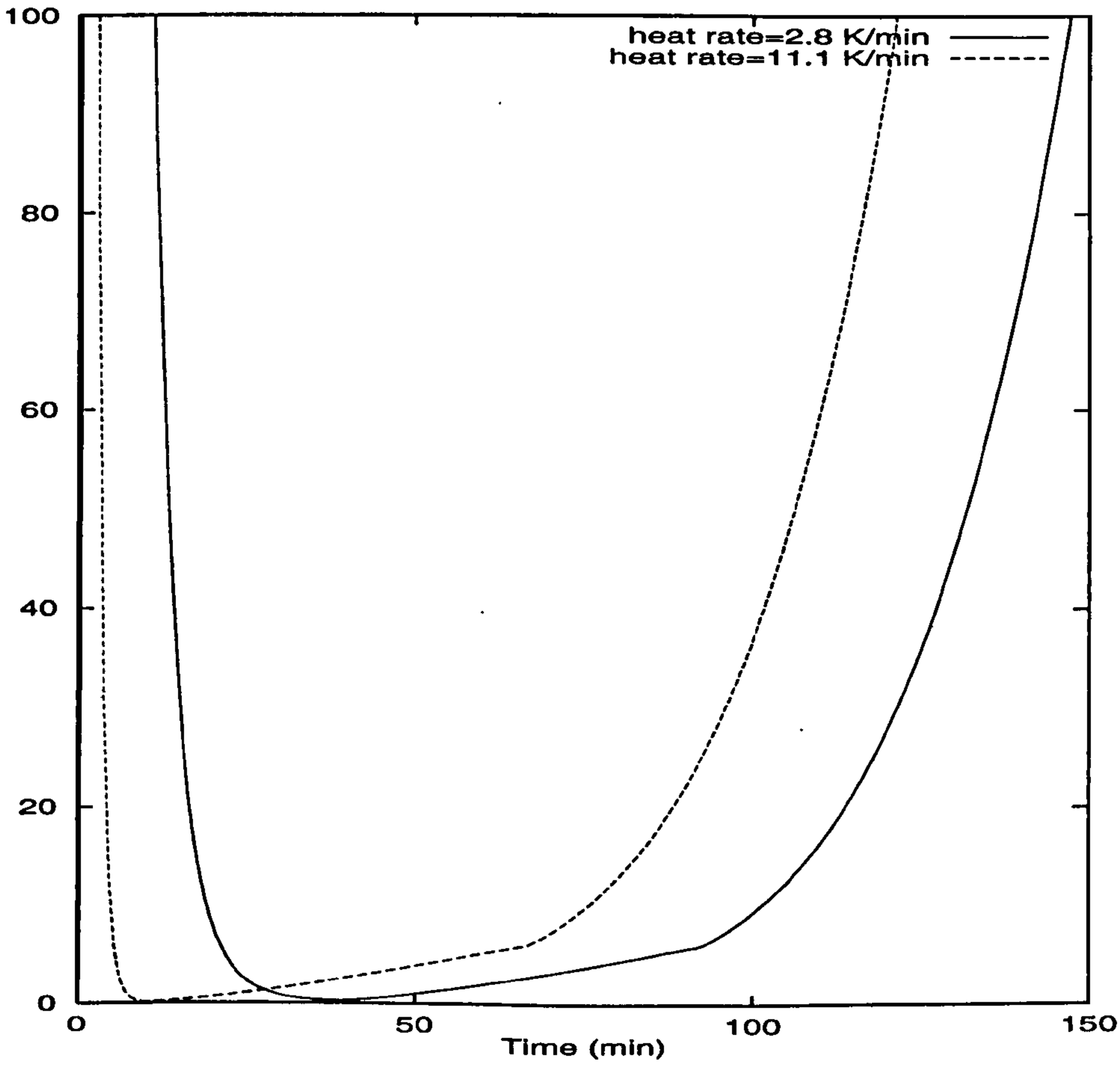

Figure 2.3: Comparison of the computed (variable) viscosity (see equation (2.62)) versus time for different heating rates for 64 ply laminate at the centre of the composite.

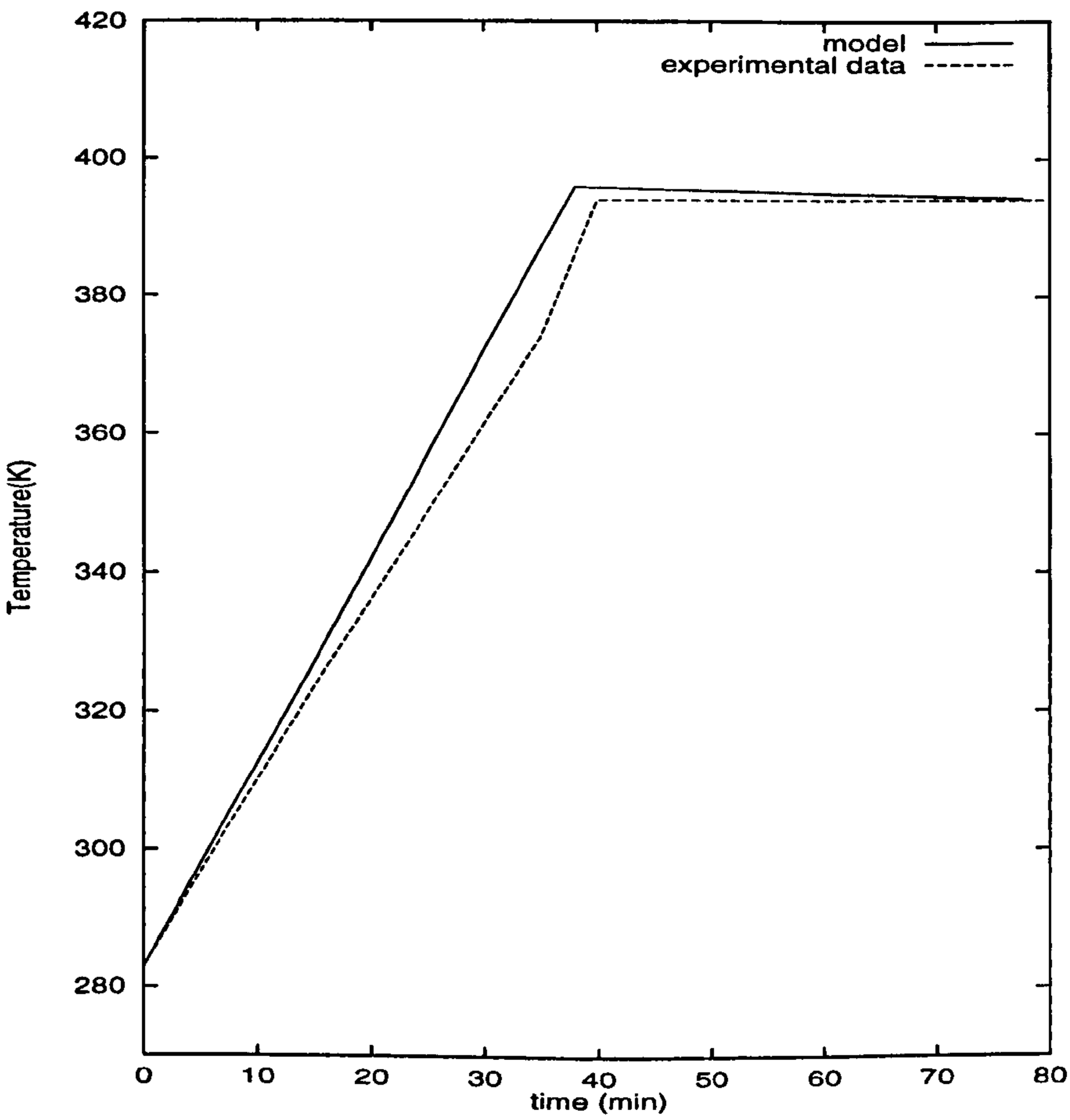

Figure 2.4: Comparison of temperature at $y/h_{2n+1}(t)$=0.25 with experimental data of Loos and Springer[12] for 64 plies.

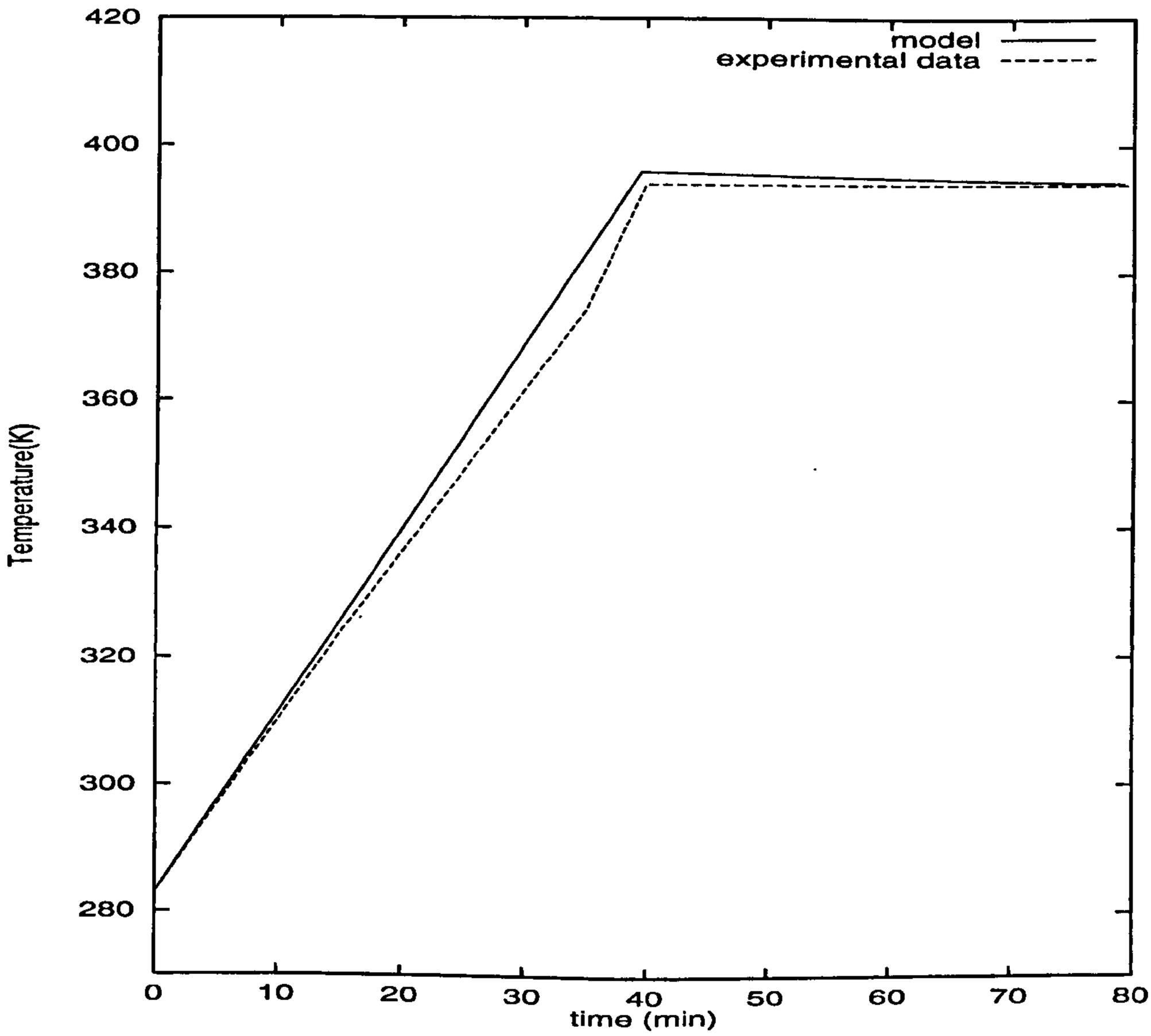

Figure 2.5: Comparison of temperature at the centre of the composite with experimental data of Loos and Springer[12] for 64 plies.

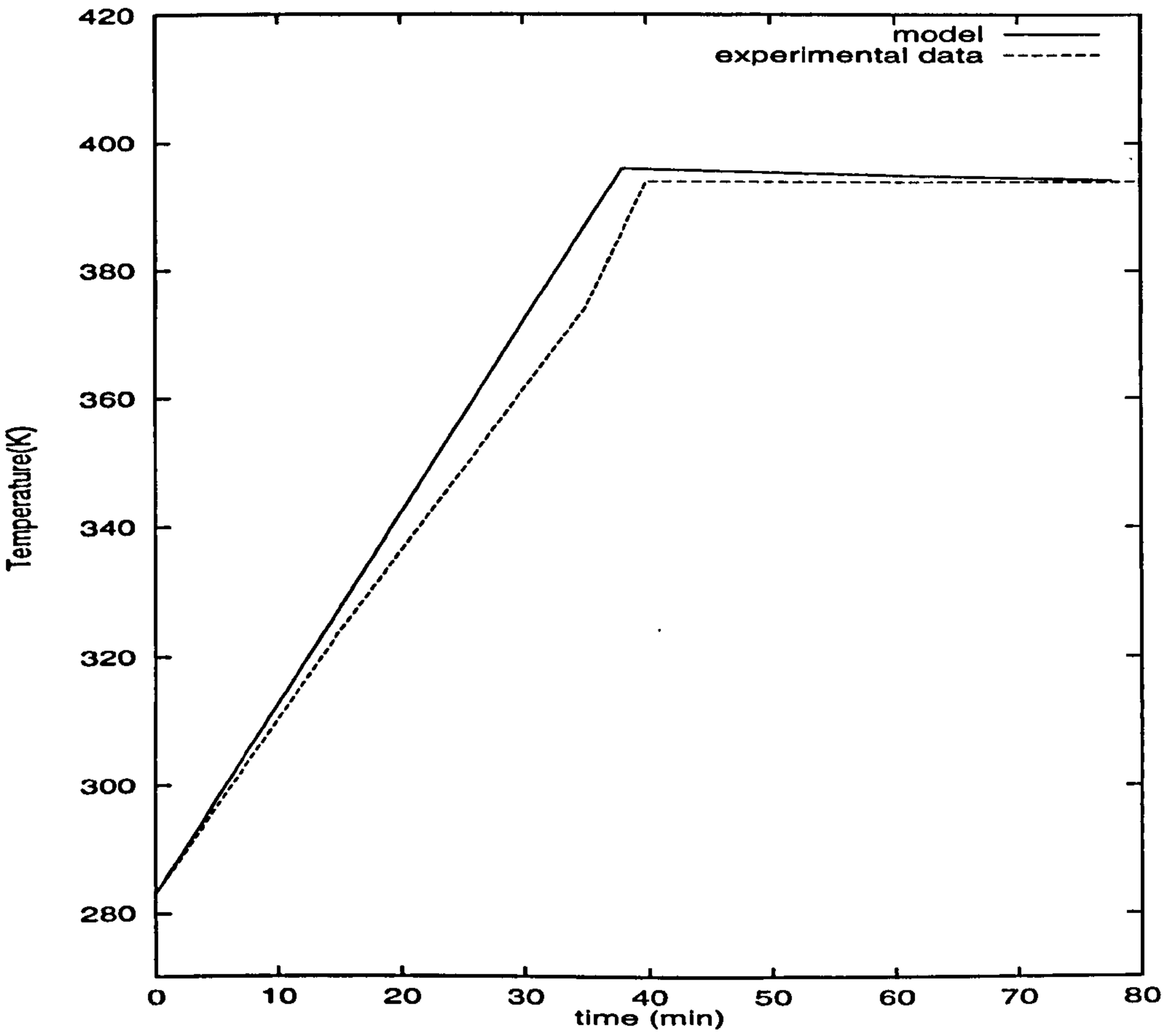

Figure 2.6: Comparison of temperature at $y/h_{2n+1}(t) = 0.75$ with experimental data of Loos and Springer[12] for 64 plies.

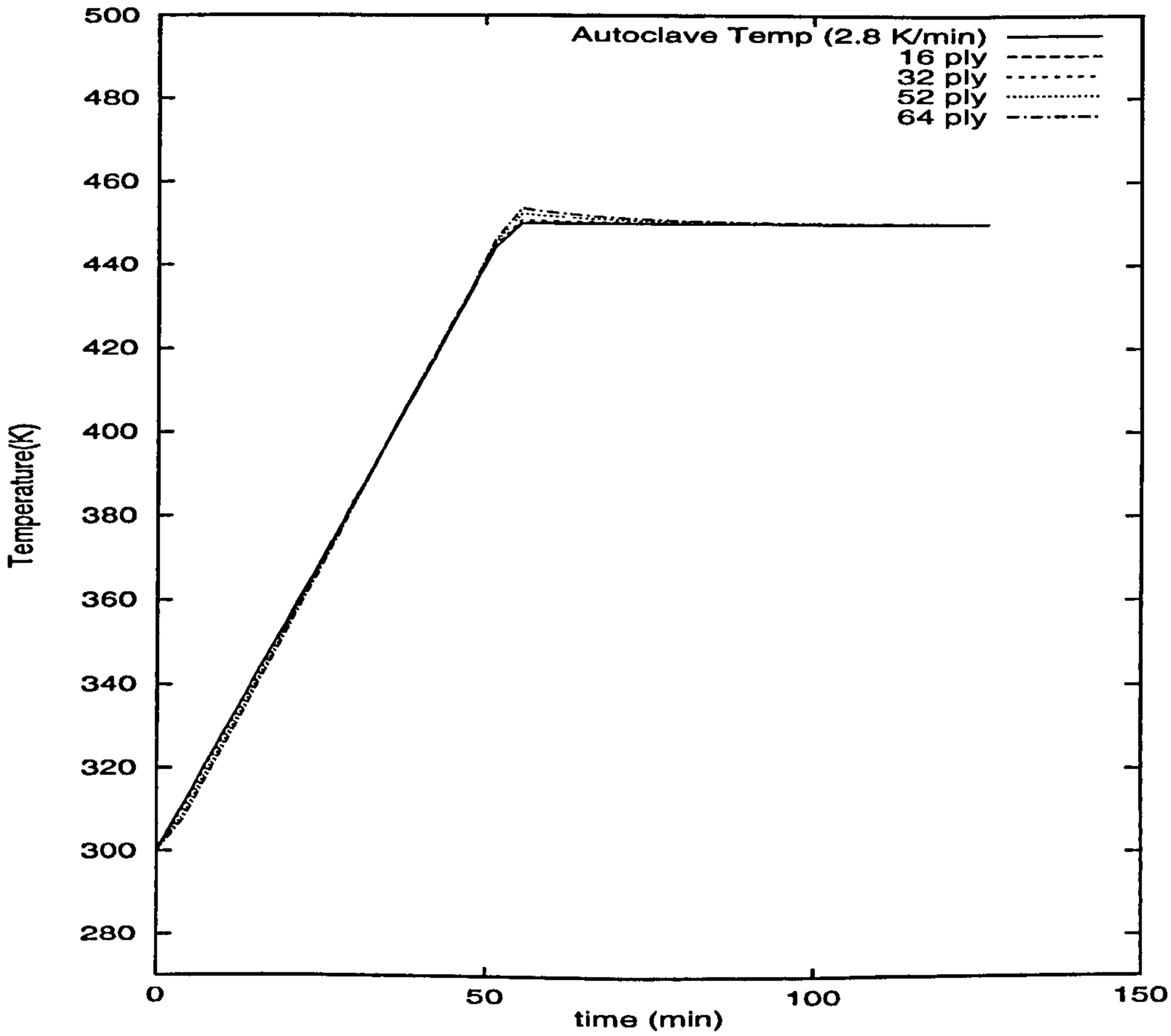

Figure 2.7: Comparison of the temperature versus time at the centre of composite for Hercules 3501-6 resin for the heating rate 2.8 K/min.

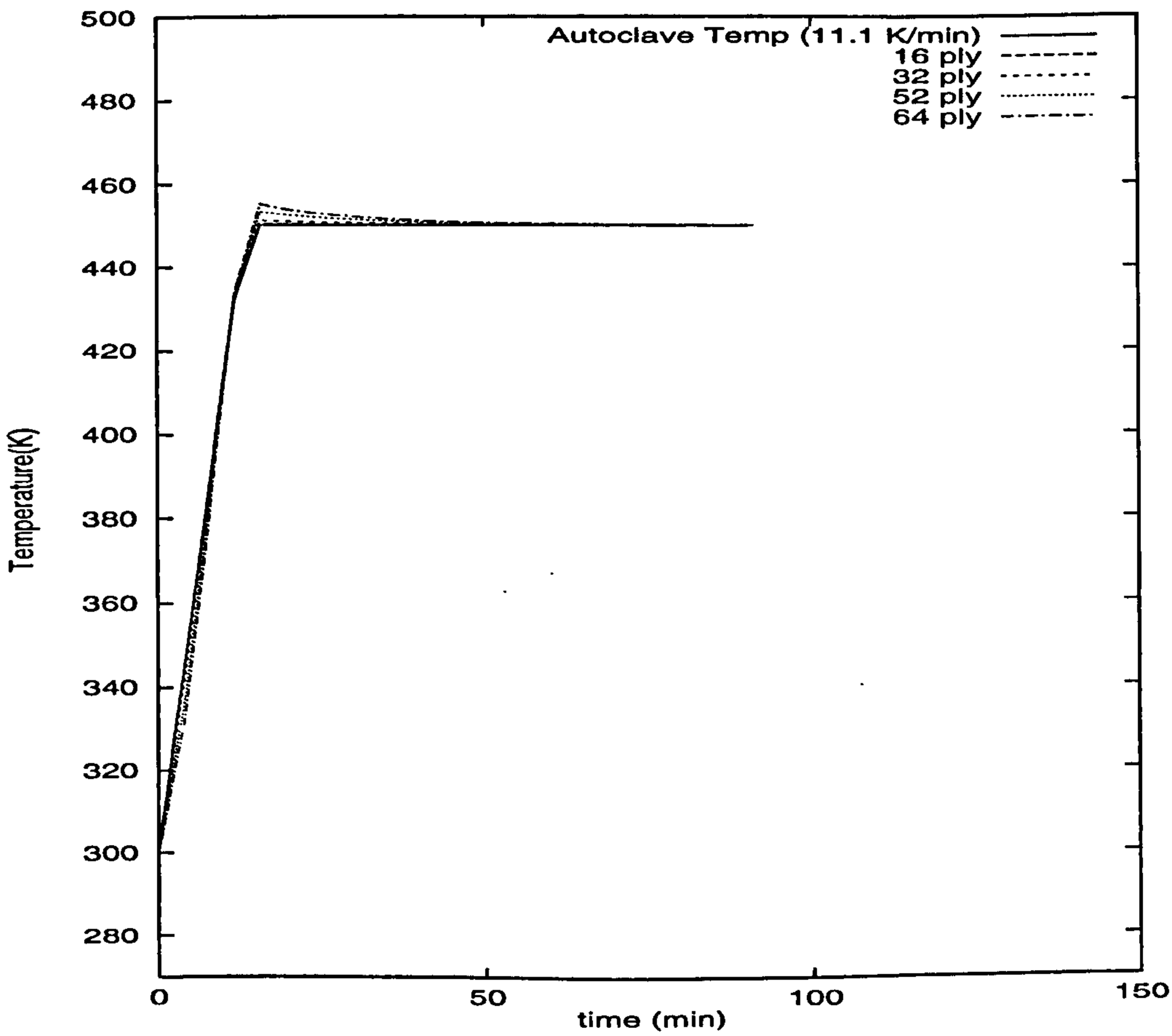

Figure 2.8: Comparison of temperature versus time at the centre of composite for Hercules 3501-6 resin for the heating rate 11.1 K/min.

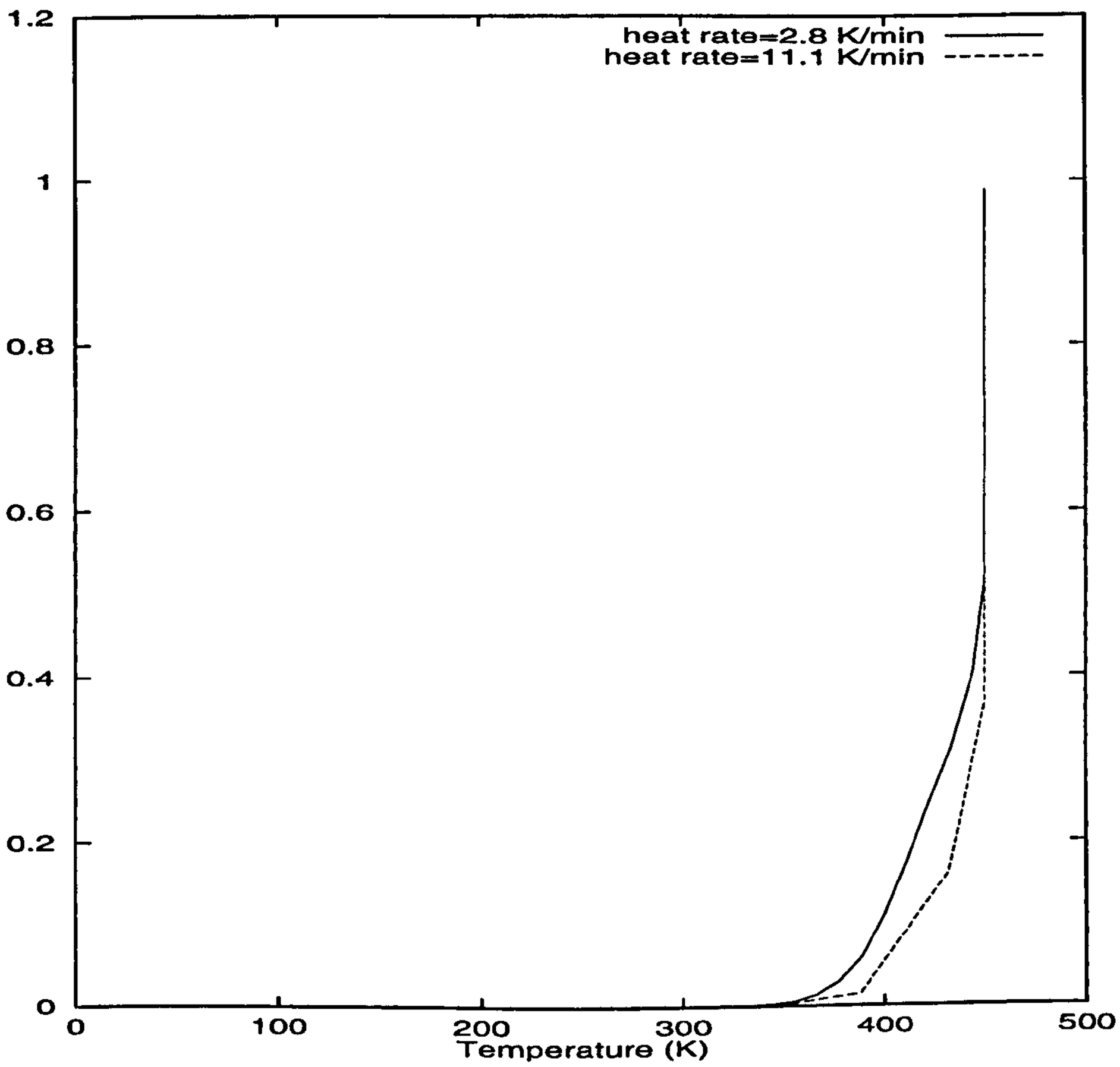

Figure 2.9: Comparison of the degree of cure versus temperature at centre of composite for Hercules 3501-6 resin for different heating rates.

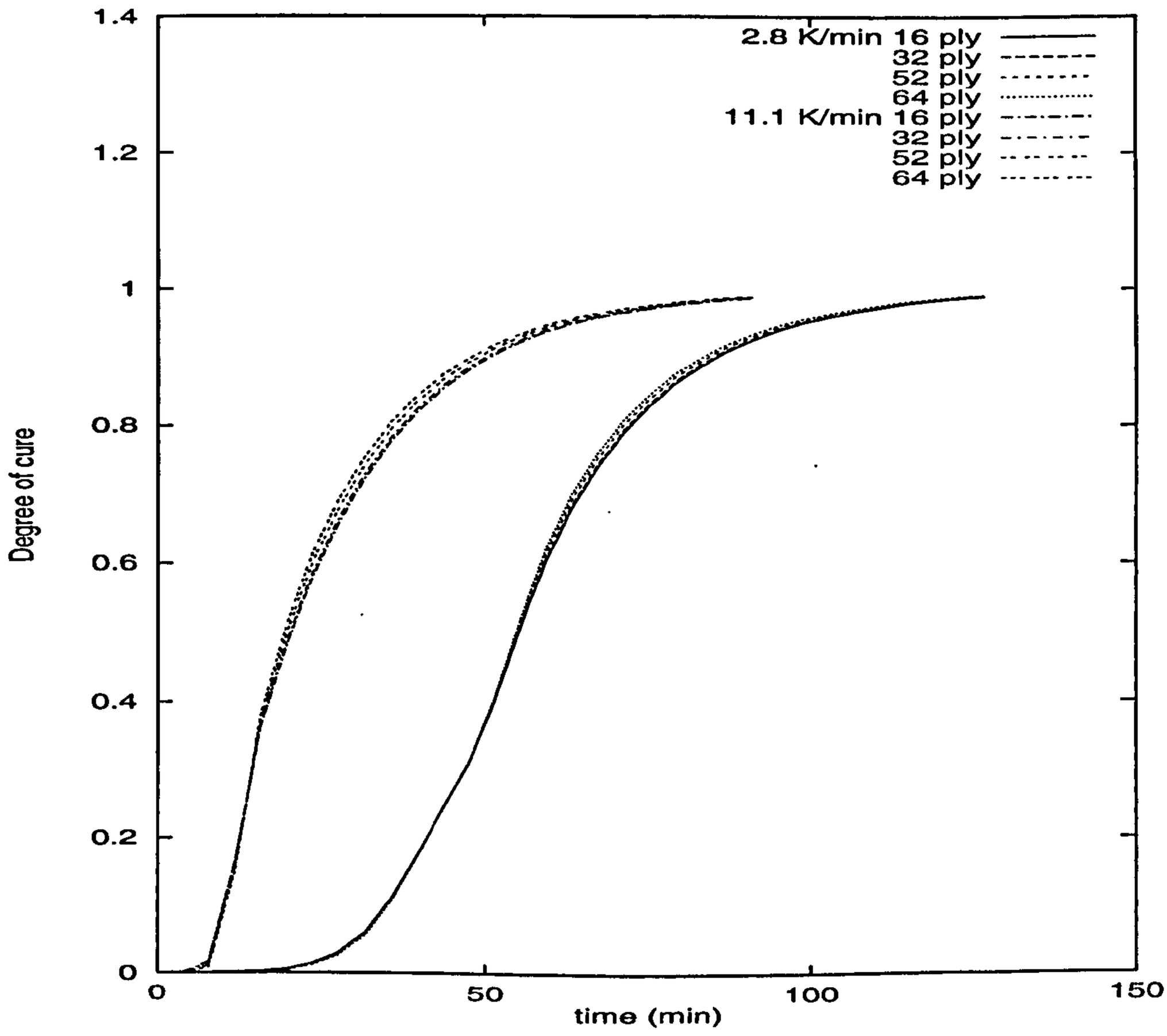

Figure 2.10: Comparison of the degree of cure versus time at the centre of composite for different heating rates for varying thickness.

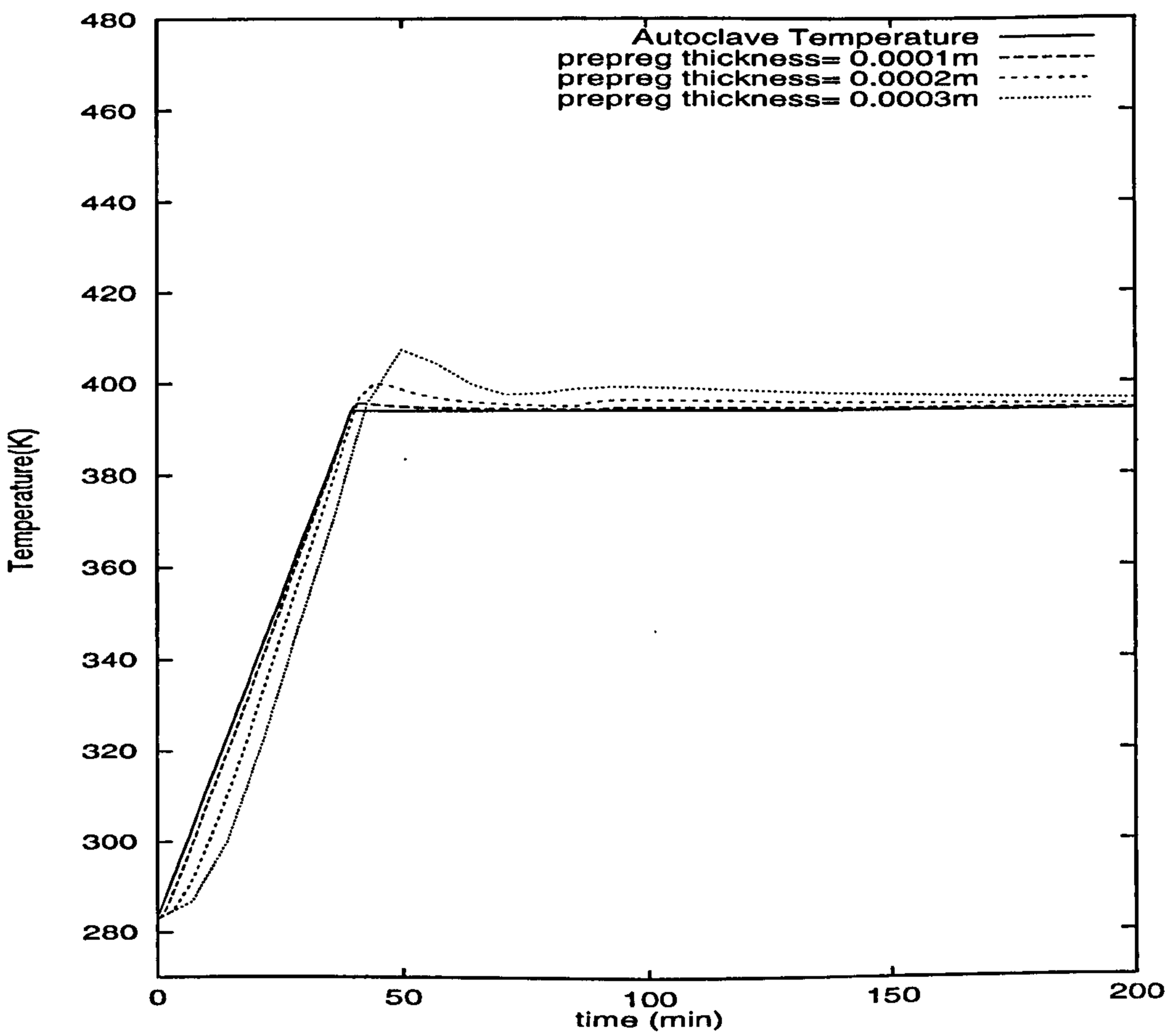

Figure 2.11: Comparison of the temperature versus time at the centre of a 64 ply laminate for varying prepreg thickness for the heating rate 2.8 K/min.

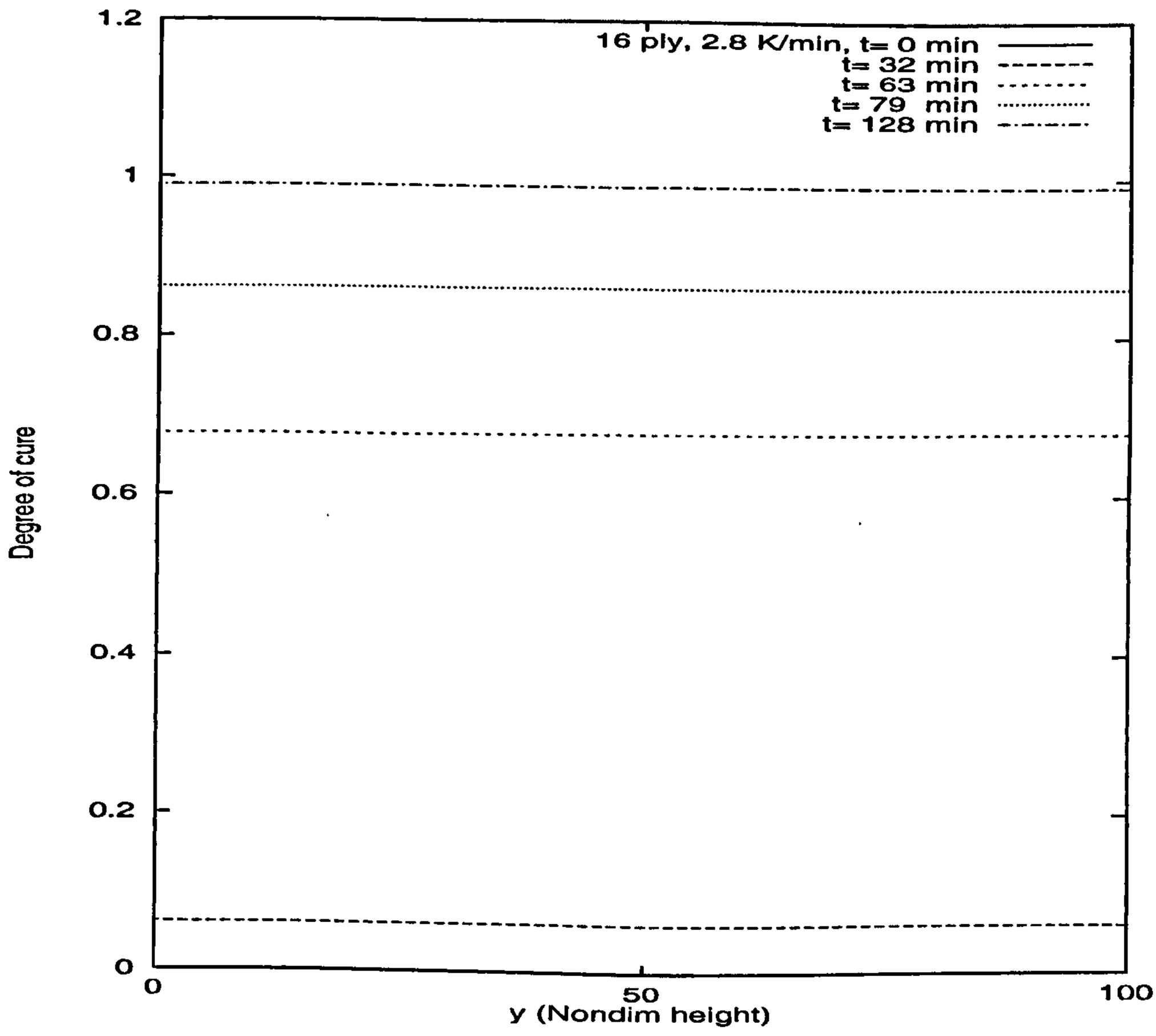

Figure 2.12: Through-the-thickness degree of cure of 16 ply laminate for the heating rate 2.8 K/min.

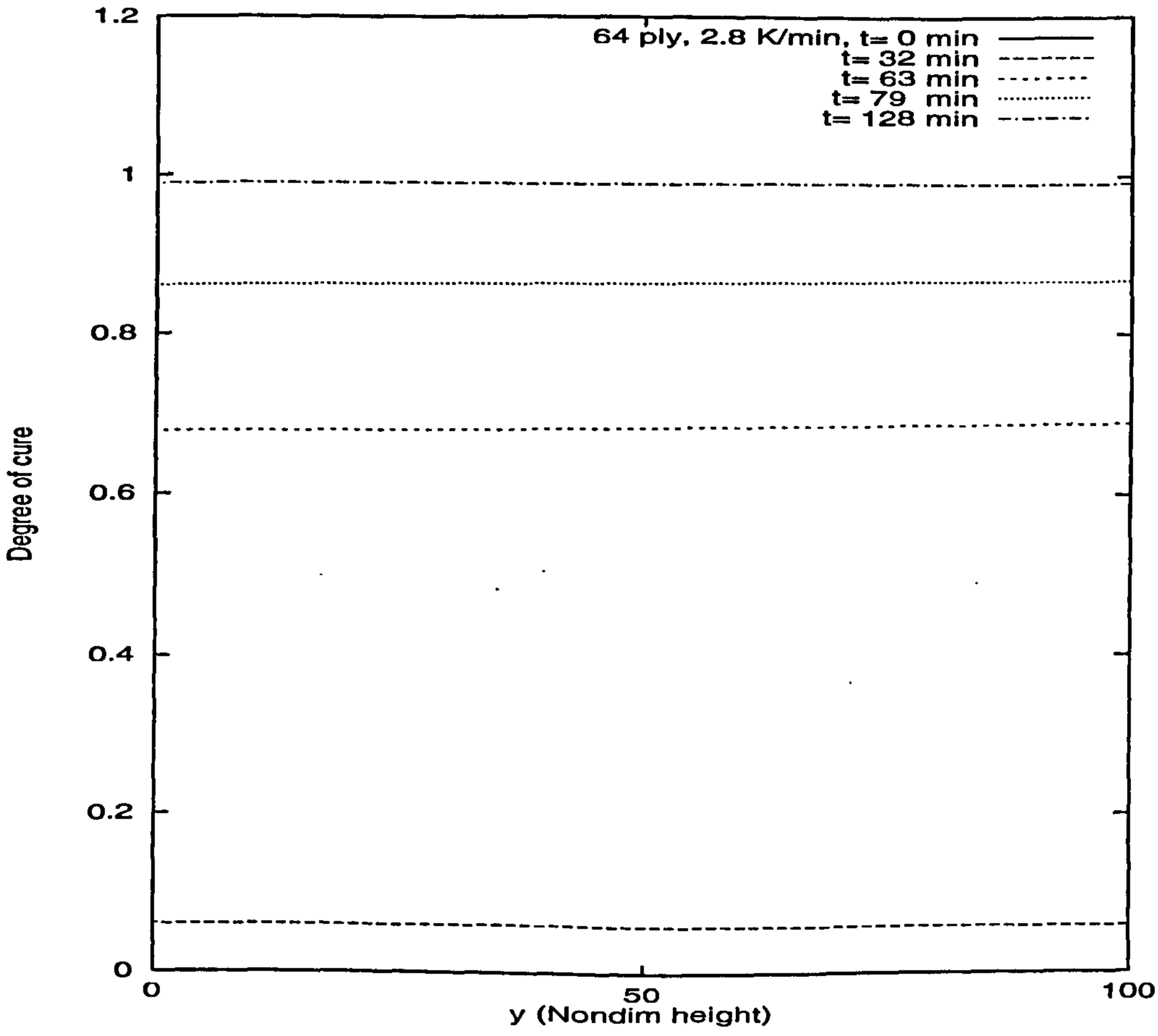

Figure 2.13: Through-the-thickness degree of cure of 64 ply laminate for the heating rate 11.1 K/min.

Chapter 3

Resin Infusion Process

3.1 Introduction

This chapter deals with the modelling and simulation of resin flow, heat transfer and the curing of a multilayer thermoset composite by the resin film infusion process. For approximately isothermal flows, the model is based on Darcy's Law and Stokes's equations where a similarity solution is obtained and subsequently used in a two-dimensional convection-diffusion heat equation coupled with a rate of cure equation. A finite difference scheme is applied to the energy equation on a moving grid and simulations for varying laminate thicknesses and number of plies are performed.

3.2 Modelling the Resin Flow

The schematic diagram for the set-up, with the chosen coordinate axis, is shown in *Figure* 3.1. A one-dimensional model is developed where the resin is assumed to be Newtonian with constant viscosity and the flow is in direction of the applied vertical force normal to the dry fibre plies. The flow through the dry fibre plies is considered as a flow through porous medium where Darcy's

law is employed.

Initially, there are $2n+1$ layers, n dry fibre plies interspersed with $n+1$ resin layers where the resin is considered to be in liquid form. A typical k dry fibre ply, which is considered as non-deformable and of constant thickness $d = h_{2k} - h_{2k-1}$, is therefore the $2k$ layer of the lay-up, for $k = 1, 2, \ldots, n$. As external pressure is applied at the top plate, $y = h_{2n+1}(t)$, the laminate is compressed, resulting in the flow of the resin into the dry fibre plies, thus, wetting the fibres and consolidating the laminate while heat is simultaneously applied in order to cure the resin into a solid composite part. The velocity

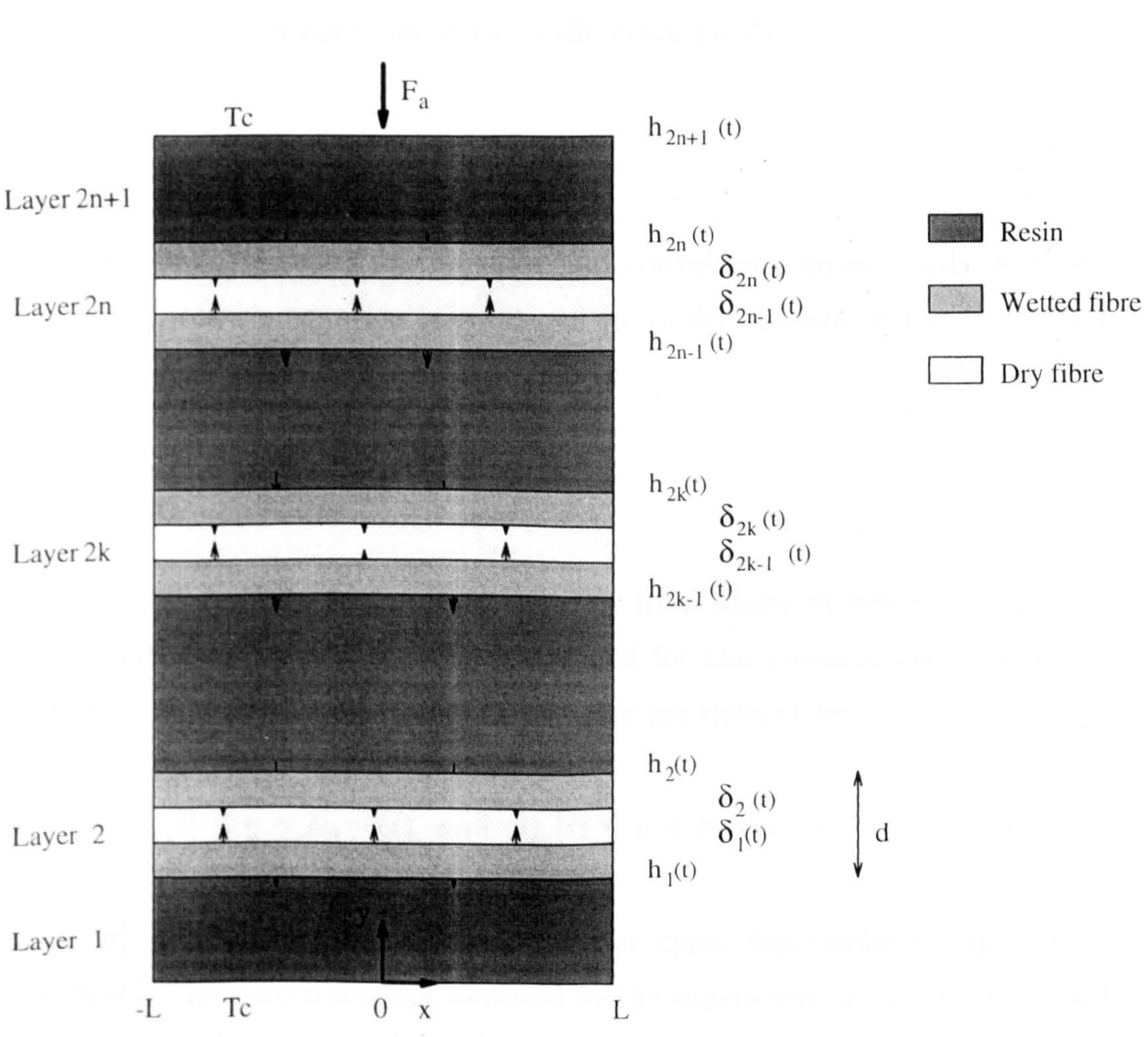

Figure 3.1: Set-up for n dry fibre plies

and pressure in the resin region $[-L, L] \times [h_{2k}, h_{2k+1}]$ are denoted by $\mathbf{v}^r_{2k+1}$ and p^r_{2k+1} while in the lower wetted fibre region $[-L, L] \times [h_{2k-1}, \delta_{2k-1}]$, the velocity and pressure are denoted by $\mathbf{v}^{w,l}_{2k-1}$ and $p^{w,l}_{2k-1}$ and in the upper wetted fibre region $[-L, L] \times [\delta_{2k}, h_{2k}]$, the velocity and pressure are denoted by $\mathbf{v}^{w,u}_{2k}$ and $p^{w,u}_{2k}$ for $k = 1, 2, \ldots, n$.

In a typical $(2k-1)$ fibre-free layer, $k = 1, 2, \ldots, n+1$, indicated by the superscript r, resin is assumed to flow only in the y-direction. Hence, the incompressiblity condition can be written as

$$\frac{\partial v^r_{2k-1}}{\partial y} = 0\,, \tag{3.1}$$

and the momentum equation in the x direction yields

$$\frac{\partial p^r_{2k-1}}{\partial x} = 0. \tag{3.2}$$

Given the high viscosity of the resin and considering quasi-steady state assumption, Stokes's equation is employed to model the flow in the y-direction where

$$\frac{\partial^2 v^r_{2k-1}}{\partial x^2} = \frac{\partial p^r_{2k-1}}{\partial y}. \tag{3.3}$$

In the dry fibre plies, as the resin can flow from above or below each ply, an upper and lower wetted region is identified for the pressure and velocity of each ply. The wetted regions of the $2k$ layer are defined by

$$h_{2k-1}(t) \le y \le \delta^l_{2k-1}(t) \;\text{ and }\; \delta^u_{2k}(t) \le y \le h_{2k}(t)\,,\; k = 1, 2, \ldots, n \tag{3.4}$$

where $\delta^l_{2k-1}(t)$ and $\delta^u_{2k}(t)$ are the lower and upper free surfaces respectively. The flow in the wetted regions, denoted by the superscript w, can be described by the continuity equation and the momentum equations in the x and y directions of an amended Darcy's law, taking account of the vertical motion of

the dry fibre plies, as

$$\frac{\partial v_{2k}^{w,i}}{\partial y} = 0 , \tag{3.5}$$

$$\frac{\partial p_{2k}^{w,i}}{\partial x} = 0 , \tag{3.6}$$

$$v_{2k}^{w,i} - \dot{h}_{2k}(t) = -\frac{\kappa}{\mu}\frac{\partial p_{2k}^{w,i}}{\partial y} , \tag{3.7}$$

for $k = 1, 2, \ldots, n$ where $i = l, u$ denotes the lower or upper wetted region respectively, $\dot{h}_{2k}(t)$ is the velocity of each dry fibre ply, κ is the permeability of the fibre ply and μ is the dynamic viscosity of the resin. In this work, both the parameters κ and μ are taken to be constant.

The boundary conditions for the velocities in the above set-up are :

- At the top and bottom plate, $y = h_{2n+1}(t)$ and $y = 0$ respectively, the no-slip condition is imposed. Thus,

$$v_{2n+1}^{r}(x, h_{2n+1}(t), t) = \dot{h}_{2n+1}(t) , \tag{3.8}$$

$$v_{1}^{r}(x, 0, t) = 0 . \tag{3.9}$$

- At the resin-wet fibre interfaces, the continuity condition is imposed whereby

$$v_{2k-1}^{r}(x, h_{2k-1}(t), t) = v_{2k}^{w,l}(x, h_{2k-1}(t), t) , \tag{3.10}$$

$$v_{2k}^{r}(x, h_{2k}(t), t) = v_{2k}^{w,u}(x, h_{2k}(t), t) , \tag{3.11}$$

for $k = 1, 2, \ldots, n$.

- At the free surfaces, $y = \delta_k(t), k = 1, 2, \ldots, 2n.$, the kinematic condition is applied whereby

$$v_{2k}^{w,l} - \dot{h}_{2k-1}(t) = \phi(\dot{\delta}_{2k-1}(t) - \dot{h}_{2k-1}(t)), \tag{3.12}$$

$$v_{2k}^{w,u} - \dot{h}_{2k}(t) = \phi(\dot{\delta}_{2k}(t) - \dot{h}_{2k}(t)) \tag{3.13}$$

for $k = 1, 2, \ldots, n$ and ϕ is the porosity of the fibre ply.

The boundary conditions for the pressure are :

- At the top bounding plate, the external force F_a acts normal to the plate at $y = h_{2n+1}(t)$ in the negative y-direction. Thus, applying a force balance over the plate of length 2L gives the pressure condition as

$$p^r_{2n+1}(x, h_{2n+1}(t), t) = \frac{F_a}{2L} \tag{3.14}$$

  where L is the half-length of the ply.

- At the bottom bounding plate, the pressure condition is

$$\frac{\partial p^r_1}{\partial y}(x, 0, t) = 0. \tag{3.15}$$

- At the resin-wet fibre interfaces, $y = h_k(t),\ k = 1, 2, \ldots, 2n$, the continuity condition is imposed whereby

$$p^r_{2k-1}(x, h_{2k-1}(t), t) = p^{w,l}_{2k}(x, h_{2k-1}(t), t), \tag{3.16}$$

$$p^r_{2k}(x, h_{2k}(t), t) = p^{w,u}_{2k}(x, h_{2k}(t), t), \tag{3.17}$$

  for $k = 1, 2, \ldots, n$.

- At the free surfaces, $y = \delta_k(t),\ k = 1, 2, \ldots, 2n$, the pressures are taken to be zero. Thus,

$$p^{w,l}_{2k}(x, \delta_{2k-1}(t), t) = 0, \tag{3.18}$$

$$p^{w,u}_{2k}(x, \delta_{2k}(t), t) = 0, \tag{3.19}$$

  for $k = 1, 2, \ldots, n$.

Flow Equations

A similarity solution is sought for the pressure and velocity in both the fibre-free and the wetted fibre or saturated regions (see Blest[61]) . In the fibre-free layers, the pressure is in terms of t only (see Appendix B),

$$p_1^r(t) = p_3^r(t) = \ldots = p_{2n+1}^r(t) = \frac{F_a}{2L}. \tag{3.20}$$

In a typical dry fibre ply of the $2k$ layer, the pressure in the upper wetted region is

$$p_{2k}^{w,u}(y,t) \;=\; \frac{\mu\phi}{\kappa}(\dot{h}_{2k} - \dot{\delta}_{2k})(y - \delta_{2k}) \tag{3.21}$$

and the $(2k+1)$ resin layer is

$$p_{2k+1}^r(t) \;=\; p_{2k}^{w,u}(h_{2k}(t),t) \;=\; \frac{\mu\phi}{\kappa}\Big(\dot{h}_{2k}(t) - \dot{\delta}_{2k}(t)\Big)\Big(h_{2k}(t) - \delta_{2k}(t)\Big). \tag{3.22}$$

In the upper wetted region of the $2k$ dry fibre ply, imposing the free surface kinematic condition gives

$$v_{2k}^{w,u}(t) = \dot{h}_{2k}(t) + \phi\Big(\dot{\delta}_{2k}(t) - \dot{h}_{2k}(t)\Big). \tag{3.23}$$

At the bottom resin layer, imposing the no-slip boundary condition at $y = 0$ yields

$$v_1^r(t) = 0$$

. Pressure in the first resin layer is

$$p_1^r(t) = \frac{\mu}{\kappa\phi}\dot{h}_1(t)(h_1(t) - h_{1,0}). \tag{3.24}$$

The position of the bottom fibre ply is

$$h_1(t) \;=\; h_{1,0} - \sqrt{\frac{\kappa\phi F_a t}{L\mu}}. \tag{3.25}$$

In the lowermost fibre ply, the free surface of the lower wetted region is

$$\delta_1(t) = \frac{\phi - 1}{\phi} h_1(t) + \frac{1}{\phi} h_{1,0}. \tag{3.26}$$

and in terms of its initial position, eliminating $h_1(t)$ in (3.26) using (3.25) yields

$$\delta_1(t) = h_{1,0} - (1 - \frac{1}{\phi})\sqrt{\frac{\kappa\phi F_a t}{L\mu}}. \tag{3.27}$$

At the top resin layer, the velocity is

$$v^r_{2n+1}(t) \;=\; \dot{h}_{2n+1}(t) \tag{3.28}$$

and from (3.22) with $k = n$, the pressure is

$$p^r_{2n+1}(t) \;=\; -\frac{\mu}{\kappa}\Big(h_{2n}(t) - \delta_{2n}(t)\Big)\Big(\dot{h}_{2n+1}(t) - \dot{h}_{2n}(t)\Big). \tag{3.29}$$

In terms of its initial position, the position of the top plate is

$$h_{2n+1}(t) = h_{2n+1,0} - (2n+1)\sqrt{\frac{\kappa\phi F_a t}{L\mu}}. \tag{3.30}$$

From the initial condition $\delta_{2k}(0) = h_{2k}(0) = h_{2k,0}$, the position of the free surfaces of the upper wetted regions in the $2k$ fibre ply can be found to be (see Appendix B)

$$\delta_{2k}(t) \;=\; h_{2k}(t) - \sqrt{\frac{\kappa F_a t}{L\mu\phi}}\;,\; k = 1, 2, \ldots, n. \tag{3.31}$$

The position of the free surfaces in the lower wetted regions in the $2k$ fibre plies are

$$\delta_{2k+1}(t) = h_{2k+1}(t) + \sqrt{\frac{\kappa F_a t}{L\mu\phi}}\ ,\ k = 0, 1, \ldots, n-1. \tag{3.32}$$

Hence, the heights of the resin-fibre interfaces and the free surface flow fronts for a typical k layer, are

$$h_{2k+1} = h_{2k+1,0} - (2k+1)\sqrt{\frac{\kappa\phi F_a t}{L\mu}}\ ,\ k = 0, 1, \ldots, n \tag{3.33}$$

$$h_{2k} = h_{2k-1} + d\ ,\ k = 1, 2, \ldots, n \tag{3.34}$$

$$\delta_{2k+1} = h_{2k+1,0} - \left(2k+1-\frac{1}{\phi}\right)\sqrt{\frac{\kappa\phi F_a t}{L\mu}}\ ,\ k = 0, 1, \ldots, n-1 \tag{3.35}$$

$$\delta_{2k} = h_{2k,0} - \left(2k-1+\frac{1}{\phi}\right)\sqrt{\frac{\kappa\phi F_a t}{L\mu}}\ ,\ k = 1, 2, \ldots, n \tag{3.36}$$

where recall that n is the total number of fibre layers and d is the constant thickness of a fibre layer.

Thus, differentiating (3.33)-(3.36), we obtain both velocities of the fibre layers and the free surface fronts

$$\dot{h}_{2k+1} = -\left(k+\frac{1}{2}\right)\sqrt{\frac{\kappa\phi F_a}{L\mu t}}\ ,\ k = 0, 1, \ldots, n \tag{3.37}$$

$$\dot{h}_{2k} = \dot{h}_{2k-1}\ ,\ k = 1, 2, \ldots, n \tag{3.38}$$

$$\dot{\delta}_{2k+1} = -\frac{1}{2}\left(2k+1-\frac{1}{\phi}\right)\sqrt{\frac{\kappa\phi F_a}{L\mu t}}\ ,\ k = 0, 1, \ldots, n \tag{3.39}$$

$$\dot{\delta}_{2k} = -\frac{1}{2}\left(2k-1+\frac{1}{\phi}\right)\sqrt{\frac{\kappa\phi F_a}{L\mu t}}\ ,\ k = 1, 2, \ldots, n. \tag{3.40}$$

3.3 Heat Transfer Model

The heat applied in the autoclave initiates an exothermic heat reaction of the resin. As the resin flows into the dry fibre layers there are three different

regions through which the heat transfer process will occur, namely the fibre-free resin regions, the wetted fibre regions and the dry fibre regions.

In the fibre-free resin layers, the two-dimensional convection-diffusion heat equation can be expressed as

$$\frac{\partial T_r}{\partial t} + v^r \frac{\partial T_r}{\partial y} = K_r \left(\frac{\partial^2 T_r}{\partial x^2} + \frac{\partial^2 T_r}{\partial y^2} \right) + \frac{H_R}{c_r} \frac{\partial \alpha}{\partial t}, \tag{3.41}$$

while in the wetted fibre layers which is considered as saturated porous layers, the heat transfer in this layer is described by

$$\frac{\partial T_w}{\partial t} + v^w \frac{\partial T_w}{\partial y} = K_w \left(\frac{\partial^2 T_w}{\partial x^2} + \frac{\partial^2 T_w}{\partial y^2} \right) + \frac{\phi H_R}{c_w} \frac{\partial \alpha}{\partial t}. \tag{3.42}$$

and in the dry fibre layers, in the absence of resins, only the conduction mode occur, hence

$$\frac{\partial T_f}{\partial t} = K_f \left(\frac{\partial^2 T_f}{\partial x^2} + \frac{\partial^2 T_f}{\partial y^2} \right) \tag{3.43}$$

where $T^i = T(x, y, t), i = r, w, f$ denote the temperature, $v^i, i = r, w$ denote the vertical velocity flow component, $\alpha(x, y, t)$ is the degree of cure of the resin and the suffices r,w and f denote the resin, wetted fibre and dry fibre layers respectively. $K_i, i = r, w, f$ are the thermal diffusivities, $c_i, i = r, w, f$ are the thermal specific heats, ϕ is the voidage of the fibre layer and H_R is the heat of reaction of the resin.

The thermal diffusivities are defined by

$$K_i = \frac{\kappa_i}{\rho_i c_i}, \text{ for } i = r, w, f \tag{3.44}$$

where κ_i are the thermal conductivities and ρ_i are the densities of the respective regions.

In the wetted fibre regions, the values of the thermal conductivity and heat

capacity are expressed by the rule of mixtures[27],

$$k_w = \phi k_r + (1-\phi)k_f, \tag{3.45}$$

$$c_w\rho_w = \phi c_r\rho_r + (1-\phi)c_f\rho_f, \tag{3.46}$$

where the suffices r and f again denoting the resin and dry fibre properties respectively. The expressions for the rate of degree of cure for the thermoset resin are obtained from [51] which are

$$\frac{\partial\alpha}{\partial t} = \begin{cases} (a_1 + a_2\alpha)(1-\alpha)(0.47-\alpha) & \alpha \leq 0.3 \\ a_3(1-\alpha) & \alpha > 0.3 \end{cases} \tag{3.47}$$

where the temperature-dependent $a_i, i = 1,2,3$ are

$$a_i = A_i exp\left(\frac{-\Delta E_i}{RT}\right), \ i = 1,2,3.$$

A_i are specified pre-exponential factors, ΔE_i are the known activation energies, and R is the universal gas constant. The degree of cure takes a value zero initially and 1 when fully cured.

Boundary Conditions

The initial temperature, T_{ini}, is assumed to be uniform across the different regions and also assumed known,

$$T_r(x,y,0) = T_w(x,y,0) = T_f(x,y,0) = T_{ini}. \tag{3.48}$$

The prescribed autoclave temperature, T_a, is assumed known and is imposed at the top and bottom bounding plates of the laminates at $y = h_{2n+1}(t)$ and $y = 0$ respectively. Thus

$$T_r(x,0,t) = T_r(x,h_{2n+1}(t),t) = T_a. \tag{3.49}$$

The laminates are also assumed to be insulated at the ends $x = \pm L$ thus

$$\frac{\partial T_r}{\partial x}(-L, y, t) = \frac{\partial T_w}{\partial x}(-L, y, t) = \frac{\partial T_f}{\partial x}(-L, y, t) = 0, \tag{3.50}$$

$$\frac{\partial T_r}{\partial x}(L, y, t) = \frac{\partial T_w}{\partial x}(L, y, t) = \frac{\partial T_f}{\partial x}(L, y, t) = 0. \tag{3.51}$$

Continuity conditions for the temperature and flux are imposed at the interface of the saturated fibre and the fibre-free layers,

$$\left.\begin{aligned} T_r(x, h_k(t), t) &= T_w(x, h_k(t), t)\ , \\ k_r \tfrac{\partial T_r}{\partial y}(x, h_k(t), t) &= k_w \tfrac{\partial T_w}{\partial y}(x, h_k(t), t) \end{aligned}\right\} k = 1, 2, \ldots, 2n.$$

and at the free surfaces,

$$\left.\begin{aligned} T_w(x, \delta_k(t), t) &= T_f(x, \delta_k(t), t)\ , \\ k_w \tfrac{\partial T_w}{\partial y}(x, \delta_k(t), t) &= k_f \tfrac{\partial T_f}{\partial y}(x, \delta_k(t), t) \end{aligned}\right\} k = 1, 2, \ldots, 2n.$$

3.4 Solution Techniques

3.4.1 Scaling

The following non-dimensionalised variables are introduced to facilitate the numerical solution procedure,

$$\tilde{x} = \frac{x}{d},\ \ \tilde{y} = \frac{y}{d},\ \ \tilde{v}^i = \frac{v^i}{V},\ \ \tilde{T}^i = \frac{(T^i - T_{ini})}{(T_a - T_{ini})} \text{ and } \tilde{t} = \frac{tK_r}{d^2}$$

for $i = r, w, f$ where d is the thickness of a dry fibre layer and V is the velocity of the uppermost plate, $\dot{h}_{2n+1}(t)$.

In the fibre-free resin layers, the non-dimensinalise heat equation becomes

$$\frac{\partial T_r}{\partial t} + Pev^r \frac{\partial T_r}{\partial y} = \left(\frac{\partial^2 T_r}{\partial x^2} + \frac{\partial^2 T_r}{\partial y^2}\right) + J_r \frac{\partial \alpha}{\partial t} \tag{3.52}$$

while in the wetted fibre layers, equation (3.42) transforms to

$$\frac{\partial T_w}{\partial t} + Pev^w \frac{\partial T_w}{\partial y} = D_w\Big(\frac{\partial^2 T_w}{\partial x^2} + \frac{\partial^2 T_w}{\partial y^2}\Big) + J_w \frac{\partial \alpha}{\partial t} \tag{3.53}$$

and in the dry fibre layers, equation (3.43) manifests itself as

$$\frac{\partial T_f}{\partial t} = D_f\Big(\frac{\partial^2 T_f}{\partial x^2} + \frac{\partial^2 T_f}{\partial y^2}\Big) \tag{3.54}$$

Note that the *tilde* has been omitted. The dimensionless numbers are

$$Pe = \frac{Vd}{K_r}, \tag{3.55}$$

$$J_r = \frac{H_R}{c_r(T_a - T_{ini})}, \tag{3.56}$$

$$J_w = \frac{\phi \rho_r H_R}{c_w \rho_w (T_a - T_{ini})}, \tag{3.57}$$

$$D_f = \frac{K_f}{K_r}, \tag{3.58}$$

$$D_w = \frac{K_w}{K_r}. \tag{3.59}$$

The rate of degree of cure equation (3.47) becomes

$$\frac{\partial \alpha}{\partial t} = \begin{cases} (C_1 + C_2\alpha)(1-\alpha)(0.47-\alpha) & \alpha \leq 0.3, \\ C_3(1-\alpha) & \alpha > 0.3 \end{cases} \tag{3.60}$$

where

$$C_i = \frac{d^2 a_i}{K_r},\ i = 1,2,3. \tag{3.61}$$

The solutions to the coupled, non-dimensionalised temperature and degree of cure equations (3.52), (3.53), (3.54) and (3.60) are carried out in a domain which changes with time.

The modified Euler method is used to discretize the first order rate of degree of cure equation (3.60). The predictor-corrector method can be expressed as

$$\alpha^*_{n+1} = \alpha_n + \Delta t f(\alpha_n) \text{ predictor} \tag{3.62}$$

$$\alpha_{n+1} = \alpha_n + \frac{1}{2}\Delta t[f(\alpha_n) + f(\alpha^*_{n+1})] \text{ corrector.} \tag{3.63}$$

The Alternating Direction Implicit (ADI) finite difference scheme with the appropriate upwinding, proposed by McKee et al.[59], is employed to discretize the energy equations (3.52), (3.53), (3.54). The ADI method in split form is given by

$$\begin{aligned}&\left[1 - \frac{ra}{2}\right](T_l)^{m+1^*}_{i,j} \\ &= \left[1 + sa\delta_y^2 - qv^l Pe\nabla_y + \frac{ra}{2}\delta_x^2\right](T_l)^m_{i,j} + \Delta t J_l g(\alpha^m_{i,j}, (T_l)^m_{i,j})\end{aligned} \tag{3.64}$$

$$\begin{aligned}&\left[1 - \frac{sa}{2} + \frac{qv^l Pe}{2}\nabla_y\right](T_l)^{m+1}_{i,j} \\ &= (T_l)^{m+1^*}_{i,j} + \left[\frac{sa}{2}\delta_y^2 - \frac{qv^l Pe}{2}\nabla_y\right](T_l)^m_{i,j}\end{aligned} \tag{3.65}$$

where $(T_l)^m_{i,j}, l = r, w, f$ represents the approximate temperature in the respective l layer of resin, wet fibre or dry fibre at the m^{th} time level for the node (i, j) where $x_i = x_0 + i\Delta x,\ i \in N$ and $y_j = y_0 + j\Delta y,\ j \in N$.
The difference notation used are

$$\nabla_x(T_l)^m_{i,j} = (T_l)^m_{i,j} - (T_l)^m_{i-1,j}$$

$$\nabla_y(T_l)^m_{i,j} = (T_l)^m_{i,j} - (T_l)^m_{i,j-1}$$

$$\delta_x^2(T_l)^m_{i,j} = (T_l)^m_{i-1,j} - 2(T_l)^m_{i,j} - (T_l)^m_{i+1,j}$$

$$\delta_y^2(T_l)^m_{i,j} = (T_l)^m_{i,j-1} - 2(T_l)^m_{i,j} - (T_l)^m_{i,j+1}$$

and

$$a = \begin{cases} D_w & \text{for the wetted fibre region} \\ D_f & \text{for the dry fibre region} \\ 1 & \text{for the resin layer} \end{cases}$$

p, q, r and s are defined as

$$p = \Delta t/\Delta x,\ q = \Delta t/\Delta y,\ r = \Delta t/\Delta x^2 \text{ and } s = \Delta t/\Delta y^2 \tag{3.66}$$

and $g\left(\alpha_{i,j}^m, (T_l)_{i,j}^m\right)$ is the exothermic reaction function from (3.60).

3.5 Numerical Result

The simulation to obtain the temperature distribution and the degree of cure distribution during the process is performed for 16, 32 and 52 plies of fibres which are initially dry. The thermal material constants employed can be found in Loos and Springer[12] are given in *Table* 2.1. Other data constants for the flow properties used for the simulation are given in *Table* 2.2 (Blest[61]). The value of constants used in the curing equations are given in *Table* 2.3.

Figure 3.2 shows the computed change in the non-dimensional thickness of the resin layers with time as pressure is applied to laminates consisting of three different number of plies. It is observed that for the given magnitude of force and viscosity ($\mu = 1$, constant), the resin infiltration into the dry fibres and the consolidation of the saturated plies are almost instantaneous for all the thicknesses.

Figures 3.3 and 3.4 shows temperature versus time at the centre of a composite consisting of different number of plies at heating rates of 2.8 K/min and 11.1 K/min respectively. At both rates of heating, exotherms are observed to occur for all the composites and the magnitude of the exotherms is seen to

increase for thicker composites. The exotherms occur due to the fact that the rate of heat generated by the exotherms is higher than the rate of heat loss to the surrounding medium, thus the rapid rise in temperature. The increased magnitude of the exotherms is expected because the low thermal conductivity of the resin acts as a thermal barrier (see Kim and Lee [20]).

Figures 3.5 and 3.6 shows the degree of cure versus time at the centre of a composite consisting of a different number of plies at heating rates of 2.8 K/min and 11.1 K/min respectively. It can be seen that the predicted time for maximum cure to be achieved increases as laminate thickness increases. The graphs also show that a higher heating rate also increases the curing process.

Figure 3.7 compares the temperature at the centre of a 16 ply composite for heating rates of 2.8 K/min and 11.1 K/min respectively. It can be seen that for the same thickness, higher exotherms are predicted for higher heating rates. *Figure* 3.8 compares the cure at the centre of a 16 ply composite for two different heating rates and it can be seen that the time to achieve maximum cure increases as the heating rate increases.

Figures 3.9 and 3.10 show a one-dimensional profile of temperature through the thickness at different times for a 16 ply and a 32 ply composite at heating rate of 11.1 K/min. From the graphs, the model predicts a fairly uniform temperature distribution for the selected cure cycle throughout the process. The figures also display the effects of the exotherms as the composite thickness increases.

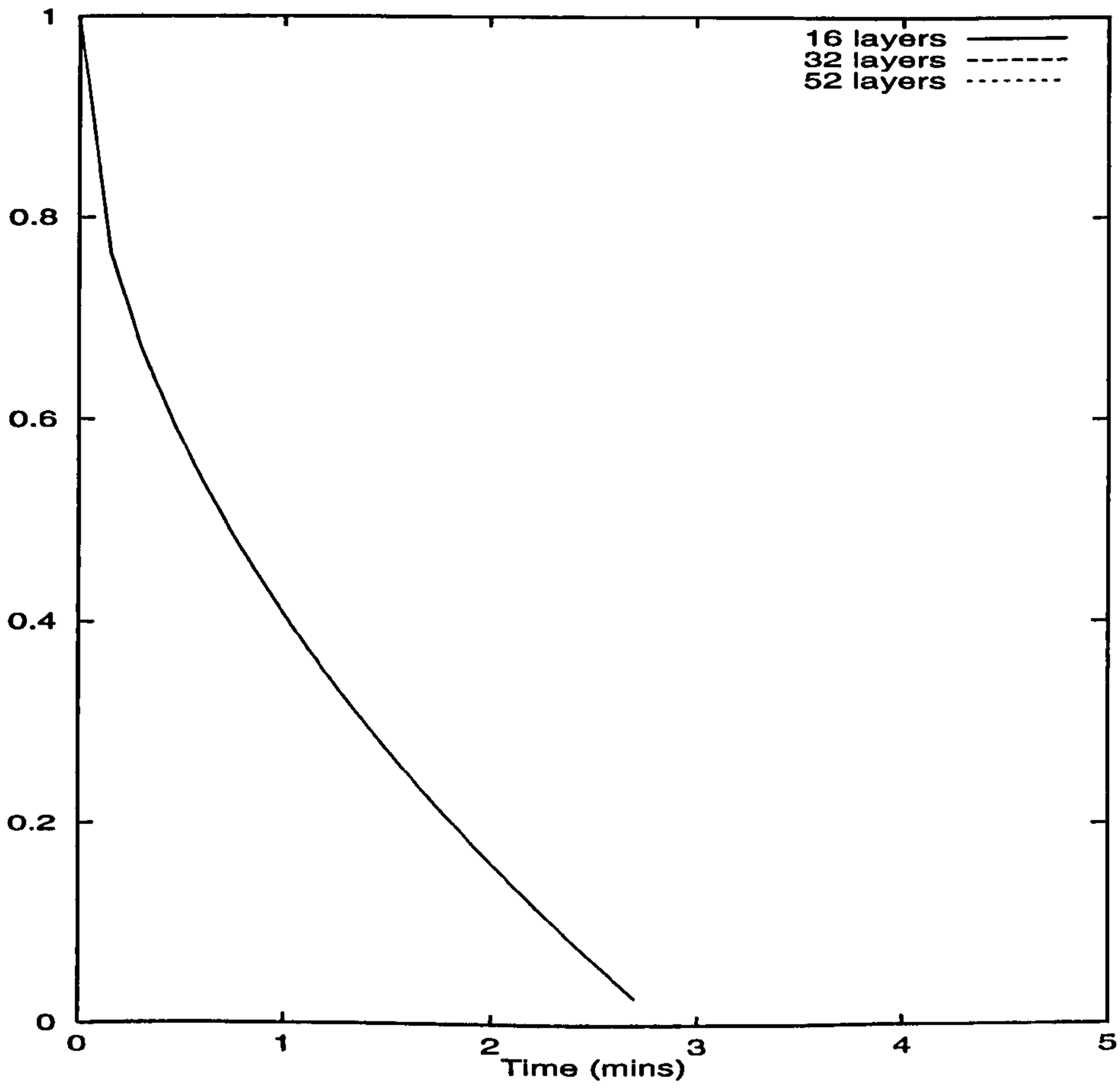

Figure 3.2: Resin thickness vs Time.

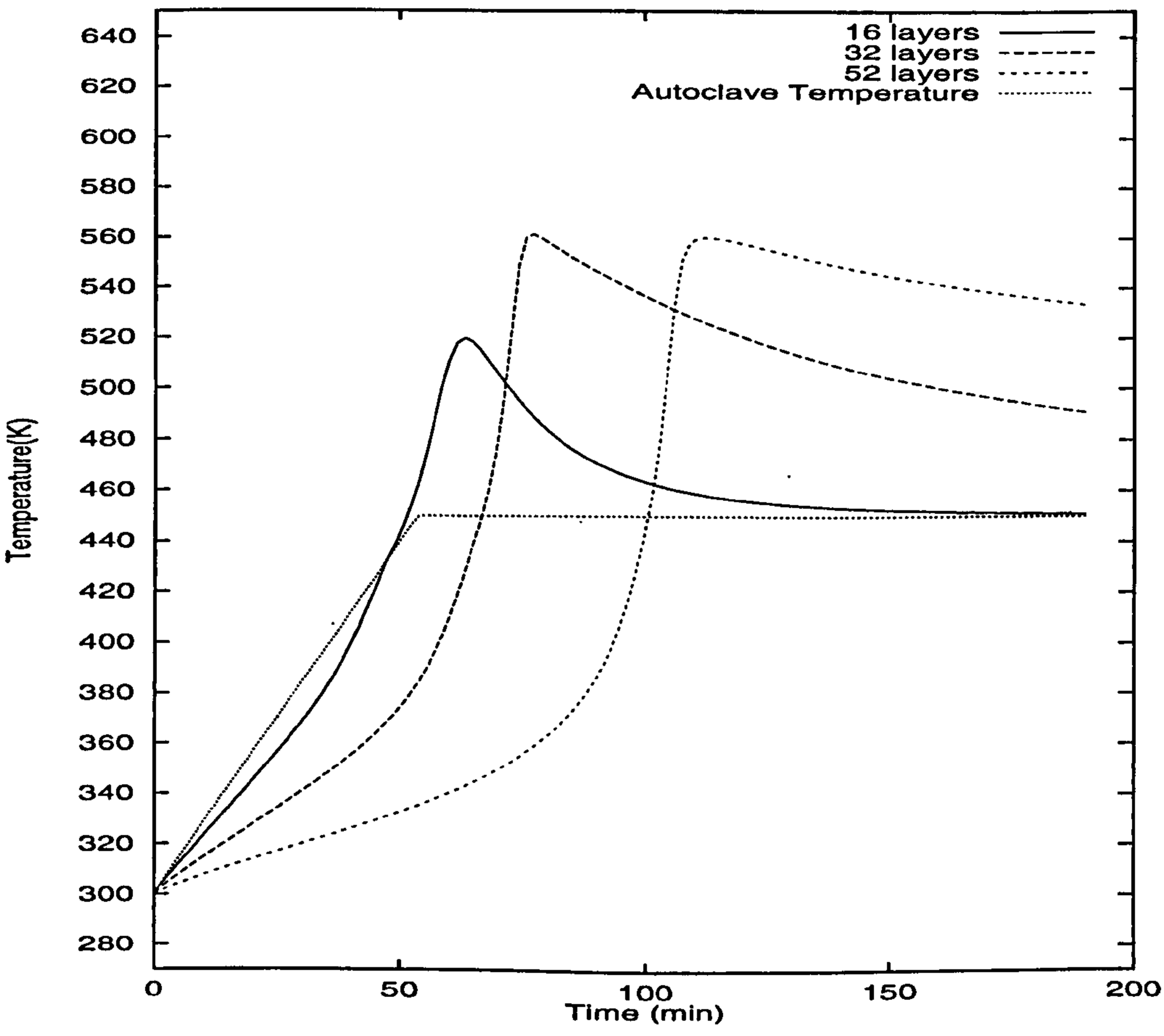

Figure 3.3: Temperature vs Time at the centre of the composites at heating rate 2.8 K/min.

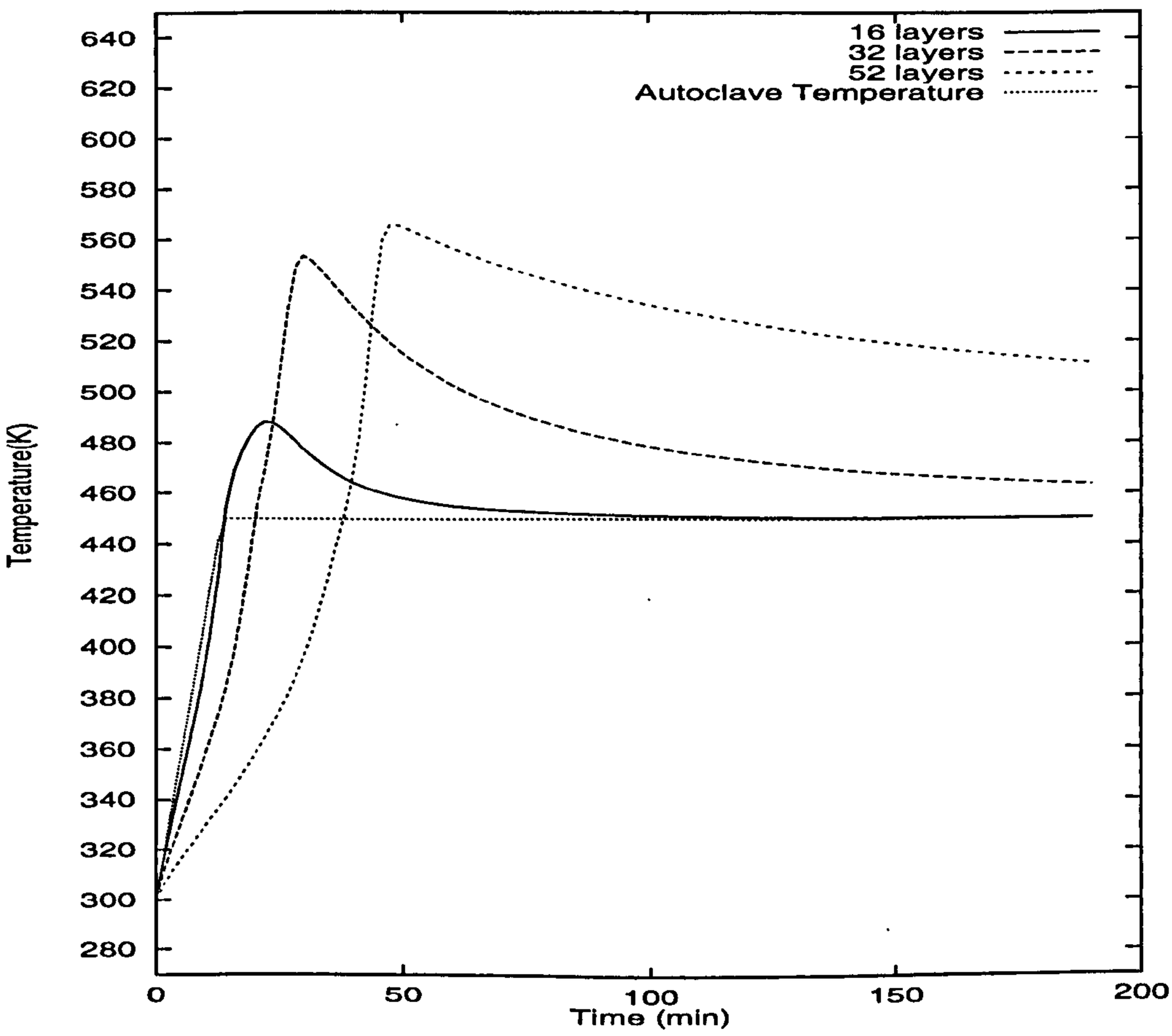

Figure 3.4: Temperature vs Time at the centre of the composites at heating rate 11.1 K/min.

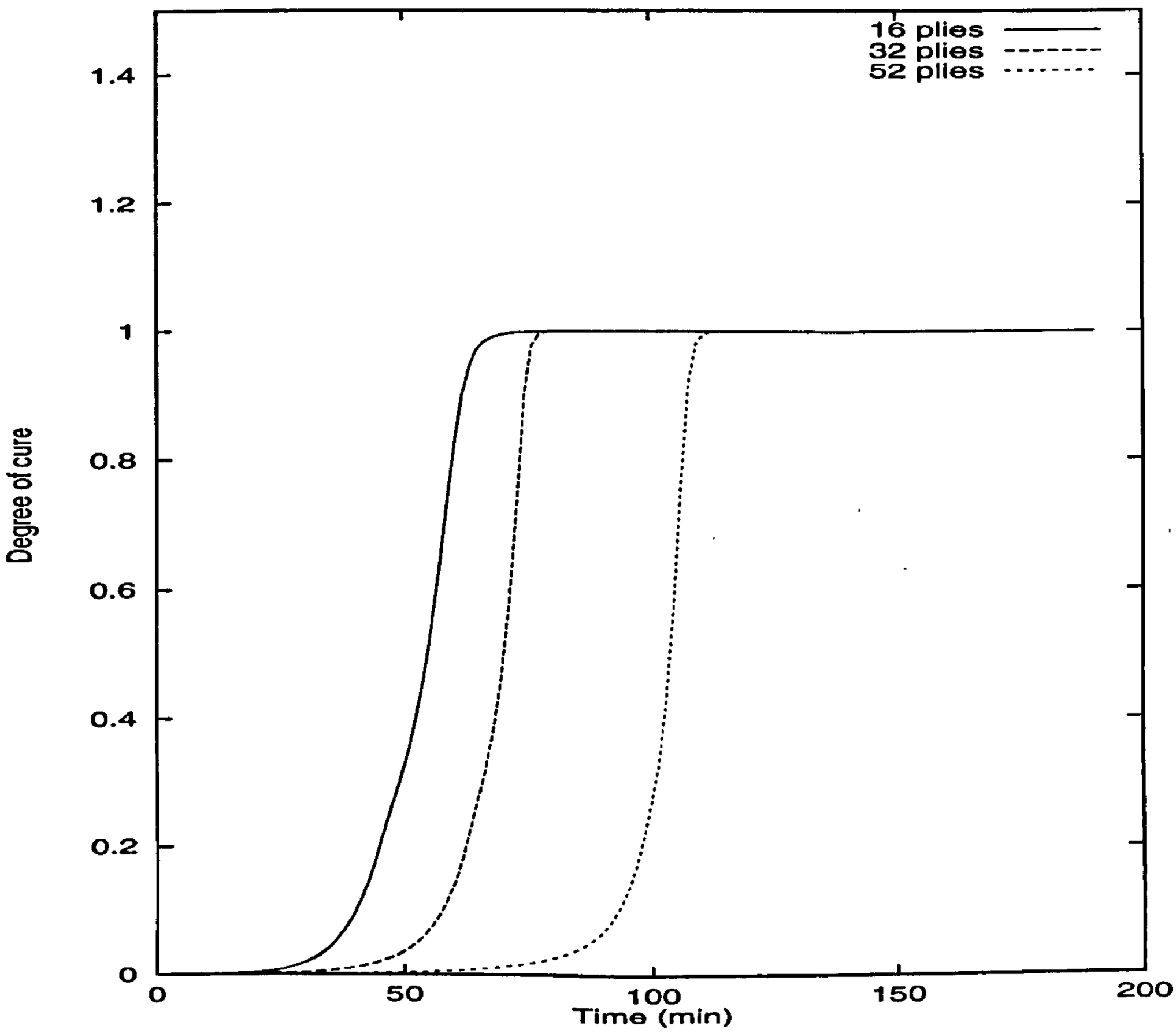

Figure 3.5: Cure vs Time at the centre of the composites at heating rate 2.8 K/min.

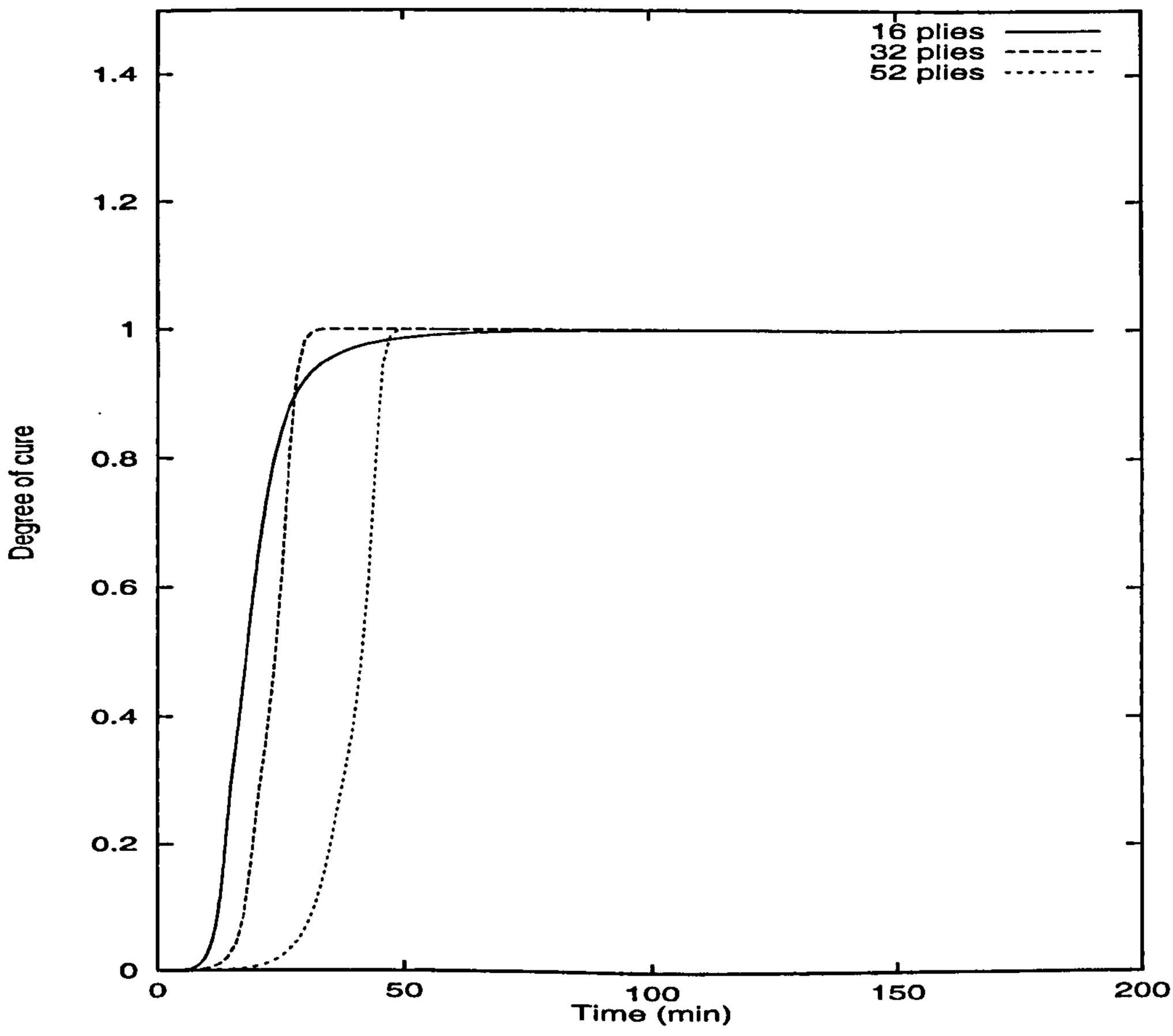

Figure 3.6: Cure vs Time at the centre of the composites at heating rate 11.1 K/min.

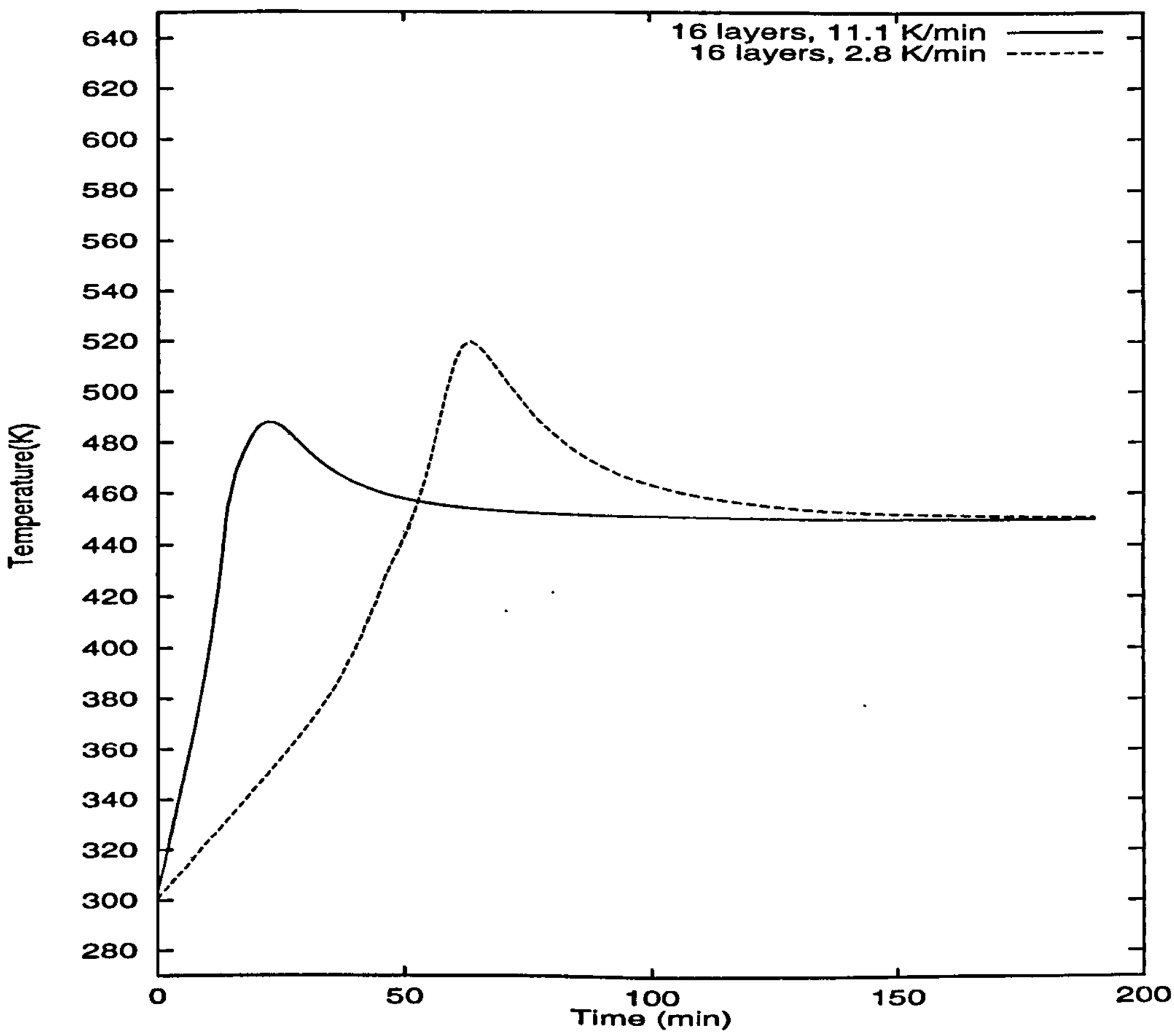

Figure 3.7: Comparison of Temperature vs Time at the centre of the composites at different heating rates.

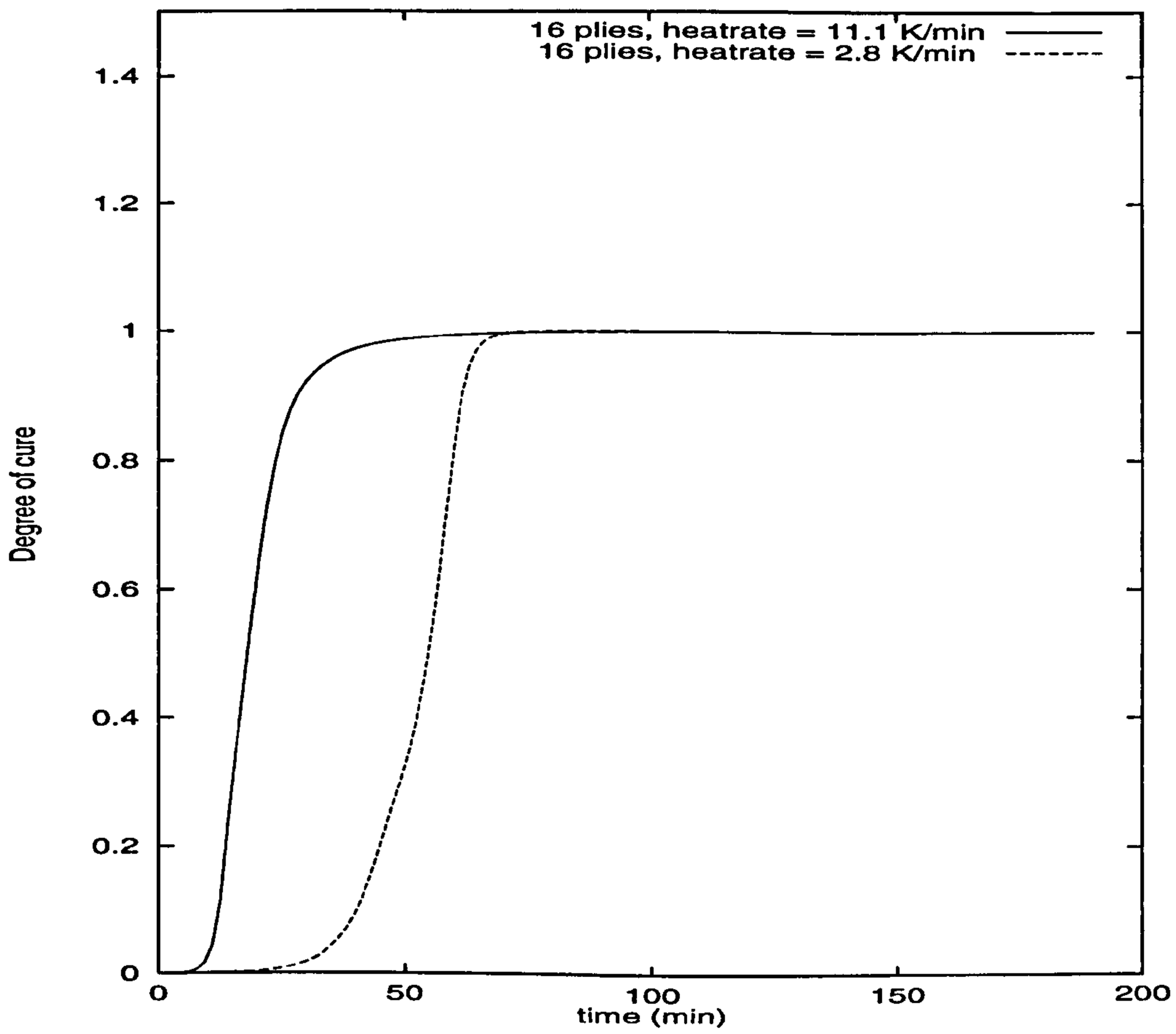

Figure 3.8: Comparison of Degree of cure vs Time at the centre of the composite at different heating rates.

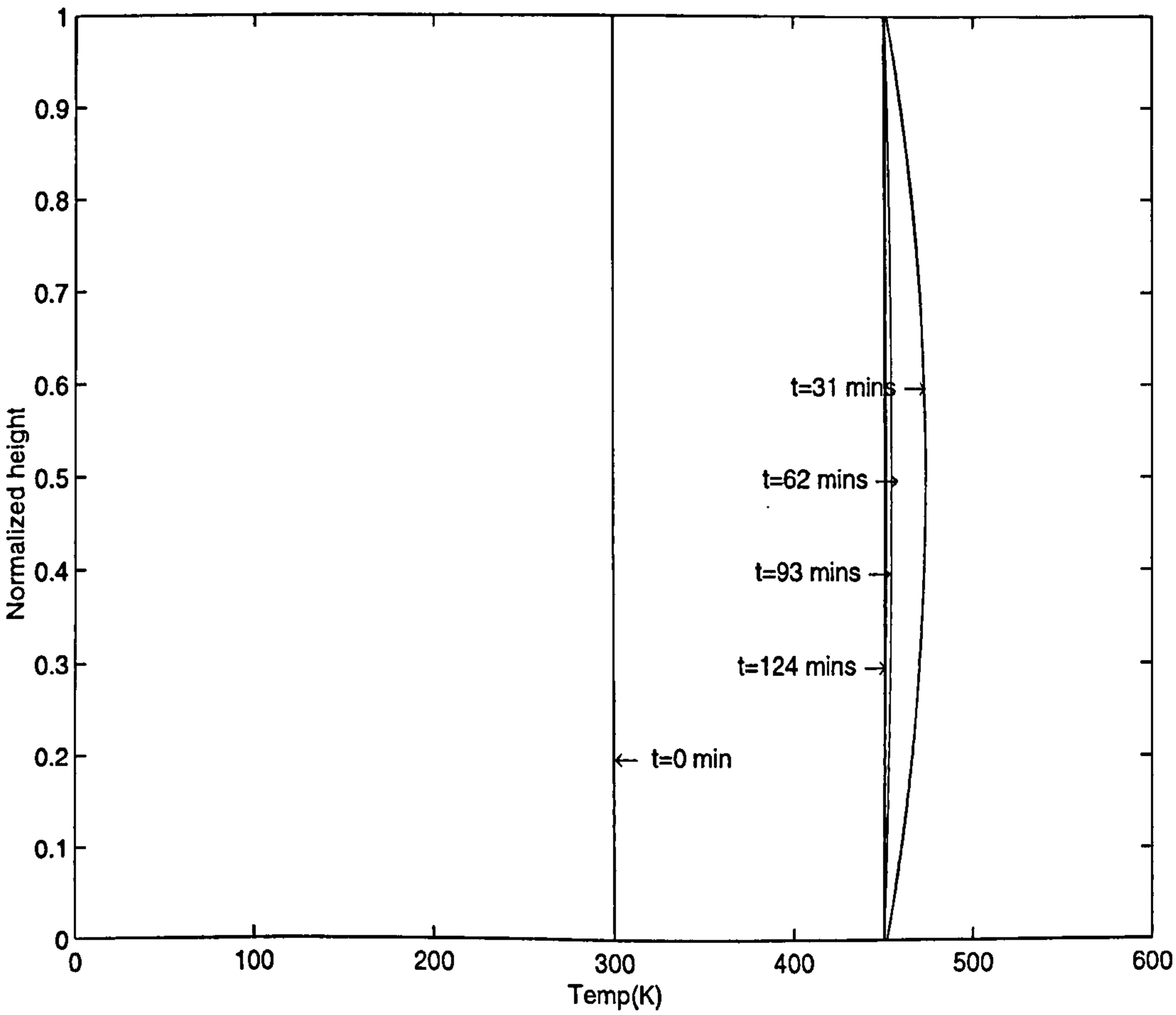

Figure 3.9: Temperature vs Normalized height at different times during the process for n=16 plies.

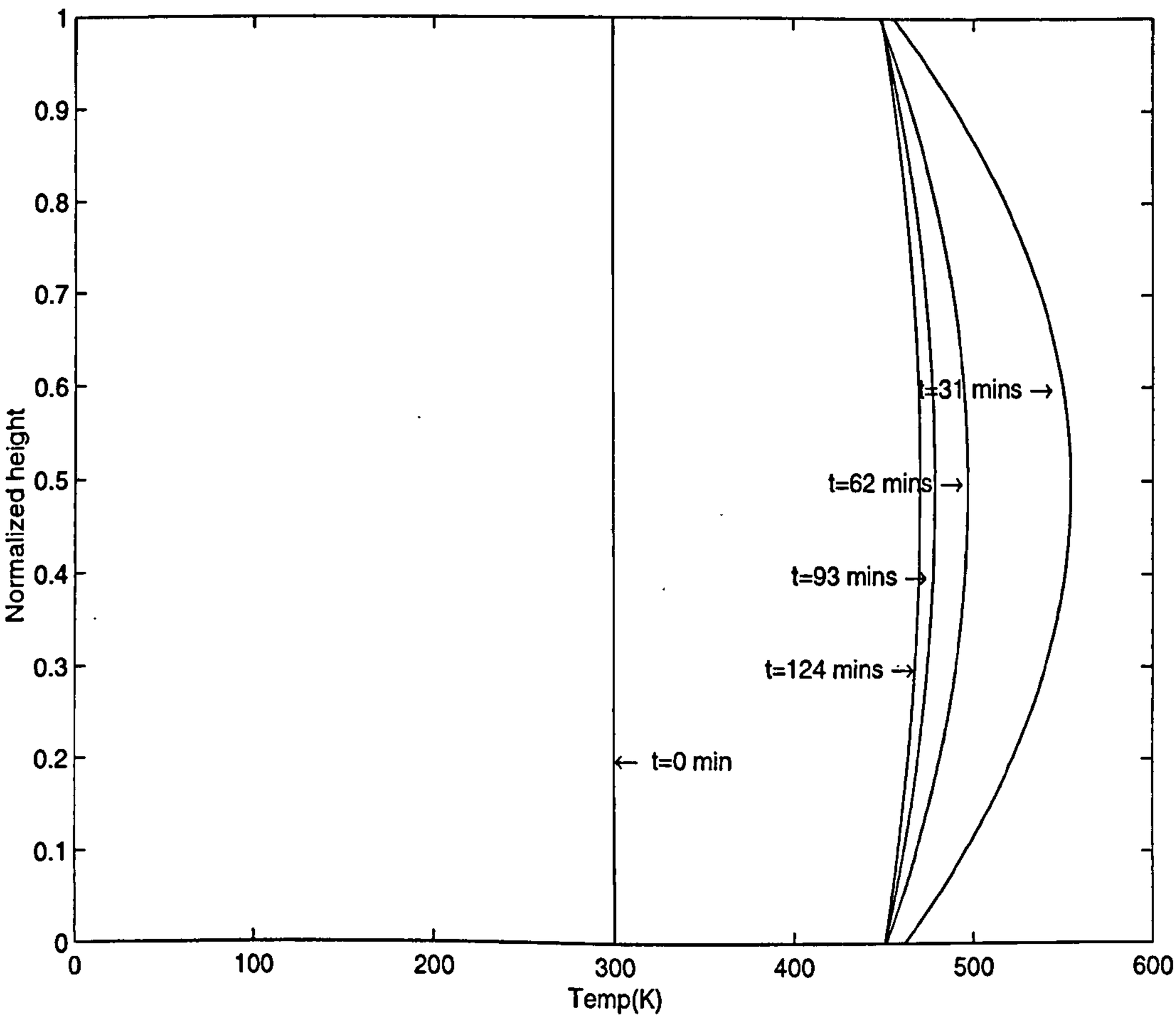

Figure 3.10: Temperature vs Normalized height at different times during the process for n=32 plies.

3.6 Experimental Investigation

In an experimental investigation carried out by P. Marshall of British Aerospace of the Sowerby Research Centre, 4 layers (equivalently, 8 plies) of stitched fabric were used. The plies in each layer were oriented alternatively at +45 degrees and -45 degrees to obtain a composite with uniform "strength" properties in both in-plane directions. Two separate cases were investigated: in the first, resin was distributed at the top and bottom of the stack of fibers, and in the second the same amount of resin was applied at the top only. The applied pressure was 85 psi (5.86×10^5 Nm^{-2}), and the temperature quickly ramped to 175 degrees C and held for a 30 minute period. Here it may be remarked that the resin utilised begins to gel after such a length of time at this temperature. In each case the final thickness of the laminar was approximately 3.5 mm.

For the first case, *Micrograph* 1 shows complete impregnation of all plies although the 5th ply from the top indicates some small defects. However when the same experimental regime was applied to the stack with resin at the top only, only 6 out of 8 plies were impregnated, as is indicated in *Micrographs* 2 and 3. It is clear that when the resin was placed at both ends of the stack of fibers, the infusion process is more successful and achieved full penetration in a shorter time; this was of course predicted by the model, and entirely to be expected.

For a one resin, one fiber set-up, equations (3.36) and (3.35) for the impermeation depth reduce to

$$\delta = \sqrt{\frac{\kappa P t}{\mu \phi}}. \tag{3.67}$$

where P here denotes the pressure.

Additional experimentation on the resin alone, over a cure cycle equivalent to that of the infusion process, shows that the viscosity is below 10 Pas. Given

the very large changes in the viscosity over the cure cycle (as much as from 1 to 10^5 Pas), an estimated viscosity of 10 Pas with an impermeation period of 15 minutes was adopted for the purpose of representing the cycle. The permeability, κ, more difficult to obtain, is estimated to lie between 5×10^{-3} and 5×10^{-4} m^2 and 10^{-3} was adopted for the order of magnitude calculation. Typical values of the porosity lie near 0.5. With these values,

$$\delta = 3.25mm \tag{3.68}$$

Given the average values taken for the parameters this is a reasonable match for the measured value of $3.5 \times (6/8) = 2.625$ mm.

Finally, there was no evidence of distinctly differing resin distributions away from the centres of the micrographed sections, allowing some support for the one-dimensional model of the fluid flow offered in this thesis.

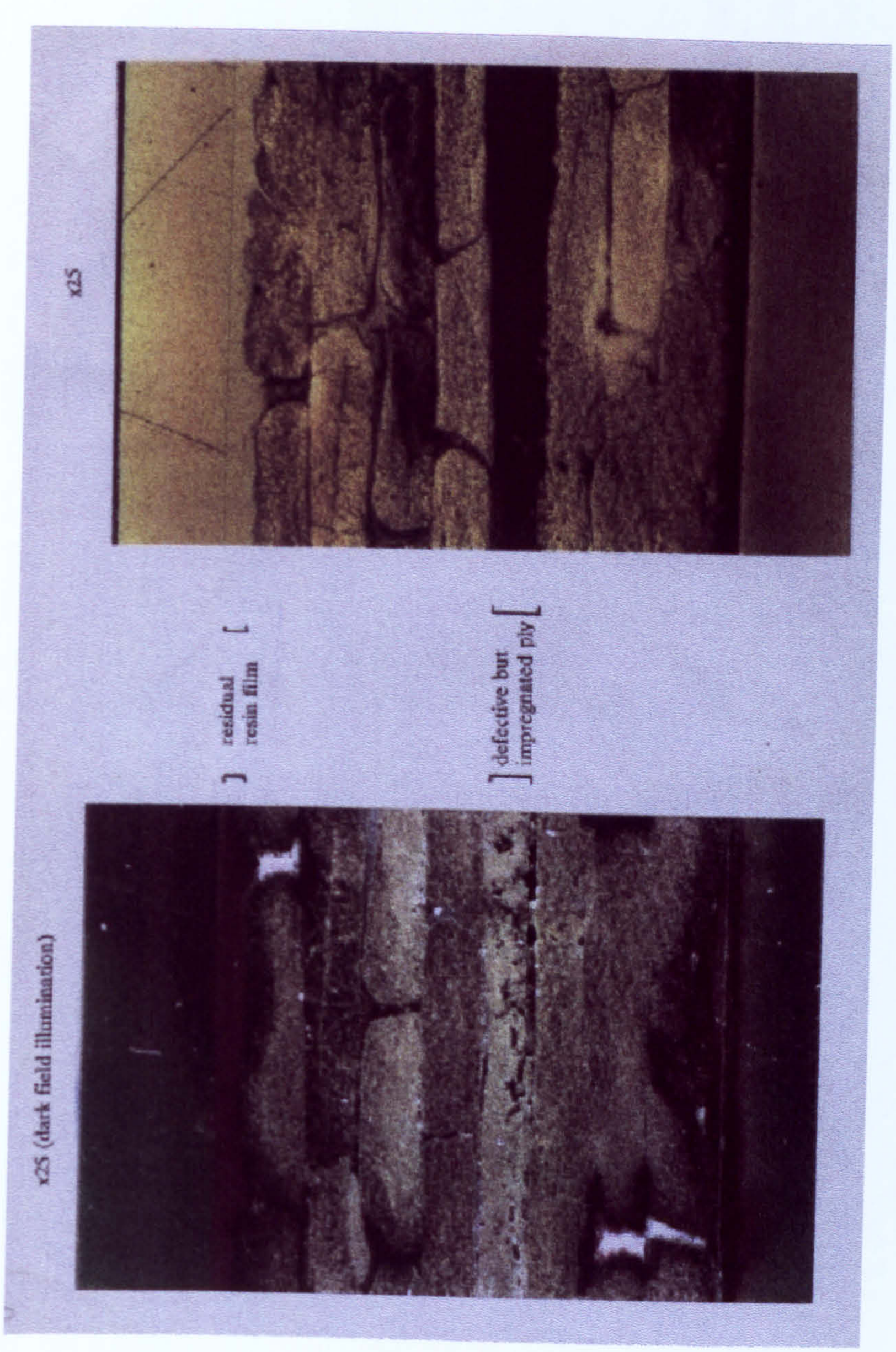

Figure 3.11: Microgr aph 1.

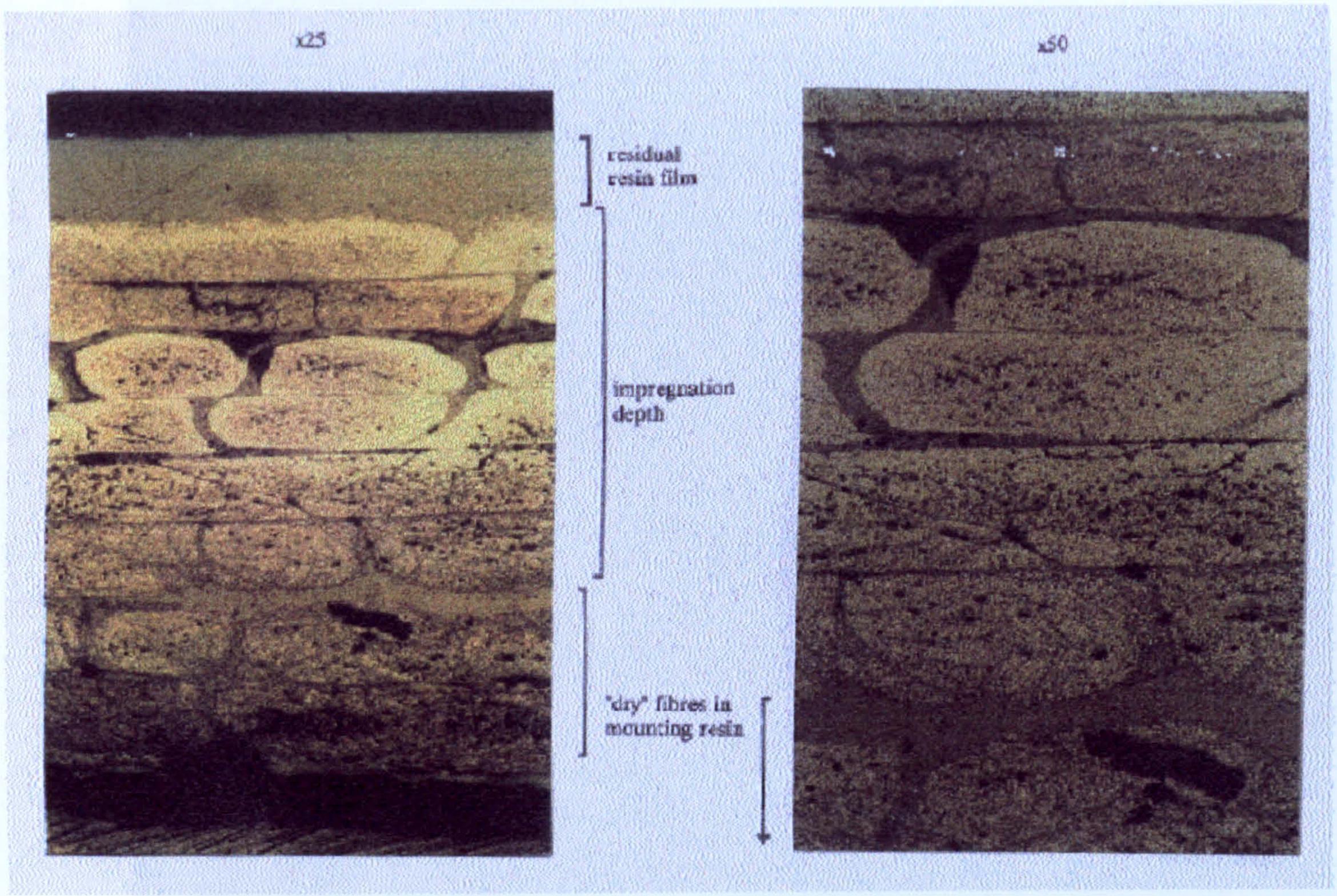

Figure 3.12: Micrograph 2.

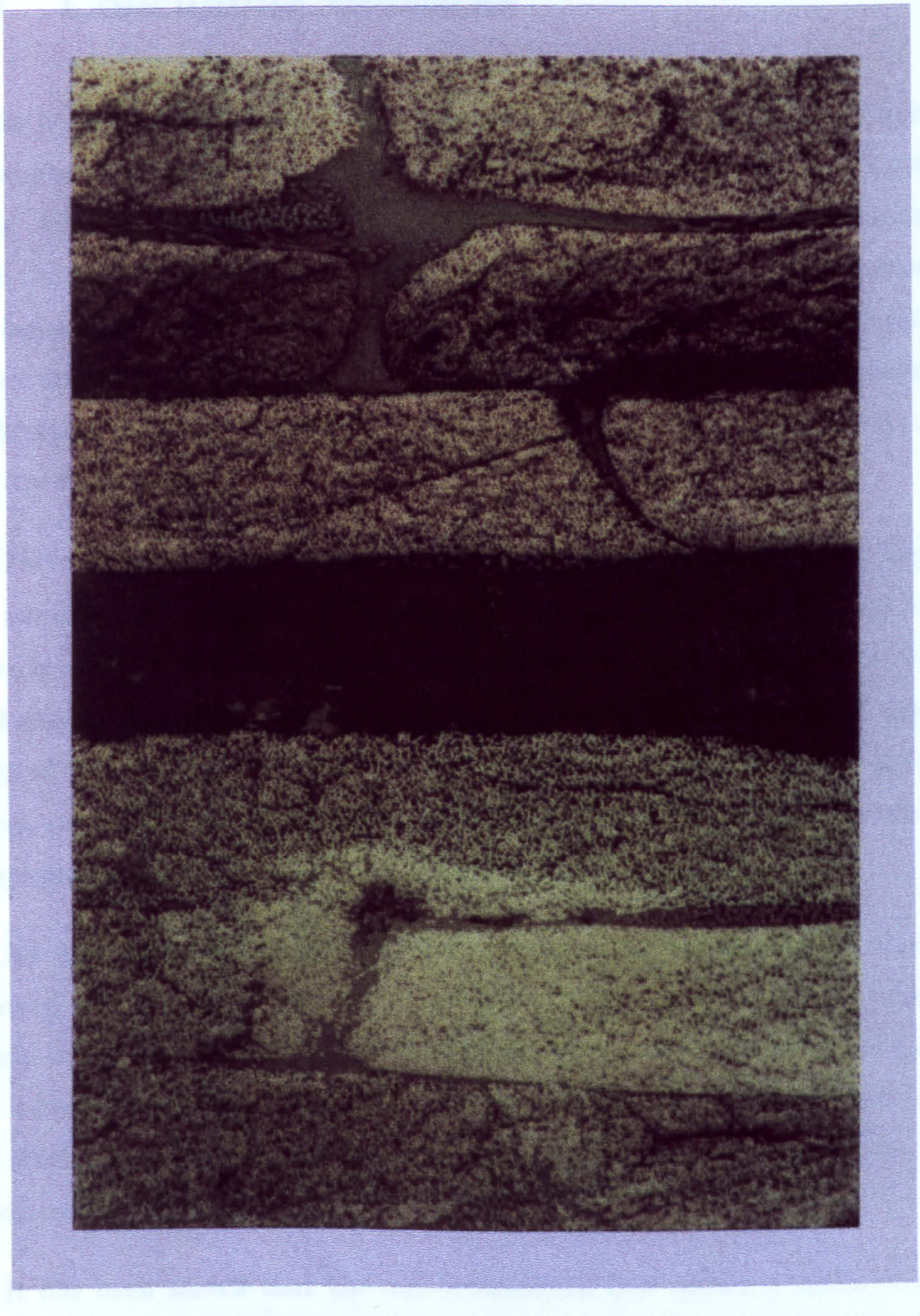

Figure 3.13: Micrograph 3.

3.7 Concluding Remarks

A mathematical model has been developed for the resin infusion process of a composite laminate with n layers of dry fibres, each separated by layers of resin. As in the prepreg case, the velocity components for the flowing resin (in both the resin and the saturated fibre layers), could be reduced to a problem of solving a system of first-order ordinary differential equations, which admits a closed analytic solution. In addition, the use of a kinematic condition resulted in the solution for the free surface boundary of the resin as it infiltrates through the dry fibre layers.

Three different regions resulted in this process namely the resin region, the saturated fibre region and the dry fibre region. Convection-diffusion equations for the temperatures in the resin and the saturated fibre layers with a heat generation term were solved by an alternating-direction implicit method coupled with a 2^{nd}-order Runge-Kutta method for the cure. In the dry fibre layers, in the absence of the resin, the diffusion equations were solved for the temperatures.

An experimental investigation was performed to investigate the fluid dynamical aspects of the process. Two cases of impregnation were performed where in the first case resin was distributed on top of a stack of fibres and in the second case the resin was distributed both on top and at the bottom of the stack. In both cases, the depth of impregnation agreed well with the value predicted by the model.

It has been shown that the one-dimensional flow model is useful in modelling the resin flow process of the Resin Infusion technique. The one-dimensional assumption was not unreasonable because the flow is being restricted due to the dam being imposed at the edges of the composite. The temperature calculated also provided a good prediction of the behaviour of the process when different heat-up rates were applied thus validating further the usefulness of the model.

Chapter 4

Conclusion and Recommendation

A mathematical model has been developed for both the prepreg curing process and the resin infusion process of a composite laminate with n layers of prepregs. Simulations are performed to predict the resin flow, heat transfer and curing of both processes. It was shown, subject to certain assumptions, that the velocity components for the flowing resin (both in the resin layers and in the saturated fibre layers) could be reduced to a problem of solving a system of first-order ordinary differential equations which, in the case where the layers of the saturated fibres are of equal thickness, admit a closed analytic solution. In the resin infusion flow model, the use of a kinematic condition enabled the free surface boundary of the resin to be determined, as it infiltrates through the dry fibre layers.

A system of convection-diffusion equations with heat generation terms was solved by an alternating-direction implicit method (for the temperatures in the prepregs and the excess resin layers) coupled with a 2^{nd}-order Runge-Kutta method for the cure. In the prepreg case numerical results have been compared with experimental data and found to give good agreement, particularly with regard to the temperature of the composite. In the resin infusion case, ex-

perimental investigations have been performed and good agreement has been found between the experimental values and the computed values with regard to the penetration depth of the resin through the dry fibre layers. It has been been shown that the flow models, validated by the temperature simulations are useful for modelling the resin flow of both processes.

Variable viscosity of the resin could have been considered in the flow model. The temperature-dependent viscosity would then couple the energy equation with the flow equations and a similarity solution of the flow model would not have been possible. A fully numerical procedure would be required to solve the Stokes's equation and the Darcy's equation which would then be employed in the heat equation to solve for the temperature of the laminate. For the Hercules 3501-6 resin, which is widely used in composites fabrication, the empirical function given by (2.62) could have been employed in the simulation. This would have resulted in the complexity of the numerical model being increased significantly to the point where it would have been nearly intractable.

The use of permeability models would further enhance the flow model. The Carman-Kozeny model (1.4) could be employed. For unsaturated flows in glass fabrics, the permeability database of Parnas [30] could be used for the characterization of the material. Further, as the degree of crosslinking of the polymer resins increases and the resin begins to solidify, the permeability of reinforcement is thus also dependent on the fluid viscosity and the degree of cure of the resin.

The reinforcement which is made of fibrous porous material will, in general, deform under stress. Several studies have proposed a deformable porous media flow model in the prepregs and RTM processes. One deformable saturated media model is to consider it to behave like a sponge which when placed under stress will experience a decrease in volume [14, 15]. For a deformable porous media which is initially dry, a model is proposed based on the theory of mixtures and using the momentum equation of both the elastic solid part and the wet part of the preform with a constitutive relation for the partial

stress tensor and internal body force [25].

Voidage is also an important issue which needs to be addressed. The presence of voids in the final stages of the process degrades the quality of the composite and the minimisation or reduction of voids is one of the most important objective of the fabrication process. In prepregs, voids are present due to entrapped volatiles between the layers during the lay-up process. In RTM and Resin Infusion, voids are present during the filling stage of the dry preforms. A two-phase model, proposed by Wood and Bader [34, 35] and Chui [36] could be incorporated into the model to further enhance the simulation procedure.

Appendix A

Derivation of Prepreg Flow Equations.

For arbitrary k consider the resin layer $[-L, L] \times [h_{2k}, h_{2+1}]$. The quasi-steady flow equations are

$$\nabla \cdot \mathbf{u}^r_{2k+1} = 0 \tag{A.1}$$

$$\nabla p^r_{2k+1} + \mu \nabla^2 \mathbf{u}^r_{2k+1} = 0 \tag{A.2}$$

where $\mathbf{u}^r_{2k+1}, p^r_{2k+1}$ are the velocity and pressure respectively in the resin layer $[-L, L] \times [h_{2k}, h_{2k+1}], k = 0, 1, \ldots, n.$

Introduce the function $f_{2k+1}(y, t)$ and set

$$u^r_{2k+1} = -x \frac{\partial f_{2k+1}}{\partial y}(y, t) \tag{A.3}$$

$$v^r_{2k+1} = f_{2k+1}(y, t). \tag{A.4}$$

Inspection of the above equations indicates that

$$\frac{\partial^2 p^r_{2k+1}}{\partial x \partial y} = 0, \quad \text{so that} \quad \frac{\partial^4 f_{2k+1}}{\partial y^4} = 0$$

which may be integrated to give

$$f_{2k+1}(y,t) = A_{2k+1}(t)y^3 + B_{2k+1}(t)y^2 + C_{2k+1}(t)y + D_{2k+1}(t). \qquad \text{(A.5)}$$

In a similar manner, consider the saturated fibre regions
$[-L, L] \times [h_{2k-1},\ h_{2k}],\ k = 1, 2, \ldots, n.$

The flow equations are

$$\nabla \cdot \mathbf{u}_{2k}^f = 0 \qquad \text{(A.6)}$$

$$\mathbf{u}_{2k}^f = \mathbf{w}_{2k} - \frac{\kappa}{\mu}\nabla p_{2k}^f \qquad \text{(A.7)}$$

where $\mathbf{u}_{2k}^f, p_{2k}^f$ are the velocity and pressure respectively in the fibre layer $[-L, L] \times [h_{2k-1}, h_{2k}], k = 1, 2, \ldots, n$, and $\mathbf{w}_{2k} = (0, \dot{h}_{2k}(t))$. Introduce the function $g_{2k}(y,t)$ and set

$$u_{2k}^f = -x\frac{\partial^2 g_{2k}}{\partial y^2}(y,t) \qquad \text{(A.8)}$$

$$v_{2k}^f = \dot{h}_{2k} + \frac{\partial g_{2k}}{\partial y}(y,t). \qquad \text{(A.9)}$$

The continuity equation is automatically satisfied; substituting these velocity components into (A.7) yields

$$g_{2k}(y,t) = \frac{1}{2}Q_{2k}(t)y^2 + R_{2k}(t)y + S_{2k}(t). \qquad \text{(A.10)}$$

Let us return to the resin layer and consider (A.2) and (A.5). Differentiating (A.3) and (A.4) appropriately then gives

$$\frac{\partial p_{2k+1}^r}{\partial x} = -6\mu A_{2k+1}x \qquad \text{(A.11)}$$

$$\frac{\partial p^r_{2k+1}}{\partial y} = 2\mu(3A_{2k+1}y + B_{2k+1}) \tag{A.12}$$

where the explicit dependency on the arguments has been neglected for clarity.

Integrate (A.11) with respect to x to obtain

$$p^r_{2k+1} = -3\mu A_{2k+1}x^2 + \xi_{2k+1} \tag{A.13}$$

where ξ_{2k+1} is an arbitrary function of y and t.

Differentiating (A.13) with respect to y and equating with (A.12) gives, after integration,

$$\xi_{2k+1} = \mu(3A_{2k+1}y^2 + 2B_{2k+1}y) + \psi_{2k+1} \tag{A.14}$$

where ψ_{2k+1} is an arbitrary function of t.

Elimination of ξ_{2k+1} in (A.13) yields

$$p^r_{2k+1} = 3\mu A_{2k+1}(y^2 - x^2) + 2\mu B_{2k+1}y + \psi_{2k+1}. \tag{A.15}$$

Applying the boundary conditions

$$p^r_{2k+1} = 0 \text{ at } x = \pm L \text{ and } y = h_{2k}, k = 0, 1, \ldots, n$$

gives

$$\psi_{2k+1} = 3\mu A_{2k+1}(L^2 - h^2_{2k}) - 2\mu B_{2k+1}h_{2k} \tag{A.16}$$

so that the pressure p^r_{2k+1} is, from (A.15),

$$p^r_{2k+1} = 3\mu A_{2k+1}(y^2 - x^2 + L^2 - h^2_{2k}) + 2\mu B_{2k+1}(y - h_{2k}). \tag{A.17}$$

From (A.3), (A.4) and (A.5) we obtain immediately that

$$u^r_{2k+1} = -x(3A_{2k+1}y^2 + 2B_{2k+1}y + C_{2k+1}) \tag{A.18}$$

$$v^r_{2k+1} = A_{2k+1}y^3 + B_{2k+1}y^2 + C_{2k+1}y + D_{2k+1}. \tag{A.19}$$

A similar analysis may be performed for the saturated fibre layers, $[-L, L] \times [h_{2k-1}, h_{2k}], k = 1, 2, \ldots, n$. We note from (A.7), that

$$u^f_{2k} = -\frac{\kappa}{\mu}\frac{\partial p^f_{2k}}{\partial x}$$

$$v^f_{2k} = \dot{h}_{2k} - \frac{\kappa}{\mu}\frac{\partial p^f_{2k}}{\partial y}.$$

Thus, using (A.8) - (A.10), we obtain

$$\frac{\partial p^f_{2k}}{\partial x} = \frac{\mu}{\kappa}\frac{\partial^2 g_{2k}}{\partial y^2}x = \frac{\mu}{\kappa}Q_{2k}x \tag{A.20}$$

and

$$\begin{aligned}\frac{\partial p^f_{2k}}{\partial y} &= \frac{\mu}{\kappa}(\dot{h}_{2k} - v^f_{2k}) \\ &= -\frac{\mu}{\kappa}\frac{\partial g_{2k}}{\partial y} = -\frac{\mu}{\kappa}(Q_{2k}y + R_{2k})\end{aligned} \tag{A.21}$$

Integrating (A.21) with respect to y yields

$$p^f_{2k} = -\frac{\mu}{\kappa}\left(\frac{1}{2}Q_{2k}y^2 + R_{2k}y\right) + \zeta_{2k}(x,t). \tag{A.22}$$

Now differentiate (A.22) with respect to x, equate $\frac{\partial \zeta_{2k}}{\partial x}(x,t)$ to (A.20), perform an integration with respect to x and substitute the expression for $\zeta_{2k}(x,t)$ in (A.22). This results in

$$p^f_{2k} = -\frac{\mu}{2\kappa}Q_{2k}(y^2 - x^2) - \frac{\mu}{\kappa}R_{2k}y + \beta \tag{A.23}$$

where β is a function of t only.

Using the boundary conditions for pressure, notably,

$$p^f_{2k} = 0 \text{ at } x = \pm L, \quad y = h_{2k-1}, k = 1, 2, \ldots, n,$$

results in

$$p^f_{2k} = -\frac{\mu}{2\kappa} Q_{2k}(y^2 - x^2 - h^2_{2k-1} + L^2) - \frac{\mu R_{2k}}{\kappa}(y - h_{2k-1}). \tag{A.24}$$

The velocity components are then obtained immediately from (A.8) - (A.10),

$$u^f_{2k} = -Q_{2k}x \tag{A.25}$$

$$v^f_{2k} = \dot{h}_{2k} + Q_{2k}y + R_{2k}. \tag{A.26}$$

So far, the velocity components and pressure have been obtained to within arbitrary functions of time in each resin and saturated fibre layer. To determine those arbitrary functions, it is necessary to consider the fluid boundary conditions at the top and bottom layer and the continuity conditions across each layer.

At $y = 0$ there is fixed impermeable plate. Consequently, there will be no–slip and no–flow, ie $u^r_1 = 0$ and $v^r_1 = 0$. Applying these conditions to (A.18) and (A.19) result in

$$u^r_1 = -x(3A_1y^2 + 2B_1y) \tag{A.27}$$

$$v^r_1 = A_1y^3 + B_1y^2. \tag{A.28}$$

At the first fibre-resin interface $y = h_1$ we equate $p^r_1(h_1)$ and $p^f_2(h_1)$ (equations (A.17) and (A.24)) to obtain

$$\begin{aligned} &3\mu A_1(-x^2 + L^2) + 3\mu A_1h^2_1 + 2\mu B_1h_1 \\ &\qquad = -\frac{\mu Q_2}{2\kappa}(-x^2 + L^2) \end{aligned} \tag{A.29}$$

using $h_0 = 0$. Equating coefficients of $(-x^2 + L^2)$ gives

$$\frac{-\mu Q_2}{2\kappa} = 3\mu A_1 \text{ or } Q_2 = -6\kappa A_1 \tag{A.30}$$

Equating horizontal velocity components at the first interface, $y = h_1$, implies

$$\begin{aligned} u_2^f(x, h_1, t) &= u_1^r(x, h_1, t) \\ \text{ie.} \qquad -Q_2 x &= -(3A_1 h_1^2 + 2B_1 h_1)x \end{aligned}$$

or, using (A.30),

$$B_1 = \frac{-6A_1\kappa - 3A_1 h_1^2}{2h_1}. \tag{A.31}$$

Thus , the velocities and pressure in the first layer are

$$u_1^r(x, y, t) = -3A_1 xy \left[y - \dot{h}_1(t) - \frac{2\kappa}{h_1(t)}\right] \tag{A.32}$$

$$v_1^r(x, y, t) = \frac{1}{2}A_1 y^2 \left[2y - 3\left(h_1(t) + \frac{2\kappa}{h_1(t)}\right)\right] \tag{A.33}$$

$$p_1^r(x, y, t) = 3\mu A_1 \left[y^2 - x^2 + L^2 - \left(h_1(t) + \frac{2\kappa}{h_1(t)}\right) y\right]. \tag{A.34}$$

The equation of the second velocity component at $y = h_1$ then gives a differential equation for $\dot{h}_1$ ie.

$$\dot{h}_1 = -\frac{1}{2}A_1 h_1(t)\left(h_1^2(t) + 6\kappa\right) \tag{A.35}$$

At this point we have established (to within an arbitrary function of time) the rate at which the bottom-most resin layer decreases in thickness as resin is squeezed out at the sides (ie $x = \pm L$). We now focus on the top-most layer where we perform a similar analysis and a force balance.

Applying a no-slip condition and a no-flow condition (through the moving plate) at $y = h_{2n+1}$ results in, after some manipulations,

$$u^r_{2n+1} = -x(3A_{2n+1}(y^2 - h^2_{2n+1}) + 2B_{2n+1}(y - h_{2n+1})) \quad (A.36)$$

$$v^r_{2n+1} = \dot{h}_{2n+1} + A_{2n+1}(y^3 - 3h^2_{2n+1}y + 2h^3_{2n+1}) + B_{2n+1}(y - h_{2n+1})^2. \quad (A.37)$$

At the interface $y = h_{2n}(t)$ the pressures in the resin and fibre layer become

$$p^r_{2n+1} = 3\mu A_{2n+1}(-x^2 + L^2) \quad (A.38)$$

$$p^f_{2n} = \frac{-\mu Q_{2n}}{2\kappa}(h^2_{2n} - x^2 + L^2 - h^2_{2n-1}) - \frac{\mu R_{2n}}{\kappa}(h_{2n} - h_{2n-1}). \quad (A.39)$$

Equating, and comparing the coefficients of $x^2 - L^2$ and the remaining terms results in

$$Q_{2n} = -6\kappa A_{2n+1} \quad (A.40)$$

$$R_{2n} = 3\kappa A_{2n+1}(h_{2n} + h_{2n-1}). \quad (A.41)$$

Applying a force balance at the top plate, where the vertical applied force is $-F_a$, gives

$$\begin{aligned} F_a &= \int_{-L}^{L} p^r_{2n+1}(x, h_{2n+1}(t), t)dx \\ &= 3\mu A_{2n+1}\left(2L(h^2_{2n+1} + L^2 - h^2_{2n}) - \frac{2}{3}L^3\right) \\ &\quad + 4L\mu B_{2n+1}(h_{2n+1} - h_{2n}) \qquad \text{using } (A.17). \end{aligned}$$

Solving for B_{2n+1} gives

$$B_{2n+1} = \frac{F_a - 6\mu L A_{2n+1}((h^2_{2n+1} - h^2_{2n}) + \frac{2}{3}L^2)}{4\mu L(h_{2n+1} - h_{2n})}. \quad (A.42)$$

We now match the horizontal components of velocity, (A.25) and (A.36), on the interface $y = h_{2n}$ ie we equate

$$u^r_{2n+1}(x, h_{2n}(t), t) = u^f_{2n}(x, h_{2n}(t), t),$$

that is,

$$-x(3A_{2n+1}(h^2_{2n} - h^2_{2n+1}) + 2B_{2n+1}(h_{2n} - h_{2n+1}) = -Q_{2n}x, \tag{A.43}$$

Eliminating Q_{2n} using (A.40) yields

$$B_{2n+1} = -\frac{3}{2}A_{2n+1}\frac{(h^2_{2n} - h^2_{2n+1} + 2\kappa)}{(h_{2n} - h_{2n+1})}. \tag{A.44}$$

We now match the vertical components of velocity, (A.26) and (A.37), on the interface $y = h_{2n}$ ie. we equate

$$v^r_{2n+1}(x, h_{2n}(t), t) = v^f_{2n}(x, h_{2n}(t), t),$$

that is,

$$\dot{h}_{2n+1} + A_{2n+1}(h^3_{2n} - 3h^2_{2n+1}h_{2n} + 2h^3_{2n+1}) + B_{2n+1}(h_{2n} - h_{2n+1})^2$$

$$= \dot{h}_{2n} + Q_{2n}h_{2n} + R_{2n}.$$

Eliminating B_{2n+1}, Q_{2n} and R_{2n} using (A.44), (A.40) and (A.41) results in

$$\begin{aligned}\dot{h}_{2n+1} - \dot{h}_{2n} \;=\; & -A_{2n+1}(h^3_{2n} - 3h^2_{2n+1}h_{2n} + 2h^3_{2n+1}) \\ & +\frac{3}{2}A_{2n+1}\left(h_{2n} + h_{2n+1} + \frac{2\kappa}{(h_{2n} - h_{2n+1})}\right)(h_{2n} - h_{2n+1})^2 \\ & -6\kappa A_{2n+1}h_{2n} + 3\kappa A_{2n+1}(h_{2n} + h_{2n-1}).\end{aligned} \tag{A.45}$$

To determine the unknown A_{2n+1} we must equate (A.42) to (A.44) which results in

$$\frac{F_a - 6\mu L A_{2n+1}((h_{2n+1}^2 - h_{2n}^2) + \frac{2}{3}L^2)}{4\mu L(h_{2n+1} - h_{2n})} = -\frac{3}{2}\frac{A_{2n+1}(h_{2n}^2 - h_{2n+1}^2 + 2\kappa)}{(h_{2n} - h_{2n+1})},$$

or, upon rearranging and simplifying,

$$A_{2n+1} = \frac{F_a}{4\mu L(3\kappa + L^2)}. \tag{A.46}$$

Eliminating B_{2n+1} in (A.36),(A.37) and (A.17) (with $k = n$) using (A.44) results in

$$\begin{aligned} u_{2n+1}^r(x,y,t) &= -3A_{2n+1}x\Big(y - h_{2n+1}(t)\Big) \times \\ &\qquad \Big(y - h_{2n}(t) + \frac{2\kappa}{h_{2n+1}(t) - h_{2n}(t)}\Big) \end{aligned} \tag{A.47}$$

$$\begin{aligned} v_{2n+1}^r(x,y,t) &= \dot{h}_{2n+1}(t) + A_{2n+1}\Big[y^3 - 3h_{2n+1}^2(t)y \\ &\quad +2h_{2n+1}^3(t) - \frac{3}{2}\Big(y - h_{2n+1}(t)\Big)^2 \times \\ &\quad \Big(h_{2n}(t) + h_{2n+1}(t) - \frac{2\kappa}{h_{2n+1}(t) - h_{2n}(t)}\Big)\Big] \end{aligned} \tag{A.48}$$

$$\begin{aligned} p_{2n+1}^r(x,y,t) &= 3\mu A_{2n+1}\Big[y^2 - x^2 + L^2 - h_{2n}^2(t) - \Big(y - h_{2n}(t)\Big) \times \\ &\quad \Big(h_{2n}(t) + h_{2n+1}(t) - \frac{2\kappa}{h_{2n+1}(t) - h_{2n}(t)}\Big)\Big] \end{aligned} \tag{A.49}$$

We are now in the position to tackle the general $2k$ saturated fibre layer and the $2k+1$ resin layer. The expressions for the pressure and velocity in the resin layer are given by (A.17) - (A.19) while the expressions for the pressure and velocity in the saturated fibre layer are given by (A.24) - (A.26). We now equate pressure and velocity at the interface $y = h_{2k}$. Matching the pressure gives

$$p_{2k+1}^r(x, h_{2k}(t), t) = p_{2k}^f(x, h_{2k}(t), t)$$

or

$$3\mu A_{2k+1}(-x^2+L^2) = -\mu\frac{Q_{2k}}{2\kappa}(h_{2k}^2-x^2-h_{2k-1}^2+L^2) - \mu\frac{R_{2k}}{\kappa}(h_{2k}-h_{2k-1}). \quad \text{(A.50)}$$

Comparing coefficients of $(-x^2+L^2)$ yield

$$Q_{2k} = -6\kappa A_{2k+1} \quad \text{(A.51)}$$

and comparing the remaining terms give

$$R_{2k} = 3\kappa A_{2k+1}(h_{2k}+h_{2k-1}). \quad \text{(A.52)}$$

Matching the horizontal velocity components, that is,

$$u_{2k+1}^r(x,h_{2k}(t),t) = u_{2k}^f(x,h_{2k}(t),t),$$

gives

$$-x\left(3A_{2k+1}h_{2k}^2+2B_{2k+1}h_{2k}+C_{2k+1}\right) = -xQ_{2k}$$

or

$$C_{2k+1} = -6\kappa A_{2k+1}-3A_{2k+1}h_{2k}^2-2B_{2k+1}h_{2k}. \quad \text{(A.53)}$$

Similarly, matching the vertical velocity components, that is,

$$v_{2k+1}^r(x,h_{2k+1}(t),t) = v_{2k}^f(x,h_{2k}(t),t),$$

gives

$$D_{2k+1} = \dot{h}_{2k}+3\kappa A_{2k+1}(h_{2k}+h_{2k-1})+2A_{2k+1}h_{2k}^3+B_{2k+1}h_{2k}^2. \quad \text{(A.54)}$$

The next step involves the matching of the pressure and velocity components at the interface $y = h_{2k+1}$.

Matching the pressure at $y = h_{2k+1}$ (from (A.17) and (A.24)) gives

$$p^r_{2k+1}(x, h_{2k+1}(t), t) \;=\; p^f_{2k+2}(x, h_{2k+1}(t), t),$$

that is,

$$\begin{aligned} &3\mu A_{2k+1}(h^2_{2k+1} - x^2 + L^2 - h^2_{2k}) + 2\mu B_{2k+1}(h_{2k+1} - h_{2k}) \\ &\quad = \; -\frac{\mu}{2\kappa} Q_{2k+2}(-x^2 + L^2). \end{aligned} \tag{A.55}$$

Equating the coefficients of $(-x^2 + L^2)$ yield

$$Q_{2k+2} \;=\; -6\kappa A_{2k+1} \tag{A.56}$$

while equating the coefficients of the remaining terms give

$$B_{2k+1} \;=\; -\frac{3}{2} A_{2k+1}(h_{2k+1} + h_{2k}). \tag{A.57}$$

Matching the horizontal velocity components from (A.18) and (A.25) at $y = h_{2k+1}$ gives

$$u^r_{2k+1}(x, h_{2k+1}(t), t) \;=\; u^f_{2k+2}(x, h_{2k+1}(t), t),$$

that is,

$$-x(3A_{2k+1}h^2_{2k+1} + 2B_{2k+1}h_{2k+1} + C_{2k+1}) \;=\; -Q_{2k+2}x$$

which gives

$$C_{2k+1} \;=\; Q_{2k+2} - 3A_{2k+1}h^2_{2k+1} - 2B_{2k+1}h_{2k+1}. \tag{A.58}$$

Elimination of Q_{2k+2} and B_{2k+1} using (A.56) and (A.57) results in

$$C_{2k+1} = (-6\kappa + 3h_{2k}h_{2k+1})A_{2k+1}. \tag{A.59}$$

Matching the vertical velocity components (from (A.19) and (A.26)) at $y = h_{2k+1}$ gives

$$v^r_{2k+1}(x, h_{2k+1}(t), t) = v^f_{2k+2}(x, h_{2k+1}(t), t),$$

that is,

$$\begin{aligned} A_{2k+1}h^3_{2k+1} + B_{2k+1}h^2_{2k+1} + C_{2k+1}h_{2k+1} + D_{2k+1} \\ = \dot{h}_{2k+2} + Q_{2k+2}h_{2k+1} + R_{2k+2}. \end{aligned} \tag{A.60}$$

Elimination of $D_{2k+1}, Q_{2k+2}, B_{2k+1}$ and C_{2k+1} using (A.54), (A.56), (A.57) and (A.59) respectively allows us to solve for R_{2k+2} :

$$\begin{aligned} R_{2k+2} = {} & 3A_{2k+1}\kappa(h_{2k} + h_{2k-1}) \\ & -\frac{1}{2}A_{2k+1}(h^3_{2k+1} - 3h^2_{2k+1}h_{2k} - h^3_{2k} + 3h^2_{2k}h_{2k+1}) \\ & -\dot{h}_{2k+2} + \dot{h}_{2k}. \end{aligned} \tag{A.61}$$

Since the saturated fibre layers are being treated as incompressible, a pressure balance may be applied over the fibre layer lying between $y = h_{2k+1}$ and $y = h_{2k+2}$, that is,

$$\int_{-L}^{L} \Big(p^f_{2k+2}(x, h_{2k+2}(t), t) - p^f_{2k+2}(x, h_{2k+1}(t), t) \Big) dx = 0.$$

Substituting from (A.24) (with k replaced by $k+1$) and integrating yields

$$\frac{-\mu Q_{2k+2}}{\kappa}(h^2_{2k+2} - h^2_{2k+1}) - \frac{\mu R_{2k+2}}{\kappa}(h_{2k+2} - h_{2k+1}) = 0.$$

Elimination of Q_{2k+2} using (A.56) then gives

$$R_{2k+2} = 3\kappa A_{2k+1}(h_{2k+2} + h_{2k+1}). \tag{A.62}$$

Equations (A.51) and (A.56) imply that $Q_{2k} = Q_{2k+2}$. Furthermore, they also imply that $A_{2k+1} = A_{2k-1}$. But $k(1 \leq k \leq n)$ is arbitrary. Thus we may set

$$A_{2n+1} = A_{2n-1} = \ldots = A_3 = A_1 = A, \text{ say.}$$

However, from (A.46)

$$A_{2n+1} = \frac{F_a}{4\mu L(3\kappa + L^2)}$$

and so

$$A = \frac{F_a}{4\mu L(3\kappa + L^2)}. \tag{A.63}$$

Hence, eliminating D_{2k+1}, B_{2k+1} and C_{2k+1} in (A.17)-(A.19) using (A.54),(A.57) and (A.59) respectively yields

$$u^r_{2k+1}(x,y,t) = -3Ax\Big[\Big(y - h_{2k}(t)\Big)\Big(y - h_{2k+1}(t)\Big) - 2\kappa\Big], \tag{A.64}$$

$$\begin{aligned} v^r_{2k+1}(x,y,t) = {} & \dot{h}_{2k}(t) - 3\kappa A\Big[2y - \Big(h_{2k-1}(t) + h_{2k}(t)\Big)\Big] \\ & + A\left[y^3 - \frac{3}{2}\Big(h_{2k}(t) + h_{2k+1}(t)\Big)y^2 + 3h_{2k}(t)h_{2k+1}(t)y\right. \\ & \left. + \frac{1}{2}h^3_{2k}(t) - \frac{3}{2}h^2_{2k}(t)h_{2k+1}(t)\right], \end{aligned} \tag{A.65}$$

$$p^r_{2k+1}(x,y,t) = 3\mu A\Big[\Big(y - h_{2k}(t)\Big)\Big(y - h_{2k+1}(t)\Big) - x^2 + L^2\Big]. \tag{A.66}$$

In the saturated fibre layer, substituting (A.56) and (A.61) into (A.24)-(A.26) yields

$$u^f_{2k}(x,y,t) = 6\kappa Ax \tag{A.67}$$

$$v^f_{2k}(x,y,t) = \dot{h}_{2k}(t) - 3\kappa A\Big[2y - \Big(h_{2k-1}(t) + h_{2k}(t)\Big)\Big] \quad \text{(A.68)}$$

$$p^f_{2k}(x,y,t) = 3\mu A\Big[\Big(y - h_{2k-1}(t)\Big)\Big(y - h_{2k}(t)\Big) - x^2 + L^2\Big] \quad \text{(A.69)}$$

Equating (A.61) and (A.62) gives, after rearrangement,

$$\dot{h}_{2k+2} - \dot{h}_{2k} = -3\kappa A(h_{2k+2} + h_{2k+1} - h_{2k} - h_{2k-1}) - \frac{1}{2}A(h_{2k+1} - h_{2k})^3. \quad \text{(A.70)}$$

Finally, we recall our assumption that the prepreg is non-deformable, that is,

$$h_{2k} = h_{2k-1} + d_k,\ k = 1, 2, \ldots, n. \quad \text{(A.71)}$$

This, in turn, implies that

$$\dot{h}_{2k} = \dot{h}_{2k-1},\ k = 1, 2, \ldots, n. \quad \text{(A.72)}$$

The system of differential equations (A.70) may be rewritten, on elimination of h_{2k-1} and h_{2k+2} using (A.71) and (A.72), as

$$\dot{h}_{2k+1} - \dot{h}_{2k} = -\frac{1}{2}A\Big[(h_{2k+1} - h_{2k})^3 + 6\kappa(2h_{2k+1} - 2h_{2k} + d_k + d_{k+1})\Big], \quad k = 1, 2, \ldots, n-1 \quad \text{(A.73)}$$

where A is given by (A.63).

Simplifying (A.45) and using (A.71) yields

$$\dot{h}_{2n+1} - \dot{h}_{2n} = -\frac{1}{2}A\Big[(h_{2n+1} - h_{2n})^3 + 6\kappa\,(h_{2n+1} - h_{2n} + d_n)\Big]. \quad \text{(A.74)}$$

To close this system we also require (A.35)

$$\dot{h}_1 = -\frac{1}{2}Ah_1\left(h_1^2 + 6\kappa\right).$$

together with the fact that $\dot{h}_{2n+1} = V$ say, a known measurable velocity. Initial conditions $h_{2k}(0), k = 1, 2, \ldots, n$, are simply obtained from the initial thickness of the resin.

Appendix B

Derivation of RFI Flow Equations.

We first note that an "internal" layer, whether it be fibre or resin has (geometrical) symmetry. The bottom resin layer (k=1) and the top layer ($k = 2n+1$) must be considered separately.
We begin, however, by making a number of observations for all layers.

Firstly, in the fibre-free $(2k-1)$ layer of resin, integrating the incompressibilty condition (3.1) yields

$$v^r_{2k-1} = v^r_{2k-1}(x,t) \quad \text{(i.e. } v^r_{2k-1} \text{ is not a function of } y\text{)}$$

and integrating the momentum equation (3.2) yields

$$p^r_{2k-1} = p^r_{2k-1}(y,t) \quad \text{(i.e. } p^r_{2k-1} \text{ is not a function of } x\text{).} \tag{B.1}$$

Hence, differentiating (B.1) with respect to x, reduces the Stoke's equation (3.3) to

$$\frac{\partial^3 v^r_{2k-1}}{\partial x^3} = 0$$

which, upon integration, yields

$$v^r_{2k-1}(x,t) \;=\; A_{2k-1}(t)x^2 + B_{2k-1}(t)x + C_{2k-1}(t). \tag{B.2}$$

Similarly, in a typical (either upper or lower) wetted regions of the $2k$ fibre layer, defined by (3.4), integrating (3.5) and (3.6) respectively yields

$$v^{w,i}_{2k} \;=\; v^{w,i}_{2k}(x,t) \tag{B.3}$$

$$p^{w,i}_{2k} \;=\; p^{w,i}_{2k}(y,t) \tag{B.4}$$

where $i = u, l$ denotes upper or lower regions respectively. Hence, differentiating (3.7) with respect to y gives,

$$\frac{\partial^2}{\partial y^2} p^{w,i}_{2k}(y,t) \;=\; 0$$

which on integrating the above yields the pressure

$$p^{w,u}_{2k}(y,t) \;=\; Q^u_{2k}y + R^u_{2k}\ , \tag{B.5}$$

$$p^{w,l}_{2k}(y,t) \;=\; Q^l_{2k}y + R^l_{2k}\ , \tag{B.6}$$

where Q and R are functions of t.

Further, the velocity expressions in the lower and upper wetted regions may be obtained from (3.7)

$$v^{w,u}_{2k}(t) \;=\; \dot{h}_{2k}(t) - \frac{\kappa}{\mu} Q^u_{2k}\ , \tag{B.7}$$

$$v^{w,l}_{2k}(t) \;=\; \dot{h}_{2k-1}(t) - \frac{\kappa}{\mu} Q^l_{2k}. \tag{B.8}$$

The dependence of $p^r_{2k-1}(y,t)$ and $v^r_{2k-1}(x,t)$ on t only will now be established. Recall that

$$v^r_{2k-1}(x,t) \;=\; A_{2k-1}(t)x^2 + B_{2k-1}(t)x + C_{2k-1}(t) \tag{B.9}$$

and

$$v_{2k}^{w,l}(x,t) \;=\; \dot{h}_{2k-1}(t) - \frac{\kappa}{\mu} Q_{2k}^{l}(t). \tag{B.10}$$

At $y = h_{2k-1}(t)$ the continuity of the normal velocity is assumed, that is

$$v_{2k-1}^{r}(x,t) \;=\; v_{2k}^{w,l}(x,t) \tag{B.11}$$

which implies, upon equating coefficients of powers of x,

$$A_{2k-1} \;=\; B_{2k-1} \;=\; 0 \tag{B.12}$$

and

$$C_{2k-1} \;=\; \dot{h}_{2k-1}(t) - \frac{\kappa}{\mu} Q_{2k}^{l}(t). \tag{B.13}$$

Thus $v_{2k-1}^{r}(x,t)$ is a function of t only, and henceforth shall be denoted by $v_{2k-1}^{r}(t)$. Note that this argument holds for all $k = 1, 2, \ldots, n$.
(The assumption of continuity of normal velocity is only really valid for high porosity (i.e. $\phi \sim 1$); the more accurate requirement might be continuity of flux that is

$$\frac{1}{\phi} v_{2k-1}^{r}(x,t) \;=\; v_{2k}^{w,l}(x,t) \;\text{ etc}).$$

Now consider the pressure in the general resin layer.
From (3.3)

$$\frac{\partial}{\partial y} p_{2k-1}^{r} \;=\; \frac{\partial^2}{\partial x^2} v_{2k-1}^{r} \;=\; 0 \tag{B.14}$$

using the fact that v_{2k-1}^{r} has now been shown to be a function of t only. This demonstrates that p_{2k-1}^{r} is independent of y. However, from (3.2), p_{2k-1}^{r} is also

independent of x, and so can only be a function of t.
Henceforth, we shall write

$$p^r_{2k-1}(y,t) \;=\; p^r_{2k-1}(t).$$

Note again that this is true for all resin layers, $k = 1, 2, \ldots, n$.
The fact that the $p^r_{2n+1}(y,t)$ is also a function of t only is established later (eg. see (B.39)).

Now from (B.5), applying the zero pressure condition of the upper free surface, $y = \delta_{2k}(t)$, yields

$$R^u_{2k} \;=\; -\,Q^u_{2k}\delta_{2k}(t). \tag{B.15}$$

The pressure is assumed to be continuous on the interface $y = h_{2k}(t)$, that is,

$$p^r_{2k+1}(t) \;=\; p^{w,u}_{2k}(h_{2k}(t),t) \;=\; Q^u_{2k}h_{2k}(t) + R^u_{2k} \tag{B.16}$$

using (B.5). However, from (B.15) we have

$$p^r_{2k+1}(t) \;=\; Q^u_{2k}(h_{2k}(t) - \delta_{2k}(t)). \tag{B.17}$$

(Note since we have shown p^r_{2k+1} is independent of y, this is true for all $y \in [h_{2k}, h_{2k+1}]$.)

But, imposing the free surface kinematic condition, (3.13), in the upper wetted $2k$ fibrous layer, gives

$$v^{w,u}_{2k}(t) \;=\; \dot{h}_{2k} + \phi(\dot{\delta}_{2k} - \dot{h}_{2k}) \tag{B.18}$$

and comparing this with (B.7) yields

$$Q^u_{2k} \;=\; -\,\frac{\mu\phi}{\kappa}(\dot{\delta}_{2k} - \dot{h}_{2k}). \tag{B.19}$$

Thus, inserting (B.19) into (B.17) gives

$$p^r_{2k+1}(t) \;=\; p^{w,u}_{2k}(h_{2k},t) \;=\; \frac{\mu\phi}{\kappa}(\dot{h}_{2k}-\dot{\delta}_{2k})(h_{2k}-\delta_{2k}). \tag{B.20}$$

Also, inserting (B.15) and (B.19) into (B.5) gives

$$p^{w,u}_{2k}(y,t) \;=\; \frac{\mu\phi}{\kappa}(\dot{h}_{2k}-\dot{\delta}_{2k})(y-\delta_{2k}). \tag{B.21}$$

We shall now consider $k=1$ separately.

At $y=0$ we have

$$v^r_1(t) \;=\; 0\,, \tag{B.22}$$

and since we have demonstrated that v^r is not a function of y (i.e. the resin in the bottom layer is static) we have

$$v^r_1(t) \;=\; 0 \;\text{ for all } y\in[\,0,h_1(t)\,].$$

At $y=h_1(t)$ we assume continuity of flow, that is

$$v^r_1(t) \;=\; v^{w,l}_2(t) \;=\; \dot{h}_1(t)-\frac{\kappa}{\mu}Q^l_2$$

which implies

$$\dot{h}_1(t)=\frac{\kappa}{\mu}Q^l_2. \tag{B.23}$$

However, we require the continuity of pressure across $y=h_1(t)$, that is

$$p^r_1(t) \;=\; p^{w,l}_2(h_1(t),t) \;=\; Q^l_2\;h_1(t)+R^l_2. \tag{B.24}$$

But the pressure $p^r_1(t)$ has been shown to be independent of y and so

$$\begin{aligned} p^r_1(t) \;&=\; Q^l_2h_1(t)+R^l_2 \quad \text{for all } y\in[0,h_1(t)] \\ &=\; \frac{\mu}{\kappa}\dot{h}_1(t)h_1(t)+R^l_2 \qquad \text{from (B.23).} \end{aligned} \tag{B.25}$$

Further on the free surface $y = \delta_1(t)$, there is zero pressure

$$p_2^{w,l}(\delta_1(t), t) \;=\; 0$$

which implies that

$$R_2^l \;=\; -\,Q_2^l \delta_1(t)$$

so that

$$p_1^r(t) \;=\; \frac{\mu}{\kappa}\dot{h}_1(t)\Big(h_1(t) - \delta_1(t)\Big). \tag{B.26}$$

At $y = \delta_1(t)$, there is also the kinematic condition that is

$$v_2^{w,l} - \dot{h}_1(t) \;=\; \phi\Big(\dot{\delta}_1(t) - \dot{h}_1(t)\Big). \tag{B.27}$$

But this expression is independent of y and so must hold for all $y \in [h_1(t), \delta_1(t)]$.

Equating (B.27) with the velocity $v_1^r(=0)$ at $y = h_1(t)$ gives

$$-\dot{h}_1(t) = \phi\Big(\dot{\delta}_1(t) - \dot{h}_1(t)\Big)$$

which, after rearranging and integrating, gives

$$(1 - \phi)h_1(t) + \phi\delta_1(t) = \textit{constant}.$$

The constant may be determined by applying the initial condition for the free surface

$$\delta_1(0) = h_1(0) = h_{1,0}$$

yielding

$$\delta_1(t) = \frac{\phi - 1}{\phi}h_1(t) + \frac{1}{\phi}h_{1,0}. \tag{B.28}$$

and so, eliminating $\delta_1(t)$ in (B.26), yields

$$p_1^r(t) = \frac{\mu}{\kappa\phi}\dot{h}_1(h_1 - h_{1,0}). \tag{B.29}$$

We consider the fibre layer $k = n$ where the velocity and pressure in the upper wetted layer are

$$v_{2n}^{w,u}(t) = \dot{h}_{2n}(t) - \frac{\kappa}{\mu}Q_{2n}^u, \tag{B.30}$$

$$p_{2n}^{w,u}(y,t) = Q_{2n}^u y + R_{2n}^u. \tag{B.31}$$

From the continuity conditions at the interface $y = h_{2n}(t)$, pressure is

$$p_{2n+1}^r(h_{2n},t) = Q_{2n}^u h_{2n} + R_{2n}^u. \tag{B.32}$$

Applying the zero free surface condition at $y = \delta_{2n}$ gives

$$0 = Q_{2n}^u \delta_{2n} + R_{2n}^u. \tag{B.33}$$

Hence,

$$R_{2n}^u = -Q_{2n}^u \delta_{2n}. \tag{B.34}$$

Applying the kinematic condition (3.13) at $y = \delta_{2n}$ gives

$$Q_{2n}^u = -\frac{\mu\phi}{\kappa}(\dot{\delta}_{2n} - \dot{h}_{2n}). \tag{B.35}$$

Hence, velocity and pressure in the $2n$ layer are

$$v_{2n}^{w,u}(t) = \dot{h}_{2n} + \phi(\dot{\delta}_{2n} - \dot{h}_{2n}), \tag{B.36}$$

$$p_{2n}^{w,u}(y,t) = -\frac{\mu\phi}{\kappa}(\dot{\delta}_{2n} - \dot{h}_{2n})(y - \delta_{2n}). \tag{B.37}$$

We now consider the topmost resin layer where the velocity of the top plate is $v^r_{2n+1}(t) = \dot{h}_{2n+1}(t)$. Matching this velocity with the velocity of the upper wetted fibre layer (B.7), at $y = h_{2n}$, yields

$$Q^u_{2n} = -\frac{\mu}{\kappa}(\dot{h}_{2n+1} - \dot{h}_{2n}). \tag{B.38}$$

In (B.5), applying the zero pressure condition at $y = \delta_{2n}(t)$ and substituting (B.38), $k = n$ gives,

$$p^r_{2n+1}(t) = p^{w,u}_{2n}(h_{2n}(t), t) = -\frac{\mu}{\kappa}(h_{2n} - \delta_{2n})(\dot{h}_{2n+1} - \dot{h}_{2n}). \tag{B.39}$$

We now turn our attention to the top resin layer, $y = h_{2n+1}$, where the applied force, $-F_a$ is opposed by the viscosity of the resin. A force balance over the top plate of length 2L gives

$$F_a = \int_{-L}^{L} p^r_{2n+1}(t)dx \tag{B.40}$$

and on integration yields

$$p^r_{2n+1}(t) = \frac{F_a}{2L}. \tag{B.41}$$

Since the pressure in this layer is a function of t only,

$$p^r_{2n+1}(t) = \frac{F_a}{2L} \quad \text{for} \quad y \in [h_{2n}, h_{2n+1}]. \tag{B.42}$$

Furthermore, since the fibre layers are assumed incompressible, the next resin layer will experience the same pressure and so on. We can therefore conclude that

$$p^r_1(t) = p^r_3(t) = \ldots = p^r_{2n+1}(t) = \frac{F_a}{2L}. \tag{B.43}$$

Equation (B.20) now becomes a differential equation in $h_{2k} - \delta_{2k}$

$$(\dot{h}_{2k} - \dot{\delta}_{2k})(h_{2k} - \delta_{2k}) \;=\; \frac{\kappa F_a}{2L\mu\phi}. \tag{B.44}$$

Integrating, and applying the initial condition $\delta_{2k}(0) = h_{2k}(0) = h_{2k,0}$, results in

$$\delta_{2k} \;=\; h_{2k} - \sqrt{\frac{\kappa F_a t}{L\mu\phi}}\;,\; k \;= 1, 2, \ldots, n. \tag{B.45}$$

From the geometry (see *Figure* (3.1)), $\delta_{2k} \leq h_{2k}$ and consequently the minus sign has been chosen. This relates the moving front from $\delta_{2k}(t)$ to $h_{2k}(t)$. However, we also require an expression for $\delta_{2k+1}(t)$. To obtain this we return to $p^r_{2k+1}(t)$ and $p^{w,l}_{2k+2}(t)$.

Requiring continuity at $y = h_{2k+1}(t)$ implies

$$p^r_{2k+1}(t) \;=\; p^{w,l}_{2k+2}(h_{2k+1}(t), t) \;=\; Q^l_{2k+2} h_{2k+1}(t) + R^l_{2k+2}. \tag{B.46}$$

From (B.6), applying the zero surface condition at the lower surface $y = \delta_{2k+1}$ implies

$$R^l_{2k+2} \;=\; -\, Q^l_{2k+2}\delta_{2k+1}(t). \tag{B.47}$$

Again, we have the kinematic condition (3.13)

$$v^{w,l}_{2k+2}(t) \;=\; \dot{h}_{2k+1} + \phi(\dot{\delta}_{2k+1} - \dot{h}_{2k+1}) \tag{B.48}$$

which implies

$$Q^l_{2k+2} \;=\; -\,\frac{\mu\phi}{\kappa}(\dot{\delta}_{2k+1} - \dot{h}_{2k+1}). \tag{B.49}$$

Thus

$$p^r_{2k+1}(t) \;=\; -\frac{\mu\phi}{\kappa}(\dot{\delta}_{2k+1} - \dot{h}_{2k+1})(h_{2k+1} - \delta_{2k+1}). \tag{B.50}$$

Using (B.43) we obtain the differential equation

$$(\dot{\delta}_{2k+1} - \dot{h}_{2k+1})(\delta_{2k+1} - h_{2k+1}) \;=\; \frac{\kappa F_a}{2L\mu\phi}. \tag{B.51}$$

Integrating the above yields

$$\frac{1}{2}(\delta_{2k+1} - h_{2k+1})^2 \;=\; \frac{\kappa F_a t}{2L\mu\phi} + constant. \tag{B.52}$$

But, constant $= 0$ since $h_{2k+1}(0) = \delta_{2k+1}(0) = h_{2k+1,0}$.

Therefore

$$\begin{aligned}(\delta_{2k+1} - h_{2k+1}) \;&=\; \pm\sqrt{\frac{\kappa F_a t}{L\mu\phi}} \\ &=\; -\sqrt{\frac{\kappa F_a}{L\mu\phi}} \text{ from physical/geometrical argument.}\end{aligned} \tag{B.53}$$

Rearranging the above gives,

$$\delta_{2k+1} = h_{2k+1} + \sqrt{\frac{\kappa F_a t}{L\mu\phi}}\;,\; k \;= 0, 1, \ldots, n-1. \tag{B.54}$$

For the general $2k+1$ resin and $2k$ fibre regions, we have

$$v^r_{2k+1} \;=\; v^{w,l}_{2k+2} \;=\; \dot{h}_{2k+1} + \phi(\dot{\delta}_{2k+1} - \dot{h}_{2k+1}) \tag{B.55}$$

$$v^{w,u}_{2k} \;=\; \dot{h}_{2k} + \phi(\dot{\delta}_{2k} - \dot{h}_{2k}). \tag{B.56}$$

At $y = h_{2k}$, $v^r_{2k+1} = v^{w,u}_{2k}$ so that

$$\dot{h}_{2k+1} - \dot{h}_{2k} + +\phi(\dot{\delta}_{2k+1} - \dot{h}_{2k+1}) - \phi(\dot{\delta}_{2k} - \dot{h}_{2k}) \;=\; 0 \tag{B.57}$$

or, upon rearranging,

$$\dot{h}_{2k+1} - \dot{h}_{2k} = \phi[\ (\dot{\delta}_{2k+1} - \dot{\delta}_{2k}) - (\dot{h}_{2k+1} - \dot{h}_{2k})\ ] \tag{B.58}$$

$$(\phi - 1)(\dot{h}_{2k+1} - \dot{h}_{2k}) = \phi(\dot{\delta}_{2k+1} - \dot{\delta}_{2k}) \tag{B.59}$$

$$= \phi\Big[\ \Big(\dot{h}_{2k+1} + \frac{1}{2}\sqrt{\frac{\kappa F_a}{L\mu\phi t}}\ \Big) - \Big(\dot{h}_{2k} - \frac{1}{2}\sqrt{\frac{\kappa F_a}{L\mu\phi t}}\ \Big)\ \Big] \tag{B.60}$$

$$= \phi\Big[\Big(\dot{h}_{2k+1} - \dot{h}_{2k}\Big) + \sqrt{\frac{\kappa F_a}{L\mu\phi t}}\ \Big]. \tag{B.61}$$

$$\text{Thus}\quad \dot{h}_{2k+1} - \dot{h}_{2k} = -\phi\sqrt{\frac{\kappa F_a}{L\mu\phi t}} \tag{B.62}$$

$$\text{and so}\quad \dot{h}_{2k+1} - \dot{h}_{2k} = -\sqrt{\frac{\kappa\phi F_a}{L\mu t}}. \tag{B.63}$$

Integrating and using

$$h_{2k+1} = h_{2k+1,0} \text{ and } h_{2k} = h_{2k,0} \text{ when } t = 0 \tag{B.64}$$

gives

$$h_{2k+1} - h_{2k} = h_{2k+2,0} - h_{2k,0} - 2\sqrt{\frac{\kappa\phi F_a t}{L\mu}}. \tag{B.65}$$

Consider (B.27), where now

$$\frac{F_a}{2L} = p_1^r(t) = \frac{\mu}{\kappa\phi}\dot{h}_1(h_1 - h_{1,0}). \tag{B.66}$$

Integrating this gives

$$h_1(t) = h_{1,0} - \sqrt{\frac{\kappa\phi F_a t}{\mu L}}. \tag{B.67}$$

We now prove the following:

$$h_{2k+1}(t) = h_{2k+1,0} - (2k+1)\sqrt{\frac{\kappa\phi F_a t}{\mu L}} \tag{B.68}$$

$$\delta_{2k+1}(t) = h_{2k+1,0} - (2k+1-\frac{1}{\phi})\sqrt{\frac{\kappa\phi F_a t}{\mu L}} \tag{B.69}$$

$$\delta_{2k}(t) = h_{2k,0} - (2k+1+\frac{1}{\phi})\sqrt{\frac{\kappa\phi F_a t}{\mu L}} \tag{B.70}$$

with $h_{2k} = h_{2k+1} + d$.

Consider

$$h_{2k+1}(t) = h_{2k+1,0} - (2k+1)\sqrt{\frac{\kappa\phi F_a t}{\mu L}},\ k = 0, 1, \ldots, n. \tag{B.71}$$

Setting $k = 0$, we obtain

$$h_1(t) = h_{1,0} - \sqrt{\frac{\kappa\phi F_a t}{\mu L}} \tag{B.72}$$

which is none other than (B.67).

Assume (B.71) is true for $k = \nu - 1$

$$h_{2\nu-1} = h_{2\nu-1,0} - (2\nu-1)\sqrt{\frac{\kappa\phi F_a t}{\mu L}}. \tag{B.73}$$

Thus (B.65) for $k = \nu$ becomes

$$\begin{aligned} h_{2\nu+1} &= h_{2\nu} + h_{2\nu+1,0} - h_{2\nu,0} - 2\sqrt{\frac{\kappa\phi F_a t}{\mu L}} \\ &= (h_{2\nu-1} + d) + h_{2\nu+1,0} - (h_{2\nu-1,0} + d) - 2\sqrt{\frac{\kappa\phi F_a t}{\mu L}} \\ &= \left(h_{2\nu-1,0} - (2\nu-1)\sqrt{\frac{\kappa\phi F_a t}{\mu L}}\right) + h_{2\nu+1,0} - h_{2\nu-1,0} - 2\sqrt{\frac{\kappa\phi F_a t}{\mu L}} \end{aligned}$$

$$= h_{2\nu+1,0} - (2\nu+1)\sqrt{\frac{\kappa\phi F_a t}{\mu L}} \tag{B.74}$$

which completes the induction argument.

From (B.54) we have

$$\delta_{2k+1}(t) = h_{2k+1}(t) + \sqrt{\frac{\kappa F_a t}{\mu\phi L}}. \tag{B.75}$$

Therefore

$$\begin{aligned}\delta_{2k+1}(t) &= \left(h_{2k+1,0} - (2k+1)\sqrt{\frac{\kappa\phi F_a t}{\mu L}}\right) + \frac{1}{\phi}\sqrt{\frac{\kappa\phi F_a t}{\mu L}} \\ &= h_{2k+1,0} - (2k+1-\frac{1}{\phi})\sqrt{\frac{\kappa\phi F_a t}{\mu L}}.\end{aligned} \tag{B.76}$$

Similarly

$$\begin{aligned}\delta_{2k}(t) &= h_{2k} - \sqrt{\frac{\kappa F_a t}{\mu\phi L}} \\ &= h_{2k-1} + d - \sqrt{\frac{\kappa F_a t}{\mu\phi L}} \\ &= h_{2k-1,0} - (2(k-1)+1)\sqrt{\frac{\kappa\phi F_a t}{\mu L}} + d - \frac{1}{\phi}\sqrt{\frac{\kappa\phi F_a t}{\mu L}} \\ &= h_{2k,0} - (2k-1+\frac{1}{\phi})\sqrt{\frac{\kappa\phi F_a t}{\mu L}}\end{aligned} \tag{B.77}$$

Thus (B.68)-(B.70) have been demonstrated to be true.

We now consider the top layer resin layer. Eliminating the pressure in (B.39) using (B.43) and eliminating $\delta_{2n}(t)$ using (B.45) with $k = n$ results in

$$\dot{h}_{2n+1} - \dot{h}_{2n} = -\sqrt{\frac{\kappa\phi F_a}{4L\mu t}}. \tag{B.78}$$

Integrating the above yields

$$h_{2n+1} = h_{2n} + h_{2n+1,0} - h_{2n,0} - \sqrt{\frac{\kappa\phi F_a t}{L\mu}}. \tag{B.79}$$

But

$$h_{2n} = h_{2n,0} - 2n\sqrt{\frac{\kappa\phi F_a t}{L\mu}}. \tag{B.80}$$

Hence

$$\begin{aligned} h_{2n+1} &= \left(h_{2n,0} - 2n\sqrt{\frac{\kappa\phi F_a t}{L\mu}}\right) + h_{2n+1,0} - h_{2n,0} - \sqrt{\frac{\kappa\phi F_a t}{L\mu}} \\ &= h_{2n+1,0} - (2n+1)\sqrt{\frac{\kappa\phi F_a t}{L\mu}}. \end{aligned} \tag{B.81}$$

In summary, the heights of the resin-fibre interfaces and the free surface flow fronts for a typical k layer, are

$$h_{2k+1} = h_{2k+1,0} - (2k+1)\sqrt{\frac{\kappa\phi F_a t}{L\mu}}\ ,\ k = 0, 1, \ldots, n \tag{B.82}$$

$$h_{2k} = h_{2k-1} + d\ ,\ k = 1, 2, \ldots, n \tag{B.83}$$

$$\delta_{2k+1} = h_{2k+1,0} - \left(2k + 1 - \frac{1}{\phi}\right)\sqrt{\frac{\kappa\phi F_a t}{L\mu}}\ ,\ k = 0, 1, \ldots, n-1 \tag{B.84}$$

$$\delta_{2k} = h_{2k,0} - \left(2k - 1 + \frac{1}{\phi}\right)\sqrt{\frac{\kappa\phi F_a t}{L\mu}}\ ,\ k = 1, 2, \ldots, n \tag{B.85}$$

where recall that n is the total number of fibre layers and d is the constant thickness of a fibre layer.

Thus, differentiating (B.82)-(B.84), we obtain both velocities of the fibre layers and the free surface fronts

$$\dot{h}_{2k+1} = -\left(k + \frac{1}{2}\right)\sqrt{\frac{\kappa\phi F_a}{L\mu t}}\ ,\ k = 0, 1, \ldots, n \tag{B.86}$$

$$\dot{h}_{2k} = \dot{h}_{2k-1}\ ,\ k=1,2,\ldots,n \tag{B.87}$$

$$\dot{\delta}_{2k+1} = -\frac{1}{2}\Big(2k+1-\frac{1}{\phi}\Big)\sqrt{\frac{\kappa\phi F_a}{L\mu t}}\ ,\ k=0,1,\ldots,n \tag{B.88}$$

$$\dot{\delta}_{2k} = -\frac{1}{2}\Big(2k-1+\frac{1}{\phi}\Big)\sqrt{\frac{\kappa\phi F_a}{L\mu t}}\ ,\ k=1,2,\ldots,n. \tag{B.89}$$

Appendix C

ADI Method

The purpose of this appendix is simply to illustrate the essential ideas of the implementation of the ADI procedure. We shall consider the application of ADI to the prepreg case (see Chapter 2). For clarity of exposition, both convection and reaction are neglected. It is not difficult to reinstate them, but the expressions become unnecessarily complicated and clarity is lost. The non-dimensionalised heat equation, for an isotropic medium, is rewritten below as

$$\frac{\partial T}{\partial t} = a\left(\frac{\partial^2 T}{\partial x^2} + \frac{\partial^2 T}{\partial y^2}\right), \tag{C.1}$$

where a is the dimensionless constant defined by

$$a = \begin{cases} J_f = D & \text{in saturated fibre region} \\ J_r = 1 & \text{in resin region.} \end{cases} \tag{C.2}$$

In equation (C.1), $T = T(x, y, t)$ represents the temperature of in the respective domains of the fibre-free and fibre regions with the initial and boundary conditions given by equations (2.69)-(2.72).

Discretizing equation (C.1) using the ADI implicit scheme given in Douglas-Rachford split form (see equations (2.80)-(2.83), see also McKee et al. [59]),

gives

$$\left[1 - \frac{ra}{2}\delta_x^2\right] T_{i,j}^{m+1^*} = \left[1 + sa\delta_y^2 + \frac{ra}{2}\delta_x^2\right] T_{i,j}^m \tag{C.3}$$

$$\left[1 - \frac{sa}{2}\delta_y^2\right] T_{i,j}^{m+1} = T_{i,j}^{m+1^*} - \left[\frac{sa}{2}\delta_y^2\right] T_{i,j}^m. \tag{C.4}$$

At each time step this is a two-stage process. An intermediate temperature, $T_{i,j}^{m+1^*}$, is calculated along lines in the x direction (omitting the interfaces) and the final temperature, $T_{i,j}^{m+1}$, is computed along lines the y direction. The intermediate temperature at the interfaces (see equations (2.73)-(2.74)) is calculated from

$$(T_f)_{i,j}^{m+1^*} = (T_r)_{i,j}^{m+1^*} \tag{C.5}$$

$$D^* \left((T_f)_{i,j+1}^{m+1^*} - (T_f)_{i,j}^{m+1^*}\right) = (T_r)_{i,j}^{m+1^*} - (T_r)_{i,j-1}^{m+1^*} \tag{C.6}$$

for $\{i,j\} \in E_k, k = 1, 2, \ldots, 2n$, where E_k denotes the set of nodal points on the k^{th} interface. The subscripts f and r denote the fibre and resin layers respectively.

The temperature, $T_{i,j}^m$, denotes an approximation to $T(i\Delta x, j\Delta y, m\Delta t)$ which is defined on a moving mesh with mesh ratios

$$r = \frac{\Delta t}{(\Delta x)^2}, \quad s = \frac{\Delta t}{(\Delta y)^2}. \tag{C.7}$$

Note that the explicit dependence upon time is not displayed; it is only Δy in the resin layers that decreases with increasing time, as the resin is squeezed from the resin layer.

The central difference is defined as

$$\delta_x^2 T_{i,j}^m = T_{i+1,j}^m - 2T_{i,j}^m + T_{i-1,j}^m \tag{C.8}$$

with the corresponding definition for δ_y^2.

To illustrate the ADI procedure, consider the case of a n layer prepreg consisting of alternate layers of impregnated fibre on a simple rectangular grid of $\mu[2n(\nu+1)+\nu]$ nodes where n is the number of prepregs, μ is the number of horizontal nodes and ν is the number of vertical internal nodes in each layer of resin and fibre (see *Figure* C.1). The number of nodes are invariant to time, that is Δy decreases in such a manner as to maintain ν is fixed.

Applying the above difference equations to each layer of the fibre and the resin for the intermediate time step yields

$$(\mathbf{I}+\frac{ra}{2}\mathbf{H})\mathbf{T}^{\mathbf{m+1^*}} = (\mathbf{I}-\frac{ra}{2}\tilde{\mathbf{H}}-sa\mathbf{V})\mathbf{T}^{\mathbf{m}}+\mathbf{b} \tag{C.9}$$

where

$$\mathbf{H}=\begin{bmatrix}
\mathcal{H}_1 & & & & & & & & & & & \\
& \ddots & & & & & & & & & & \\
& & \mathcal{H}_\nu & & & & & & & & & \\
& & [\ \ \mathcal{K}\ \ ] & & & & & & & & & \\
& & & \mathcal{H}_1 & & & & & & & & \\
& & & & \ddots & & & & & & & \\
& & & & & \mathcal{H}_\nu & & & & & & \\
& & & & & [\ \ \mathcal{K}\ \ ] & & & & & & \\
& & & & & & \mathcal{H}_1 & & & & & \\
& & & & & & & \ddots & & & & \\
& & & & & & & & \ddots & & & \\
& & & & & & & & & \mathcal{H}_\nu & & \\
& & & & & & & & & [\ \ \mathcal{K}\ \ ] & & \\
& & & & & & & & & & \mathcal{H}_1 & \\
& & & & & & & & & & & \ddots \\
& & & & & & & & & & & & \mathcal{H}_\nu
\end{bmatrix},$$

for the $2n+1$ layers. The matrix $\mathbf{H}$ is $\mu[2n(\nu+1)+\nu] \times \mu[2n(\nu+1)+\nu]$. The block matrices $\mathcal{H}_k,\ k = 1, 2, \ldots, \nu$ are defined as

$$\mathcal{H}_\mathbf{k} = \begin{bmatrix} 2 & -2 & & & \\ -1 & 2 & -1 & & \\ & \ddots & \ddots & \ddots & \\ & & -1 & 2 & -1 \\ & & & -2 & 2 \end{bmatrix}_{\mu\times\mu}, \ k = 1, 2, \ldots, \nu. \tag{C.10}$$

where the '-2's appear as a consequence of the derivative boundary conditions. The block matrix $\mathcal{K}$ is

$$\mathcal{K} = \begin{bmatrix} 1 & \ldots & -(D^*+1) & \ldots & & & D^* & \ldots \\ & 1 & \ldots & & -(D^*+1) & \ldots & & D^* & \ldots \\ & & \ddots & & & \ddots & & & \ddots \\ \ldots & & 1 & \ldots & & & -(D^*+1) & \ldots & \ldots \end{bmatrix}$$

that is,

$$\mathcal{K} = \begin{bmatrix} \mathbf{I}_\mu \ \vdots \ -(1+D^*)\mathbf{I}_\mu \ \vdots \ D^*\mathbf{I}_\mu \end{bmatrix}_{\mu\times 3\mu}.$$

Note that the matrix, $\mathcal{K}$ is a $\mu \times 3\mu$ matrix and 'overlaps' with the previous matrix $\mathcal{H}_\nu$ and the next matrix $\mathcal{H}_1$. Thus $\mathbf{H}$ is a block matrix except at the 'interface'. This allows the essential idea of ADI to be exploited, the values on the interfaces or the intermediate step being computed explicitly in Gauss-Seidel fashion after the intermediate temperatures of the resin and fibre have been calculated. Using the latest updates to calculate the intermediate

temperature on the interfaces implies that $\tilde{\mathbf{H}}$ takes the form of:

$$\tilde{\mathbf{H}} = \begin{bmatrix}
\mathcal{H}_1 & & & & & & & & & & & & & & & & & & & \\
& \ddots & & & & & & & & & & & & & & & & & & \\
& & \mathcal{H}_\nu & & & & & & & & & & & & & & & & & \\
& & [\quad 0 \quad] & & & & & & & & & & & & & & & & & \\
& & & \mathcal{H}_1 & & & & & & & & & & & & & & & & \\
& & & & \ddots & & & & & & & & & & & & & & & \\
& & & & & \mathcal{H}_\nu & & & & & & & & & & & & & & \\
& & & & & [\quad 0 \quad] & & & & & & & & & & & & & & \\
& & & & & & \mathcal{H}_1 & & & & & & & & & & & & & \\
& & & & & & & \ddots & & & & & & & & & & & \\
& & & & & & & & \ddots & & & & & & & & & & \\
& & & & & & & & & \mathcal{H}_\nu & & & & & & & & & \\
& & & & & & & & & [\quad 0 \quad] & & & & & & & & & \\
& & & & & & & & & & \mathcal{H}_1 & & & & & & & & \\
& & & & & & & & & & & \ddots & & & & & & & \\
& & & & & & & & & & & & \mathcal{H}_\nu & & & & & & \\
& & & & & & & & & & & & [\quad 0 \quad] & & & & & & \\
& & & & & & & & & & & & & \mathcal{H}_1 & & & & & \\
& & & & & & & & & & & & & & \ddots & & & & \\
& & & & & & & & & & & & & & & \mathcal{H}_\nu & & &
\end{bmatrix},$$

where $[\quad \mathbf{0} \quad]$ is the $\mu \times 3\mu$ null matrix.

The matrix $\tilde{\mathbf{H}}$ is $\mu[2n(\nu+1)+\nu] \times \mu[2n(\nu+1)+\nu]$.

The matrix $\mathbf{V}$ is

$$\mathbf{V} = \begin{bmatrix} V_1 & & & & & & & & & & & & \\ & \mathcal{V}_2 & & & & & & & & & & & \\ & & \ddots & & & & & & & & & & \\ & & & \mathcal{V}_\nu & & & & & & & & & \\ & & & [\ \mathbf{0}\ ] & & & & & & & & & \\ & & & & \mathcal{V}_1 & & & & & & & & \\ & & & & & \ddots & & & & & & & \\ & & & & & & \ddots & & & & & & \\ & & & & & & & \mathcal{V}_\nu & & & & & \\ & & & & & & & [\ \mathbf{0}\ ] & & & & & \\ & & & & & & & & \mathcal{V}_1 & & & & \\ & & & & & & & & & \ddots & & & \\ & & & & & & & & & & \mathcal{V}_{\nu-1} & & \\ & & & & & & & & & & & V_\nu \end{bmatrix},$$

where

$$V_1 = \left[2\mathbf{I}_\mu \ \vdots \ -\mathbf{I}_\mu \right], \tag{C.11}$$

$$\mathcal{V}_\mathbf{k} = \left[-\mathbf{I}_\mu \ \vdots \ 2\mathbf{I}_\mu \ \vdots \ -\mathbf{I}_\mu \right], \ k = 1, \ldots, \nu, \tag{C.12}$$

and

$$V_\nu = \left[-\mathbf{I}_\mu \ \vdots \ 2\mathbf{I}_\mu \right]. \tag{C.13}$$

The matrix $\mathbf{V}$ is $\mu[2n(\nu+1)+\nu] \times \mu[2n(\nu+1)+\nu]$.

The vector $\mathbf{b}$ is

$$\mathbf{b} = [\ b_1, b_2, \ldots, b_\mu, 0, \ldots, 0, b_1, b_2, \ldots, b_\mu\ ]^T, \tag{C.14}$$

where

$$b_i \;=\; saT_c\,,\;\; i = 1, 2, \ldots, \mu. \tag{C.15}$$

In the intermediate step, the matrix H is almost tridiagonal. The individual matrices $\mathcal{H}_k$ are tridiagonal and the corresponding vector temperature values are computed directly using the Thomas algorithm (see Varga [63]). When this is accomplished, we return to the temparature nodes on the interfaces and then computed them explicitly from the values of $T_{i,j}^{m+1^*}$ which have already been computed.

To calculate the temperature value $T_{i,j}^{m+1}$, the order of the nodes are rearranged. Instead of an ordering along lines parallel to the x-axis, a new ordering is introduced along lines parallel to the y-axis. The resultant matrix is then block diagonal with each block a tridiagonal matrix each of which may be solved by the Thomas algorithm.

As time progresses, the resin layers are reduced (recall that the fibre layers are assumed incompressible and hence have a fixed thickness) and consequently in these regions the mesh moves. To take account of this, after each time step, the position of the mesh is computed and linear interpolation in the y-direction is employed to compute the corrected value of the temperature on that new mesh. The scheme for the final time step is

$$\left[\mathbf{I} + \frac{sa}{2}\tilde{\mathbf{V}}\right]\mathbf{T}^{\mathbf{m+1}} \;=\; \mathbf{T}^{\mathbf{m+1^*}} + \left[\frac{sa}{2}\tilde{\mathbf{V}}\right]\mathbf{T}^{\mathbf{m}}. \tag{C.16}$$

The tridiagonal matrix $\check{\mathbf{V}}$ can be expressed as

$$\check{\mathbf{V}} = \begin{bmatrix} V_1 \\ & \mathcal{V}_2 \\ & & \ddots \\ & & & \mathcal{V}_\nu \\ & & & [\ \mathcal{K}\ ] \\ & & & & \mathcal{V}_1 \\ & & & & & \ddots \\ & & & & & & \ddots \\ & & & & & & & \mathcal{V}_\nu \\ & & & & & & & [\ \mathcal{K}\ ] \\ & & & & & & & & \mathcal{V}_1 \\ & & & & & & & & & \ddots \\ & & & & & & & & & & \mathcal{V}_{\nu-1} \\ & & & & & & & & & & & V_\nu \end{bmatrix},$$

and the matrix $\mathbf{V}$ is

$$\mathbf{V} = \begin{bmatrix} V_1 \\ & \mathcal{V}_2 \\ & & \ddots \\ & & & \mathcal{V}_\nu \\ & & & [\ 0\ ] \\ & & & & \mathcal{V}_1 \\ & & & & & \ddots \\ & & & & & & \ddots \\ & & & & & & & \mathcal{V}_\nu \\ & & & & & & & [\ 0\ ] \\ & & & & & & & & \mathcal{V}_1 \\ & & & & & & & & & \ddots \\ & & & & & & & & & & \mathcal{V}_{\nu-1} \\ & & & & & & & & & & & V_\nu \end{bmatrix},$$

Note that this matrix is $\mu[2n(\nu+1)+\nu] \times \mu[2n(\nu+1)+\nu]$ and that V_1, V_ν and $\mathcal{V}_\mathbf{k}$, $(k = 1, 2, \ldots, \nu)$ have all been defined previously (eg. (C.11)-(C.13)).

The solution to the linear system of tridiagonal matrix is obtained directly using the Thomas algorithm (see Varga [63]).

For the matrix equation

$$\mathbf{Az} = \mathbf{b} \tag{C.17}$$

where

$$\mathbf{A} = \begin{bmatrix} d_1 & c_1 & 0 & \ldots & 0 \\ a_2 & d_2 & c_2 & & 0 \\ 0 & \ddots & \ddots & \ddots & 0 \\ \vdots & \ddots & a_{n-1} & d_{n-1} & c_{n-1} \\ 0 & \ldots & 0 & a_n & d_n \end{bmatrix} \text{ and } \mathbf{b} = \begin{bmatrix} b_1 \\ b_2 \\ \vdots \\ b_{n-1} \\ b_n \end{bmatrix}, \tag{C.18}$$

defining

$$w_1 = \frac{c_1}{d_1};\ w_i = \frac{c_i}{d_i - a_i w_{i-1}},\ 2 \leq i \leq n-1, \tag{C.19}$$

and

$$g_1 = \frac{b_1}{d_1};\ g_i = \frac{b_i - a_i g_{i-1}}{d_i - a_i w_{i-1}},\ 2 \leq i \leq n, \tag{C.20}$$

the components of z_i of the solution vector $\mathbf{z}$ are then given recursively by the following backward substitution procedure

$$z_n = g_n;\ z_i = g_i - w_i z_{i+1},\ 1 \leq i \leq n-1. \tag{C.21}$$

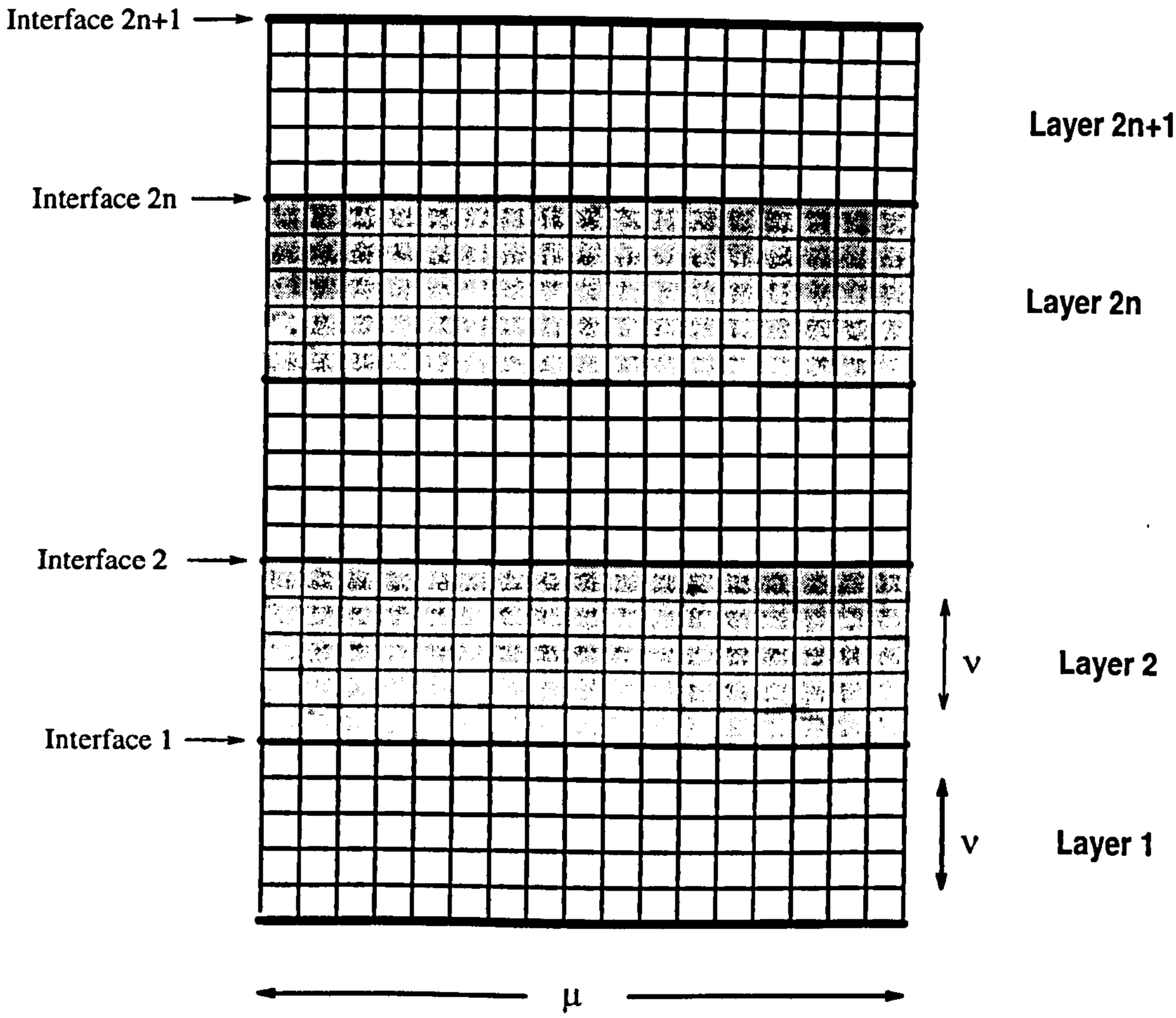

Figure C.1: Grid for n prepregs.

Bibliography

[1] Dominy, J., Structural Composites in Civil Gas Turbine Aero Engines, Composites Manufacturing, 1994, **5**, 2, 69-72.

[2] Mallick, P.K., FIBER REINFORCED COMPOSITES: Materials, Manufacturing and Design, Marcel Dekker, Inc., USA, 1993.

[3] Hoa, S.V., Computer-Aided Design of Polymer-Matrix Composite Structures, 1995, Marcel Dekker, Inc, New York.

[4] Seemann, W.H., Plastic Transfer Moulding Techniques for the Production of Fibre Reinforced Composites, 1989, US Patent No. 4902215.

[5] Williams, C., Summerscales, J. and Grove, S., Resin Infusion under Flexible Tooling (RIFT): a review, Composites Part A, 1996, **27A**, 517-524.

[6] Hasko, G., Dexter, H.B., Loos, A. and Kranbuehl, D., Application of Science-Based RTM for Fabricating Primary Aircraft Structural Elements, J. Advanced Materials, 1994, **26**, 1, 9-15.

[7] Guy, T.A., Sanger, K.B. and Ruskowski, E., Low Cost Fabrication Methods Applied to Low Observable Structure, AIAA-95-1156-CP, 1995, 1-7.

[8] Peters, S. T., Handbook of Composites, Chapman and Hall, UK, 1998.

[9] Ciriscioli, P.R. and Springer, G.S., Smart Autoclave Cure of Composites, Technomic, Lancaster, P.A., 1990.

[10] Lindt, J. T., Engineering Principles of the Formation of Epoxy Resin Composites, SAMPE Quarterly, 1982, October.

[11] Gutowski, T. G., A Resin Flow Fibre Deformation Model for Composites, SAMPE Quarterly, 1985,**16**, 4, 58-64.

[12] Loos, A.C. and Springer, G. S. , Curing of Epoxy Matrix, J. Composite Materials, 1982, **17**, 135-169.

[13] Gutowski, T. G., Morigaki, T. and Cai, Z., The Consolidation of Laminate Composites, J. Composite Materials, 1987, **21**, 172-188.

[14] Dave, R., Kardos, J. L. and Dudukovic, A Model for Resin Flow During Composite Processing: Part 1- General Mathematical Development, Polymer Composites, 1987, **8**, 1, 29-38.

[15] Dave, R., A Unified Approach to Modeling Resin Flow During Composite Processing, J. Composite Materials, 1990, **24**, 23-41.

[16] Young, W. B., Resin Flow Analysis in the Consolidation of Multi-Directional Laminated Composites, Polym. Comp., 1995, **16**, 3, 250-257.

[17] Young, W. B., Consolidation and Cure Simulations for Laminated Composites, Polymer Composites, 1996, **17**, 1, 142-148.

[18] Hojjati, M. and Hoa, S. V., Curing Simulation of Thick Thermosetting Composites, Composites Manufacturing, 1994, **5**, 3, 159-169.

[19] Kinsey, S. P. , Haji-Sheikh, A. and Lou, D. Y. S. , A Thermal Model for Cure of Thermoset Composites, J. Materials Processing Technology, 1997, **63**, 442-449.

[20] Kim, J.S. and Lee, D.G., Development of an Autoclave Cure Cycle with Cooling and Reheating Steps for Thick Thermoset Composite Laminates, J. Composite Materials, 1997, **31**, 22, 2264-2282.

[21] Ciriscioli, P. R., Wang,Q. and Springer,G. S. , Autoclave Curing - Comparisons of Model and Test Results, J. Composite Materials, 1987, **26**, 1, 90-102.

[22] Yi, S. and Hilton, H.H., Effects of Thermo-Mechanical Properties of Composites on Viscosity, Temperature and Degree of Cure in Thick Thermosetting Composite Laminates during Curing Process, J. Composite Materials, 1998, **32**, 7, 600-622.

[23] Ahn,K.J., Seferis, J.C., Price,J.O. and Berg,A.J., Permeation Measurements Through Prepreg Laminates, SAMPE Journal- Society for the Advancement of Material and Process Engineering, 1991, 27,6,p19-25.

[24] Harper,J.F., Miller,N.A. and Yap,S.C., The Influence of Temperature and Pressure during the Curing of Prepreg Carbon-Fibre Epoxy-Resin, Polymer-Plastics Technology and Engineering, 1993,23,4,pp. 269-275.

[25] Ambrosi, D. and Preziosi, L., Modelling Matrix Injection through Elastic Porous Preforms, Composites Part A, 1998, **29A**, 5-18.

[26] Givler, R.C. and Altobelli, S.A., A Determination of the Effective Viscosity for the Brinkman-Forchheimer Flow Model, J. Fluid Mech., 1994, **258**, 355-370.

[27] Nield, D. A. and Bejan, A. , Convection in Porous Media, Springer-Verlag, New York, 1992.

[28] Liu, S. and Masliyah, J.H., Single Fluid Flow in Porous Media, Chem. Eng. Comm., 1996, **148-150**, 653-732.

[29] Advani, S.G., Flow and Rheology in Polymer Composites Manufacturing, Elsevier Science B.V., The Netherlands, 1994.

[30] Parnas, R.S, Kathleen, M.F. and Dal-Favero, M.E., A Permeability Database for Composites Manufacturing, 1997, Polymer Composites, **18**, 5, 623-633.

[31] Ni, J., Zhao, Y., Lee L.J., and Nakamura, S., Analysis of Two-Regional Flow in Liquid Composite Molding, Polymer Composites, 1997, **18**, 2, 254-269.

[32] Pearce, N., Guild, F. and Summerscales, J., A Study of the Effects of Convergent Flow Fronts on the Properties of Fibre Reinforced Composites Produced by RTM, Composites Part A, 1998, **29A**, 141-152.

[33] Abraham, D. and McIlhagger, R., Investigations into Various Methods of Liquid Injection to Achieve Mouldings with Minimum Void Contents and Full Wet Out, Composites Part A, 1998, **29A**, 533-539.

[34] Wood, J.R. and Bader, M.G., Void Control for Polymer Matrix Composites (1): Theoretical and Experimental Methods for Determining of the Growth and Collapse of Gas Bubbles, Composites Manufacturing, 1994, **5**, 3, 139-147.

[35] Wood, J.R. and Bader, M.G., Void Control for Polymer Matrix Composites (2): Experimental Evaluation of a Diffusion Model for the Growth and Collapse of Gas Bubbles, Composites Manufacturing, 1994, **5**, 3, 149-158.

[36] Chui, W.K., Glim, J., Tangerman, F.M., Jaridine, A.P., Madsen,J.S., Donellan, T.M. and Leek, R., Process Modeling in Resin Transfer Molding as a Method to enhance Product Quality, 1997, Siam Rev., **39**, 4, 714-727.

[37] Coulter, J.P. and Ğuceri, S.I., Resin Impregnation During the Manufacture of Thermaplastic Matrix Composite Materials, Advances in Thermoplastic Matrix Composite Materials, G.M. Newaz, Ed., American Society for Testing and Materials, 1989, 14-32.

[38] Coulter, J.P. and Ğuceri, S.I., Resin Impregnation during Composite Manufacturing: Theory and Experimentation, Comp. Sci. Technol., 1989, **35**, 317-330.

[39] Ahn, K.J., Seferis, J.C. and Letterman, L., Autoclave Resin Infusion Process: Analysis and Prediction of Resin Content, SAMPE QUARTERLY, 1990, **21**, 2, 3-10.

[40] Bruschke, M.V. and Advani, S.G., A Numerical Approach to Model Non-Isothermal Viscous Flow through Fibrous Media with Free Surfaces. Int. J. Numerical Meth. in Fluids, 1994, **19**, 575-603.

[41] Wymer, S.A. and Engel, R.S., A Numerical Study of Nonisothermal Resin Flow in RTM with Heated Uniaxial Fibres., J. Composite Materials, 1994, **28**, 1, 53-65.

[42] Kang, M. K., Lee, W. I., Yoo, J. Y. and Cho S. M. , Simulation of Mold Filling Process during Resin Transfer Molding, J. Materials Processing and Manufacturing Science, 1995, **3**, 279-313.

[43] Malkin, A.Y., Baranov, A.V. and Timifeev, S.V., Molding of Resins with Impregnation of a Reinforcing Layer, J. Polymer Engineering, 1995, **14**, 2-3, 141-159.

[44] Sadiq, T.A.K., Advani, S.G. and Parnas, R.S., Experimental Investigation of Transverse Flow through Aligned Cylinders, Int. J. Multiphase Flow, 1995, **21**, 5, 755-774.

[45] Loos, A.C. and MacRae, J.D., A process simulation model for the manufacture of a balde-stiffened panel by resin film infusion., Comp. Sci. Technol., 1996, **56**, 273-289.

[46] Mogavero,J. and Advani, S.G., Experimental Investigation of Flow Through Multi-Layered Preforms, 1997, Polymer Composites, **18**, 5, 649-655.

[47] Yu, H.W. and Young, W.B., Optimal Design of Process Parameters for Resin Transfer Molding, J. Composite Materials, 1997, **31**, 11, 1113-1139.

[48] Pillai,K.M. and Advani,S.G., Numerical Simulation of Unsaturated Flow in Woven Fibre Preforms During the Resin Transfer Molding Process, Polymer Composites, 1998, **19**, 1, 71-80.

[49] Lekakou, C. and Bader, M.G., Mathematical Modelling of Macro- and Micro-infiltration in Resin Transfer Moulding (RTM), Composites Part A, 1998, **29A**, 29-37.

[50] Kamal, M. R. and Sorour S., Kinetics and Thermal Characterization of Thermoset Resin, Polymer Engineering and Science, 1973, **13**, 59.

[51] Lee, W.I., Loos, A.C. and Springer, G.C., Heat of Reaction, Degree of Cure, and Viscosity of Hercules 3501-6 Resin, J. Composite Materials, 1982, **16**, 510-261.

[52] Dusi, M.R., Lee, W.I., Ciriscioli, P.R. and Springer, G.S., Cure Kinetics and Viscosity of Fibreite 976 Resin, J. Composite Materials, 1987, **21**, 1, 243-261.

[53] Bogetti, T.A. and Gillespie, J.W.,Jr., Two-Dimensional Cure Simulation of Thick Thermosetting Composites, J. Composite Materials, 1991,**25**,239-273.

[54] Telikicherla, M.K., Altan, M.C. and Lai, F.C., Autoclave Curing of Thermosetting Composites: Process Modeling for the Cure Assembly, Int. Comm. in Heat and Mass Transfer, 1994, **21**, 6,785-797.

[55] Tredoux, L. and Van der Westhuizen, J. , Development of a Numerical Code that simulates Combined Heat Transfer, Resin Flow and Compaction during Composites Processing, Composites Manufacturing, 1995, **6**, 85-92.

[56] Young, W.B., Compacting Pressure and Cure Cycle for Processing of Thick Composite Laminates, 1995, Composites Science and Technology, **54**, 299-306.

[57] White, S.R. and Kim, Y.K., Staged Curing of Composite Materials, 1996, Composites Part A, **27A**, 3, 219-227.

[58] Buckmaster, J. and Vedarajan, T.G., Self-Heating Effects in Thermoset Composites, J. Composite Mater.,1997, **31**, 1, 2-21.

[59] McKee, S., Wall, D. and Wilson, S., An Alternating Direction Implicit Scheme for Parabolic Equations with Mixed Derivative and Convective Terms, J. Comput. Phys., 1996, **126**, 64-76.

[60] Beavers, G. S. and Joseph, D. D., Boundary Conditions at a Naturally Permeable Wall, J. Fluid Mech., 1967, **30**, 197-207.

[61] Blest, D.C., Fluid Mechanical aspects of the Manufacture of Laminar-Composites, MSc Thesis, University of Strathclyde, 1993.

[62] Baldini, G. and Petracco, M. ,(1994) , Models for Water Percolation during Penetration of Expresso Coffee, Fasano, A. and Primicierio, M. eds., Proc. ECMI, 1993, 131-138.

[63] Varga, R.S., Matrix Iterative Analysis, 1962, Prentice-Hall, USA.